Multi-instrument observations of ionospheric irregularities over South Africa

A thesis submitted in partial fulfillment of the
requirements for the degree of

MASTER OF SCIENCE

of

Rhodes University

by

Emirant Bertillas Amabayo

June 2011

Abstract

The occurrence of mid-latitude spread F (SF) over South Africa has not been extensively studied since the installation of the DPS-4 digisondes at Madimbo (30.88°E, 22.38°S), Grahamstown (33.32°S, 26.50°E) and Louisvale (28.51°S, 21.24°E). This study is intended to quantify the probability of the occurrence of F region disturbances associated with ionospheric spread F (SF) and L-band scintillation over South Africa. This study used available ionosonde data for 8 years (2000-2008) from the three South African stations. The SF events were identified manually on ionograms and grouped for further statistical analysis into frequency SF (FSF), range SF (RSF) and mixed SF (MSF). The results show that the diurnal pattern of SF occurrence peaks strongly between 23:00 and 00:00 UT. This pattern is true for all seasons and types of SF at Madimbo and Grahamstown during 2001 and 2005, except for RSF which had peaks during autumn and spring during 2001 at Madimbo. The probability of both MSF and FSF tends to increase with decreasing sunspot number (SSN), with a peak in 2005 (a moderate solar activity period). The seasonal peaks of MSF and FSF are more frequent during winter months at both Madimbo and Grahamstown. In this study SF was evident in $\sim 0.03\%$ and $\sim 0.06\%$ of the available ionograms at Madimbo and Grahamstown respectively during the eight year period. The presence of ionospheric irregularities associated with SF and scintillation was investigated using data from selected Global Positioning System (GPS) receiver stations distributed across South Africa. The results, based on GPS total electron content (TEC) and ionosonde measurements, show that SF over this region can most likely be attributed to travelling ionospheric disturbances (TIDs), caused by gravity waves (GWs) and neutral wind composition changes. The GWs were mostly associated with geomagnetic storms and sub-storms that occurred during periods of high and moderate solar activity (2001-2005). SF occurrence during the low solar activity period (2006-2008) can probably be attributed to neutral wind composition changes.

Acknowledgement

I would like to extend my sincere gratitude to my supervisors Dr. Lee-Anne McKinnell and Dr. Pierre Cilliers for their continuous guidance and unlimited support during this study. Thanks to the South African National Space Agency (SANSA) Space Science staff for their hospitality, encouragement and support during my study. Special thanks goes to the National Astrophysics and Space Science Programme (NASSP) administration of University of Cape Town for the financial offer for this study and Rhodes University management for enrolling me for this study.

Thanks to Dr. Gopi Krishna Seemala of Boston College and Dr. Ben Opperman of SANSA Space Science for respectively providing the GPS_TEC and ASHA algorithms used in GPS data analysis. The assistance of Dr. John Bosco Habarulema, Ngwira Chigomezyo, Stefan Lotz, Nkanyiso Mbatha (with Matlab programming) and their content based guidance (including Dr. Ndiitwa Christopher) is highly acknowledged. Thanks to all my friends and colleagues (inside and outside Hermanus) who assisted me in many different ways.

My sincere thanks goes to my wife and the entire family for their patience during the period of this study.

Dedication

I dedicate this thesis to Onzia Prossy and Fetaru Patience. I thank you for fulfilling my life and this serves for your patience and inspiration during this study.

Contents

List of Tables

List of Figures

Chapter 1

Introduction

The aim of this study is to characterise the ionospheric irregularities that cause spread F (SF) and GPS L-band scintillation in the mid-latitude region over South Africa. SF generally occurs in the F region of the ionosphere, particularly when the region becomes diffuse due to irregularities which scatter the radio wave. The ionosphere is the partially ionised region of the atmosphere that lies between $\sim$ 50 km and $\sim$ 1000 km above the Earth's surface. The signal received from the ionosphere is the superposition of a number of waves refracted from different heights and locations in the ionosphere at slightly different times. At low latitudes, SF occurs mostly during the night hours and around the equinoxes. At mid-latitudes, SF occurrence is believed to be less likely than at low and high latitudes, with more likelihood at night and in winter. At high latitudes (i.e $\gtrsim 40^{\circ}$ geomagnetic latitude), SF tends to be a nighttime phenomenon, appearing mostly around the equinoxes. Meanwhile, around the magnetic poles, SF is often observed both day and night. At all latitudes there is a tendency for SF to occur when there is a decrease in F region frequencies (Davies, 1990).

The ionosphere is characterised by its ability to transmit and reflect radio waves and forms an integral part of space weather. Space weather is being used globally for quantitative description of the physical changes in the near Earth-space environment in response to variations in solar radiation, solar plasma ejection, and the electromagnetic status of the interplanetary medium (Purohit *et al.*, 2010). Radio wave transmissions from the Global Positioning System (GPS) satellites have been used to obtain information about the Earth's ionosphere simultaneously from a global network of stations (Hoffmann-Wellenhof *et al.*, 1992; Wanninger, 1993; Kintner *et al.*, 2007; Yizengaw *et al.*, 2007). Space weather events associated with solar flares and coronal mass ejections (CMEs) cause ionospheric irregularities that scatter trans-ionospheric radio signals. The scattering of these signals produces fluctuations in both amplitude and phase of GPS signals, and GPS cycle slips, thus disrupting

satellite communications and navigation (Du *et al.*, 2000; Purohit *et al.*, 2010). Everything that depends on efficient long-range radio transmission is affected by adverse space weather. This includes long-distance phone calls, satellite television, GPS systems, and most importantly, the high frequency (HF) radios used by ships and aeroplanes (McKinnell *et al.*, 2007).

A mid-latitude ionospheric scintillation study by Radicella and Ezquer (2002) suggests a low scintillation activity level in the mid-latitude regions. A similar mid-latitude ionospheric scintillation study over Kokobunji (35.7°N, 139.5°E) in East Asia was conducted by Hajkowicz and Minakoshi (2003) and the results show strong evidence of scintillation activity during summer nighttime. A study conducted by Hajkowicz and Dearden (1988) using data from Brisbane (geographic latitude 27.5°S and longitude 152.5°E) reported that the magnitude and occurrence of scintillation activity strongly depended on the time of the day, season and solar cycle. Similar studies by Hajkowicz (1994) using data from Brisbane pointed out maximum occurrence of mid-latitude SF in association with sunspot minimum during mid-latitude ionospheric scintillation activity. Southern hemisphere mid-latitude seasonal ionospheric scintillation dependence was investigated by Hajkowicz (1989) and this author observed a consistent principal maximum during summer solstice. The current study investigates SF and ionospheric scintillation over Southern Africa and particularly over the South African region.

1.1 Project motivation

The ionosphere affects the signals received from GPS satellites, by degrading the signals and the accuracy of differential corrections, and in some cases causing loss of carrier lock. Signal degradation causes errors in GPS position fixes which in turn complicates effective operation of communication and navigation systems. The degradation is caused by irregularities in electron density which creates a medium through which the signals are refracted and diffracted as they traverse the ionosphere (Davies, 1990). The presence of moving irregularities in the ionosphere causes rapid random fluctuations in signal intensity and phase, referred to as amplitude and phase scintillations respectively. The above impact of ionospheric scintillation on GPS signals have raised concerns and identified a need to understand the nature of the irregularities responsible for scintillation in the mid-latitude regions. SF is a type of ionospheric phenomenon in which the pulses returned from the ionosphere are of a much longer duration than the transmitted signals. SF can be observed by either radio techniques such as ionosonde, radar, and scintillation or by optical techniques which observe the F region night-glow emissions using conventional photometers or wide-angle imaging

systems (Fagundes *et al.*, 1999).

The mid-latitude ionosphere is highly dynamic and this makes it difficult to predict SF probability on a nightly basis. SF affects radio communication and navigation systems utilising the Earth-space propagation environment/path. Though the probability of SF occurrence is small at mid-latitudes, there is still need to study the SF pattern in such regions, because of its strong influence on trans-ionospheric radio wave communication. SF is closely related to the scintillation of radio signals from satellites and radio stars (Davies, 1990), thus disrupting radio signals from astronomical sources, and possibly affecting radio astronomy studies (Fagundes *et al.*, 1999).

Models such as WBMOD (WideBand MODel) and the ionospheric scintillation model of North West Research Associates have been used to model observations in the northern hemisphere (Secan *et al.*, 1997). However, currently no significant model exists for predicting ionospheric scintillation over the mid-latitude regions of the southern hemisphere. As a result, there is an incomplete understanding of ionospheric scintillation over mid-latitude regions compared to high and low latitudes, particularly in Southern Africa. The frequency of occurrence of southern hemisphere ionospheric scintillation and SF at mid-latitudes and the mechanisms responsible for their formation are not yet well established. The Regional Space Weather Centre for Africa of the International Space Environment Centre, based at the South African National Space Agency (SANSA) Space Science (located at Hermanus (34.42°S, 19.22°E)) in South Africa launched a campaign in December 2006 to study ionospheric scintillation over Southern Africa and the South Atlantic by means of signals from GPS satellites.

1.2 Objective of the study

The main objective of this study is to identify and characterise the ionospheric irregularities that give rise to SF and ionospheric scintillations at mid-latitude stations located in South Africa, by analysing data from instruments which operate in the HF and L-band spectrum, namely ionosonde, dual frequency GPS and GPS Ionospheric Scintillation and Total Electron Content (TEC) monitor (GISTM). Dual frequency GPS receiver data from selected receivers distributed all over South Africa was used to derive $VTEC$, S_4-proxy scintillation index (S_{4p}) and hence the rate of change of TEC index ($ROTI$). Ionosonde data was analysed to look for irregularity signatures on ionograms. Corresponding GISTM and dual frequency GPS receiver data, if available, was also analysed. This helped to infer the extent and motion of

the irregularities that gave rise to SF and ionospheric scintillation. This in turn helped to develop an understanding of the extent, nature and origin of irregularities causing SF and ionospheric scintillation as observed at the mid-latitude stations.

1.3 Relevance of the study

The study of SF and ionospheric scintillation patterns over South Africa is aimed at providing a basis for developing a prediction model. Predictions by a SF and ionospheric scintillation forecasting model may be used to reschedule observation times and maintain the operation of spacecrafts. It can be used to advise users of the Earth-space environment on the likely occurrence of SF and ionospheric scintillation. A SF and ionospheric scintillation occurrence model could help to reduce the amount of work required to make corrections to space weather and radio astronomy data. Therefore, this study provides the basic understanding of SF and ionospheric scintillation required for developing a model that will be applicable to all radio communication prediction, as well as general radio science operations within a mid-latitude ionosphere.

1.4 Thesis layout

This thesis consists of six Chapters including this one. Chapter 2 gives the theoretical background of the SF phenomenon, its variability and brief theoretical introduction to ionosondes (i.e. pulse sounder) used for observation of SF. Chapter 3 provides background information on ionospheric scintillation and some basic parameters used to characterise this phenomenon. Chapter 4 provides a description of the data source, types of data used and the procedure of analysis. Chapter 5 presents the results and the observations. Chapter 6 offers a discussion, conclusion and recommendation for future work.

Chapter 2

Theory of the ionosphere and SF

This Chapter reviews the literature on the morphology of the ionosphere and the SF phenomenon. It provides essential background on various factors which influence SF, such as time of the day, seasons and solar activity. It also describes the nature of irregularities that cause mid-latitude SF. The associated plasma processes governing the generation of the irregularities, and variability of SF are also discussed.

2.1 The ionosphere

The ionosphere is formed primarily through the ionisation of the atoms and molecules in the upper atmosphere by ultraviolet (UV) radiation from the Sun. Recombination of electrons and positive ions takes place continuously. The ionosphere is divided into the D, E and F regions. Each layer is characterised by its altitude range, composition and electron density concentration. The F region splits into the F1 and F2 layers during the day (McNamara, 1991; Moldwin, 2008). There is no solar radiation to produce ionisation at night, however, recombination continues to take place and so the D, E and F1 layers gradually diminish. At sunset, the F2 layer persists although its density slowly decreases throughout the night. The solar activity determines the amount of radiation produced and consequently influences the ionisation in the ionosphere. The ionisation process is greatly affected by time of the day, season and geographical location (polar, auroral zones, mid-latitudes, and equatorial regions). The local winter hemisphere is away from the Sun and as a result the received radiation is spread out over a larger area in the winter hemisphere, thus receiving less solar flux than during the summer.

The plasma emitted by the Sun contains protons and electrons with a small percentage of alpha particles and heavier nuclei. This plasma flows out into space at a typical speed of

400 km/s, which can increase to about 1000 km/s during disturbed periods. Solar flares and coronal mass ejections (CMEs) are two major solar eruptions that inject huge amounts of radiation and charged particles into interplanetary space (Davies, 1990). These eruptions are known for potentially fuelling geomagnetic storms as they strike the Earth's magnetosphere. Solar wind flowing towards the Earth at speeds exceeding 500 km/s may be associated with CMEs. Matter ejected by solar flares and CMEs into the solar wind can therefore influence ionisation and recombination processes in the ionosphere which in turn may increase or reduce the thickness of ionospheric layers.

2.1.1 Effect of the ionosphere on radio propagation

The ionosphere influences radio propagation to distant places on the Earth. The ionosphere is a highly dynamic medium characterised by irregularities in electron density, and is also a highly dispersive medium at GPS frequencies. The electrical properties of the ionosphere allow it to transmit, reflect and refract radio waves as they traverse the ionosphere. Small scale irregularities cause scintillation of radio waves on trans-ionospheric links (Forte and Radicella, 2005). The ionospheric scintillation phenomenon occurs near the F2 layer and is observable in ionosonde data through a spreading of the HF radar return in both altitude and frequency (i.e. SF). Ionospheric scintillation is defined as a rapid temporal variation in the amplitude and phase of trans-ionospheric signals associated with structures of increased or decreased electron density. It is often attributed to the Rayleigh-Taylor (R-T) gravitational instability processes which operate on the steep upward gradient of the bottomside of the F region (Huang *et al.*, 1996, 2002; Hoang *et al.*, 2010).

2.1.2 Ionospheric E layer propagation

The E layer is the layer of the ionosphere that lies between 90 km to 120 km above the Earth's surface. This layer is ionised by soft x-ray (1-10 nm) and far ultraviolet (UV) solar radiation of molecular oxygen. It can reflect radio waves at oblique incident angles with frequencies below $\sim$ 10 MHz, but absorbs radio waves above this frequency. After sunset an increase in the maximum height of the E layer increases the frequency at which radio waves can travel a given distance by reflection. Besides the regular layers of the ionosphere, there are occasional irregular layers that affect the propagation of radio waves. The most significant of these is the sporadic E layer often denoted as Es (Davies, 1990). The Es phenomenon can be observed on the ionograms in Figure 2.1.

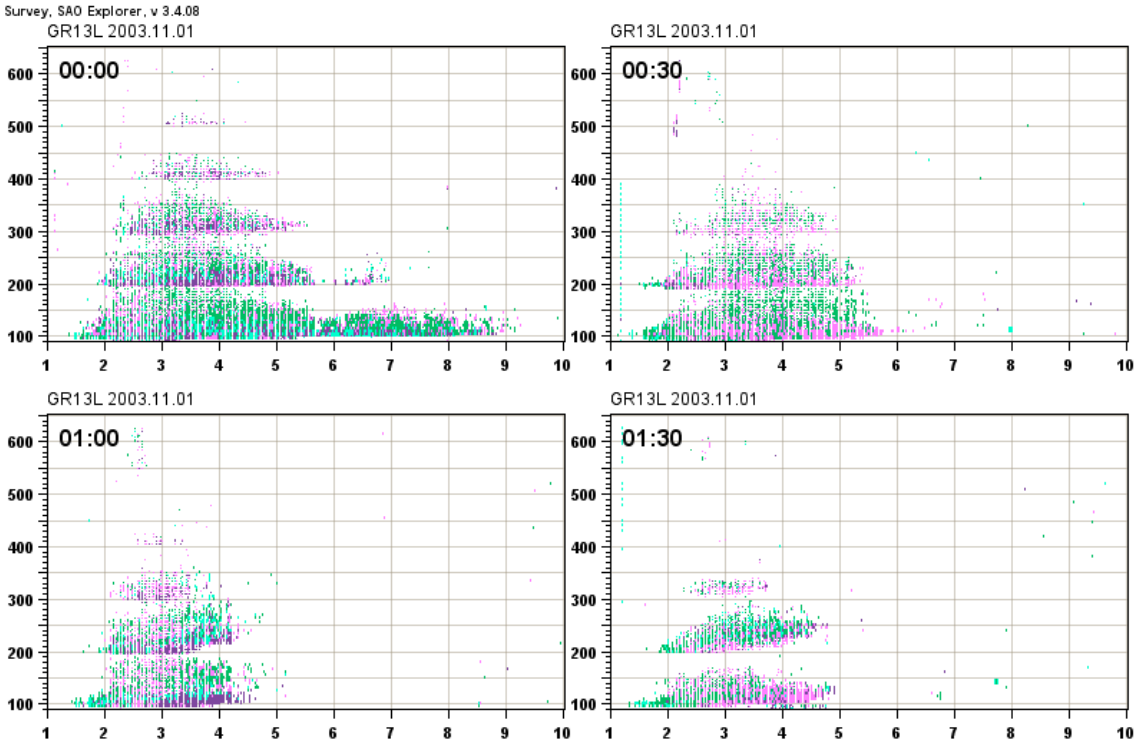

Figure 2.1: Occurrence of Es layer at different virtual heights as recorded by the ionosonde at Grahamstown (33.3°S, 26.50°E).

The existence of the Es layer is dependent upon the geomagnetic latitude and the formation of this layer has been explained using wind shear theory by authors like Bencze *et al.* (2004) and McNamara (1991). This theory attributes the formation of the Es layer to the vertical shear of the horizontal wind which changes the vertical ion (and electron) distribution due to the interaction between the wind and geomagnetic field (i.e. by $\overline{U} \times \overline{B}$ drift). The main source for mid-latitude Es clouds is wind shear produced by internal buoyancy or gravity waves, that create travelling ionospheric disturbances (TIDs). Most of these TIDs are produced by severe thunderstorm cell complexes with overshooting tops that penetrate the stratosphere. This layer is characterised by two basic parameters, the maximum (or critical) frequency (foEs) and the blanketing frequency (fbEs). The fbEs is equivalent to the background ion density above which the Es layer is non-transparent to sounding radio waves.

According to Bencze *et al.* (2004), the Es layer can reflect radio waves up to 50 MHz during intense Es events which often last from a few minutes to several hours. The Es layer is characterised by small, thin clouds of intense ionisation and can reflect radio signals up to 225 MHz. When Es propagation occurs, propagation paths that are unreachable often open up and this excites radio amateurs. The frequency of Es propagation is high when

high signal levels are attained and this is generally common during the summer months. The Es phenomenon is commonly experienced on the 10-m band, especially from May to August, although it may appear at any time. The foEs of this transient layer varies with time and space, and is less at the mid-latitudes than elsewhere. The Es layer is known to be more persistent during local summer and daytime than during winter and nighttime (Davies, 1990).

2.1.3 F layer propagation

The F region which extends from $\sim$ 200 km to $\sim$ 600 km above the Earth's surface is sometimes referred to as the Appleton layer. In the most dense regions of the F layer an increase in the density of mobile electrons increases the refractive index of the layer. Thus radio signals are refracted gradually over long vertical distances. Radio waves become useful for terrestrial propagation only when they are refracted enough to bring them back to the Earth. It is for this reason that the F2 layer supports most of the sky wave propagation of radio waves, thus facilitating HF radio communications over long distances (Davies, 1990). However, ionospheric effects are less apparent in the very high frequencies (VHF), ranging from 30 to 300 MHz. The maximum frequency of internal oscillation of a plasma known as plasma frequency (ω_p), is proportional to the square root of the electron density. Frequency of 30 MHz is above ω_p of the peak electron density in the ionosphere. As a result above this particular frequency, most radio waves travel through the ionosphere, except those at very oblique incident angles.

2.2 Ionospheric measurements

Different instruments are used to characterise the ionosphere at different altitudes. Below about 90 km (i.e. lower ionosphere) measurements are made by Incoherent Scatter Radars, or instruments on rockets and balloons. Ground-based ionosondes are used for recording ionospheric behaviour between about 90 km and 350 km (the bottomside ionosphere), and satellite-based ionosondes are used for measuring above $\sim$ 350 km (the topside). In situ electron density measurements at various fixed altitudes in the range 250 km to 800 km are conducted by means of low Earth orbit (LEO) satellites. In addition, recent research has shown that ionospheric information can be obtained by means of ionospheric tomography using the TEC information available in dual frequency GPS receiver data (Fremouw and Secan, 1992; Yizengaw *et al.*, 2007). This is due to the dispersive delay of trans-ionospheric signals, such as GPS L-band signals. The group (equivalent or virtual) height of an iono-

spheric layer (see Figure 2.2) represents the apparent height of the ionospheric layer, as determined from the time interval between the transmitted signal and the ionospheric echo at vertical incidence, assuming that the pulse propagates at the speed of light. The virtual height (in a complicated way) depends on the electron density profile, the geomagnetic field, and the frequency of the wave (Davies, 1990).

2.2.1 Mechanism of refraction of radio signals

Kelley (2009) stated that, if the ionosphere were uniform, refraction would yield a single great circle path with some minimum time delay. However, when the plasma density has an east-west structure, additional, larger time delays occur, which can be used to characterise the structure. Figure 2.2 illustrates the phenomenon of refraction in the ionosphere.

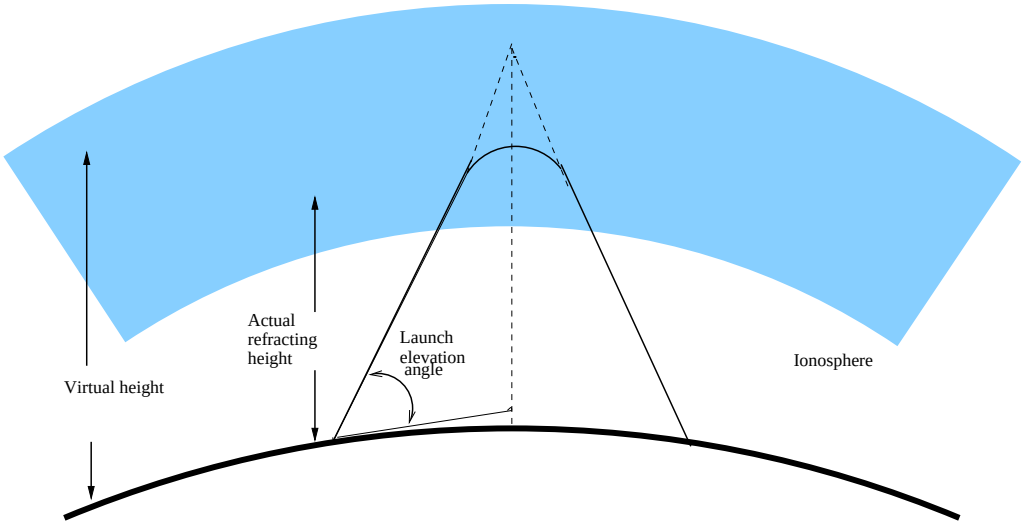

Figure 2.2: Schematic illustration of refraction of radio signals in the ionosphere over long distances.

When a radio wave reaches the ionosphere, the electric field in the wave forces the electrons in the ionosphere into oscillation at the same frequency as the radio wave. Some of the radio wave energy is sacrified to this resonant oscillation. The oscillating electrons will then either be lost to recombination or will re-radiate the original wave energy. Total refraction occurs when the collision frequency of the ionosphere is less than the radio frequency, and if the electron density in the ionosphere is great enough (Davies, 1990). The critical frequency is the highest (or limiting) frequency at or below which a radio wave is reflected by an ionospheric layer at vertical incidence. If the transmitted frequency is higher than ω_p, then the electrons cannot respond fast enough and they are not able to re-radiate the signal. The cut-off frequency (fmin) is the frequency below which a radio wave fails to penetrate a

layer of the ionosphere at the incidence angle required for transmission between two specified points by refraction from the layer.

2.2.2 Theory of ionosondes

An ionosonde is a pulsed radar device that vertically transmits a sweeped frequency signal into the ionosphere. It is the type of HF radar most frequently used today as an ionospheric sounding device. There are two types of modulation methods that are used in an ionosonde: the sweep frequency pulsed method and the chirp method. The operation of pulse and chirp sounders are similar, thus only the pulse ionosonde operation is illustrated in Figure 2.3. world and the data from some of them is sent regularly to various World Data Centres. This allows global monitoring of the main features of the ionosphere Davies (1990).

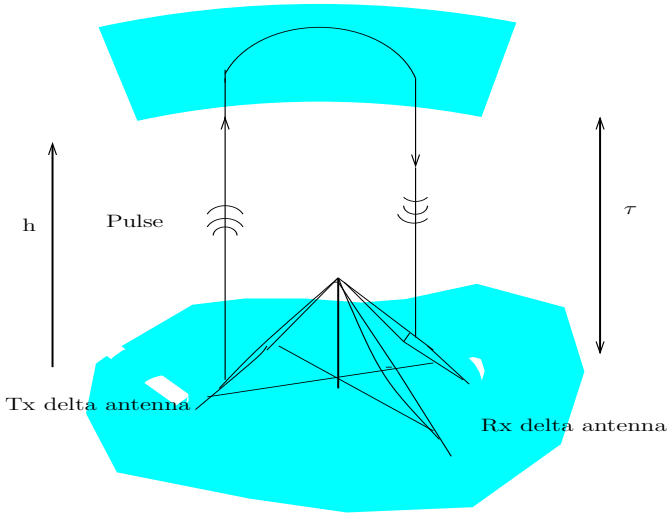

Figure 2.3: Schematic diagram illustrating the components and operation of the pulse ionosonde.

The ionosonde transmits short pulses from the transmitter (Tx) consisting of a number of cycles that sweep over a wide frequency range, generally from ∼2 to ∼6 MHz or higher, straight up into the ionosphere (Figure 2.3). The receiver (Rx) output of the detected signals is displayed on the oscilloscope with a time base synchronised to start with the transmission of the pulse. The delayed echo is then seen as a deflection of the trace in the Y-direction. The frequencies of the echoes are then recorded against delay time as the frequency changes. The resulting record is a plot of echo delay time (in the X-direction) versus frequency (in the Y-direction). In the first place, the axis in the Y-direction is a time axis which is then re-calibrated to a frequency axis by means of frequency markers inserted onto the ionogram. The echo delay time axis is likewise re-calibrated in terms of height according to equation

2.1.

$$h^{'} = \frac{c\tau}{2}, \tag{2.1}$$

where $h^{'}$ is the apparent (or virtual) height of reflection, c is the speed of light and τ is the echo delay time.

The factor of 2 in equation 2.1 arises from the fact that the pulse has to traverse the distance $h^{'}$ twice. The critical frequency ($f_{critical}$) is a function of electron density and hence varies with the ionisation at a particular altitude (Davies, 1990). Since the ionosphere is in a plasma state this frequency is then referred to as ω_p. However, modern ionosondes make use of the desktop PC to capture data and to display, electronically scaled and archived ionograms.

The relationship between virtual (or group) height ($h^{'}$), group refractive index ($\mu^{'}$) and time of flight (t) is represented by the equation:

$$h^{'} = \frac{c\tau}{2} = c\int_0^{h_r} \frac{dh}{u} = \int_0^{h_r} \mu^{'} dh, \tag{2.2}$$

where u is the group speed and h_r is the real height of reflection. The virtual height of the F layer at night increases linearly with frequency until penetration occurs at critical frequencies foF2 and fxF2 for the Ordinary (O) and Extraordinary (X) waves respectively in the ionosphere. The X-wave penetration at a frequency fxF2 implies retardation at the lower frequencies due to ionisation which in turn decreases with increasing frequency. The frequency at which the signal (pulse) penetrates the ionosphere can be converted to electron density by using the equation 2.3 (Davies, 1990).

$$f_{critical} = 9 \times 10^{-3}\sqrt{N_e}, \tag{2.3}$$

where N_e is the electron density in electrons/cm^3 and $f_{critical}$ is the frequency of penetration of a particular layer (in MHz).

The above ionospheric parameters can be obtained from ionosonde data. Currently, South Africa operates four ionosonde stations, over 56 GPS receivers and one GISTM receiver. The ionosonde and GPS stations from which data was obtained for this study are shown in Figure 2.4.

2.2.3 Selected ionospheric observatories in South Africa

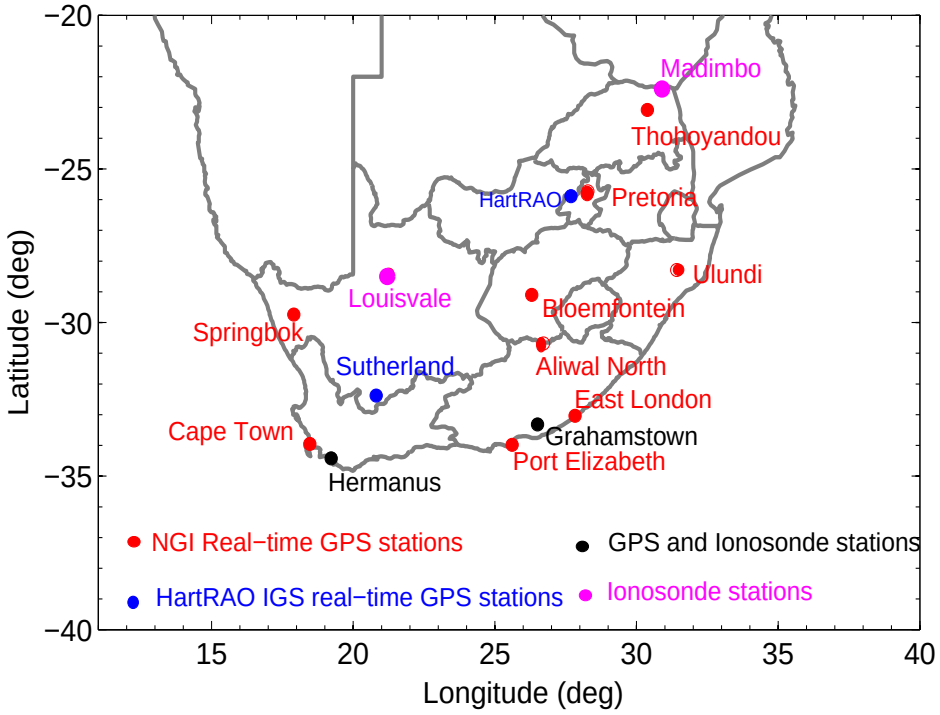

Figure 2.4: Map of South Africa showing the current ionosonde stations and selected dual frequency GPS stations. The GPS receivers are owned by International GPS Service (IGS) and National Geo-spatial Information (NGI).

An ionospheric field station equipped with an ionosonde has been operational in Grahamstown (33.32°S, 26.50°E) in the Eastern Cape since 1973, where a Barry Research Chirp Sounder was initially located. In 1996 a new digisonde (Lowell DPS-4 model) was installed, at the Grahamstown field station. In 2000 two more ionosondes (Lowell DPS-4 model) were added to the South African network, namely Louisvale (28.51°S, 21.24°E) in the Northern Cape and Madimbo (22.38°S, 30.88°E) in Limpopo Province. A fourth digisonde was added to the network in 2008, when a new model DPS-4D was installed in Hermanus (34.42°S, 19.22°E) in the Western Cape. Currently the digisondes at Grahamstown, Madimbo and Louisvale are being upgraded to the DPS-4D model. The geographical and geomagnetic longitudes and latitudes (denoted by (Glong, Glat) and (Mlong, Mlat) respectively) of the ionosonde and GPS stations are provided in Table 2.1 together with station codes.

The magnetic coordinates of the stations shown in Table 2.1 are computed using the facility available on the website ($http://wdc.kugi.kyoto-.ao.jp/igrf/gggm/$). The stations are

Table 2.1: Geophysical parameters of the ionosonde stations and selected dual frequency GPS receiver stations.

		Geogra. coordinates		Geomag. coordinates	
Station	code	long (°E)	lat (°S)	long (°E)	lat (°S)
		Ionosonde stations			
Grahamstown	GR13L	26.50	33.32	92.09	34.09
Hermanus	HE13N	19.22	34.42	84.67	33.90
Louisvale	LV12P	21.24	28.51	88.04	28.48
Madimbo	MU12K	30.88	22.38	98.89	24.16
		Trignet GPS stations			
Aliwal North	ANTH	26.72	30.68	92.95	31.55
Bloemfontein	BFTN	26.30	29.10	92.90	29.93
Cape Town	CTWN	18.47	33.95	84.06	33.31
East London	ELDN	27.83	33.04	93.48	34.05
Grahamstown	GRHM	26.50	33.32	92.09	34.09
Hermanus	HNUS	19.22	34.42	84.67	33.90
Port Elizabeth	PELB	25.61	33.98	91.04	34.58
Pretoria	PRET	28.28	25.73	95.60	26.98
Springbok	SBOK	17.88	29.67	84.49	29.03
Thohoyandou	TDOU	30.38	23.08	98.25	24.75
Ulundi	ULDI	31.42	28.29	98.17	30.03
		IGS GPS stations			
HartRAO	HRAO	27.69	25.89	94.98	27.04
Sutherland	SUTH	20.81	32.38	86.72	32.19

chosen such that they provide vast information all over South Africa. This provides a basis for comparing features of the events identified at different latitudes within South Africa.

2.2.4 Ionograms and their interpretation

The ionosonde generates and amplifies a signal on a range of frequencies and then transmits the signals through the atmosphere into the ionosphere. As the signals enter the ionosphere they start slowing down because the ionosphere is a diffuse medium (plasma) and becomes more diffuse as the altitude increases. Ionograms provide information about not only the shape of the different layers of the ionosphere, but also about the structure of the electron/ion plasma. Rough traces, indicating non-homogeneity, are seen predominantly at night, at equatorial or higher latitudes, and during disturbed conditions. As the frequency increases, each wave is refracted less by the ionisation in the layer, and so each penetrates further before it is reflected. Eventually, a frequency is reached that enables the wave to penetrate the layer without being reflected. For the ordinary mode wave, this occurs when the transmitted

frequency just exceeds the peak plasma, or critical frequency of the layer (McNamara, 1991).

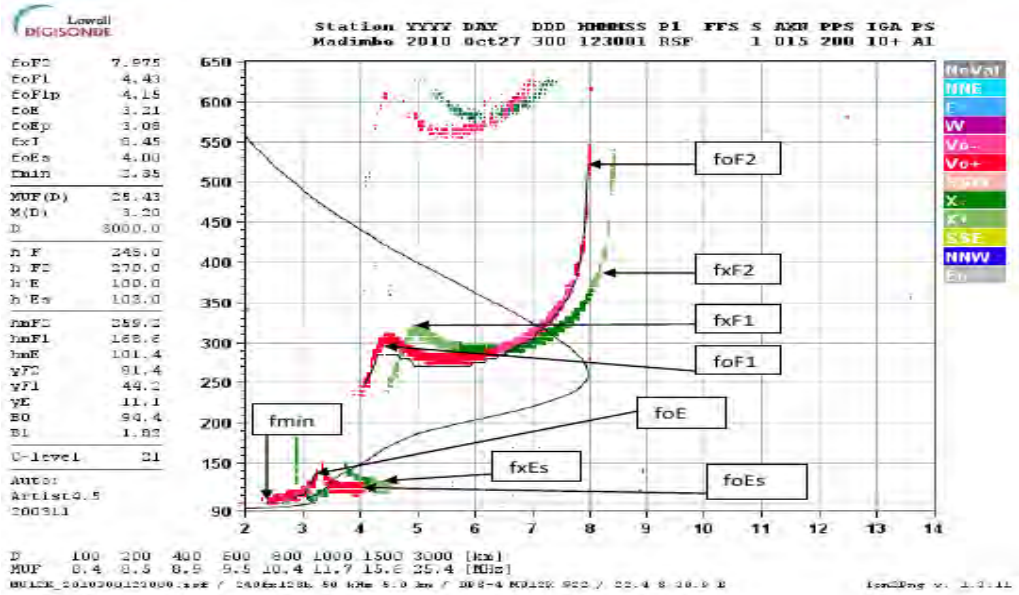

(a)

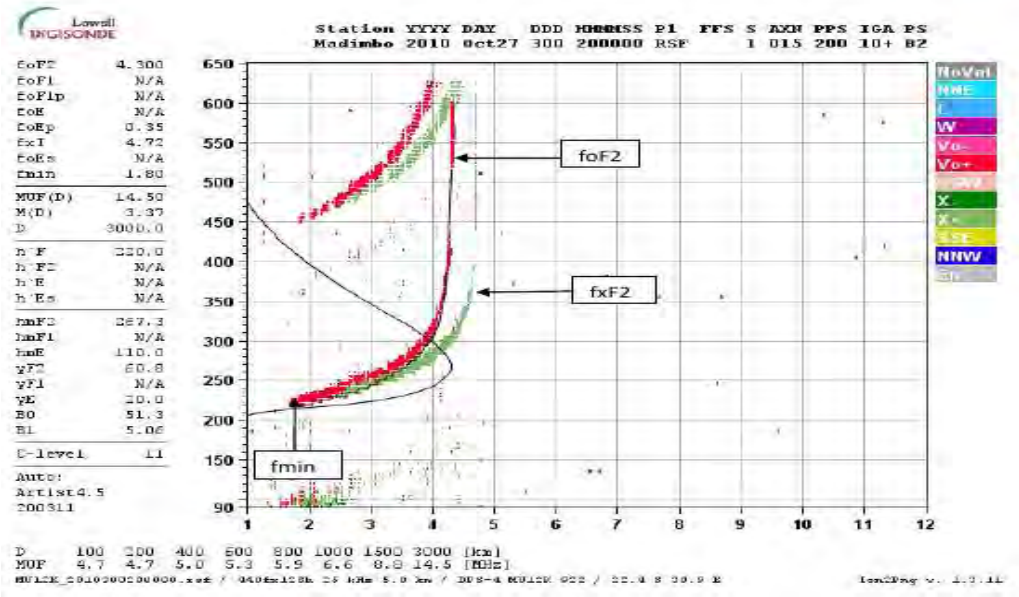

(b)

Figure 2.5: (a) Daytime (12:30:01 UT) and (b) nighttime (20:00:00 UT) ionograms without SF as observed at Madimbo on 27 October, 2010.

As the transmitted radio signal begins to penetrate the ionosphere, it splits up into O and X wave components due to the Earth's magnetic field. Both wave components have different critical frequencies for the different layers of the ionosphere.

2.3 The spread F (SF) phenomenon

SF refers to plasma irregularities of different characteristic scale sizes that occur during the night in the F region ionosphere. Ionospheric irregularities are temporal and spatial variations of the electron density lasting from minutes to a few hours. At the lower (equatorial) geographic latitudes ($\pm$ 0° - 20°) within the F region ionosphere these irregularities give rise to equatorial SF. Occurrence of similar irregularities in the mid-latitude F region causing SF originate from density perturbations, which in turn are believed to be caused by gravity waves (GWs) propagating in the F region (Abdu, 2001; Hoang *et al.*, 2010). SF development is enhanced when GWs raise the height of the F layer.

According to Radicella and Ezquer (2002) the daytime random ionospheric scintillation at mid-latitudes are related to Es layer events, while nighttime ones are associated with SF. At high latitudes, the morphology and intensity distribution of the irregularities shows that particle precipitation in the auroral oval and polar cusp are the primary agents which drive density fluctuations. In general, SF is caused by the scattering of signals from irregularities embedded in the signal path, both in depth and away from the zenith. SF occurrence increases with a decrease in foF2, and it is believed that above a certain threshold of foF2 no SF exists (Davies, 1990).

2.3.1 Variability of SF

The occurrence of mid-latitude SF depends mainly on solar activity, time of the day, time of the year, magnetic declination, geomagnetic activity and latitude. A good knowledge of mid-latitude SF and factors affecting its occurrence helps to model this phenomenon.

Geographical variations

SF occurrence is dominant at night in the equatorial regions (latitudes bounded by $\pm$20°) and at high latitude regions ($\geq$ 40° geomagnetic latitude). SF is evident mainly during the night, although it also occurs to a lesser extent during the day. The probability of occurrence of SF increases with latitude and hence is expected to occur less between 20° and 40° geomagnetic latitude (Davies, 1990).

Diurnal variations

The magnetic field lines at equatorial F region heights are mapped to the lower and higher latitudes. During the daytime, the high plasma conductivity of the E region will suppress

any electric field inhibiting the development of the plasma instability (Wernik *et al.*, 2004). However, after sunset, the E region conductivity drops considerably and the electric fields generated within the bottomside of the F region can develop plasma instabilities. The rapid post-sunset uplifting of the F region supports the onset of ionospheric plasma irregularities. Fluctuations in the ion drift velocity or plasma density, caused by GWs or other large scale structures, can initiate the generation of the initial perturbation (Davies, 1990). It therefore follows that SF is predominantly a nighttime phenomenon. In the polar regions during winter, there is no diurnal variation and hence SF occurs both during daytime and nighttime (Davies, 1990).

Geomagnetic activity

Perturbations induced by a geomagnetic storm in the ionosphere have been of great interest to space scientists over decades. During geomagnetic storms, electron density variations may be positive (increase) or negative (decrease), which in turn influences the SF phenomenon. Equatorial region SF occurs on magnetically quiet days and disappears with the onset of a magnetic storm (Davies, 1990). Mid-latitude SF is highly supported by magnetic storm activity while the exact opposite occurs close to the magnetic equator. However, there exists strong correlation between SF and magnetic storm activity during autumnal and vernal equinoxes. The correlation is moderate during summer (near north solstice) and poor in winter (Davies, 1990). Geomagnetic activity is known to strongly disrupt SF occurrence before local midnight near solar maximum. Sastri (1999) studied the post-midnight onset of SF at Kodaikanal (10.2°N, 77.5°E, dip 4°N) during the June solstice of solar minimum, and found that the F layer height does not play a pivotal role in the midnight onset of SF. This author also stated that the post-midnight onset of SF may not be entirely due to local plasma instability, but may result from plasma irregularities that were generated earlier to the west of the region observed and drifted onto the signal path. According to Buresova (2005), the storm effects in the F2 region ionosphere are predominantly attributed to ionospheric response to storm effects in the thermosphere. The effects in the lower ionosphere are predominantly caused by the storm-associated precipitating energetic particles.

Seasonal variations

In the polar latitude regions, seasonal variations change widely from year to year (Davies, 1990). Maximum SF occurrence at night is registered near equinoxes, followed by winter and least in summer near the magnetic dip pole regions. In the equatorial latitudes SF occurs most (90-100% at night and 50-60% around noon) near the equinoxes or during local

summer. The seasonal SF study over South Africa conducted by Lambert (1988), with data from Johannesburg (26.07°S, 28.10°E) and Hermanus (34.42°S, 19.22°E), revealed a seasonal maximum in winter, equinoctial minima, and a secondary maximum in summer. A similar study conducted by Huang *et al.* (2011) over Changchun (125.26°E, 43.83°N) and Urumqi (87.63°E, 43.75°N), both in China, show that the annual maxima of SF occurrence over the two stations are during summer and winter.

Sunspot dependence

SF occurrence increases with an increase in sunspot number (SSN) in regions of high geomagnetic latitude (greater than 60°N). Subbarao and Murthy (2006) stated that equatorial SF observed on an ionogram showed a positive correlation with solar activity in the Indian zones. Near the magnetic equator the sunspot influence appears through the effect of magnetic disturbance on SF. There exists strong negative correlation at sunspot maximum between the appearance of SF and the magnetic disturbance, and it disappears during low solar activity. Near the geomagnetic equator SF is an evening and nighttime phenomenon, beginning around sunset and most likely occurring between 21:00 and 01:00 local time (LT), occurring earlier at sunspot maximum (Davies, 1990).

2.3.2 R-T instability

R-T instability develops at the interface between two fluids of different densities when the lighter fluid pushes the heavier fluid. The polar region magnetic field is coupled to the magnetosphere and interstellar medium, thus allowing energy to flow directly into the ionosphere. This coupling may result in the formation of aurora, and can create great turbulence, leading to intense scintillation on trans-ionospheric radio signals. The nearly horizontal magnetic field at low latitudes provides a conducive environment for the generation of irregularities by the generalised R-T instability (GRT) mechanism. This mechanism occurs very frequently in the post-sunset equatorial ionosphere, resulting in the explosive release of the stored gravitational energy in the ionosphere. Irregularities of different scale sizes, ranging from centimetres to kilometres, develop and create an intense scintillation environment, leading to communication and navigational problems (Abdu, 2001).

Consider a finite plasma in a magnetic field under the influence of gravity, as shown in Figure 2.6. A perturbation of the interface between the fluids causes sinusoidal variations in the plasma density. The gravitational force on the electrons and ions causes them to drift parallel to the boundary. The $E \times B$ drift produced in the opposite direction amplifies the

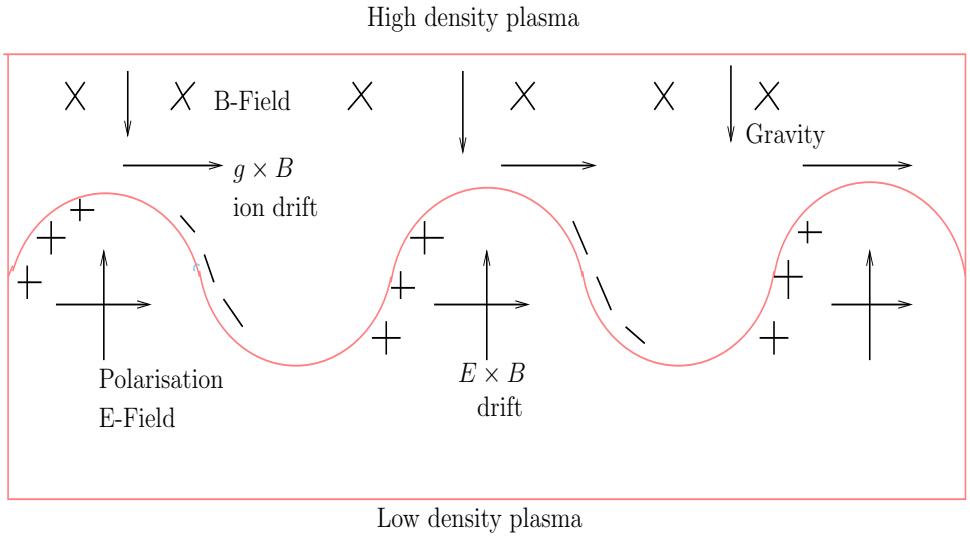

Figure 2.6: Schematic illustration of the R-T instability mechanism.

initial perturbation. When such a disturbance moves onto the surface of the interface in the form of a wave, they generate the so-called GWs and these provide a seed mechanism for the R-T instability (Huang *et al.*, 2002; Hoang *et al.*, 2010). When GWs propagate perpendicularly to the magnetic field, they generate polarised electric fields, and these are amplified non-linearly by the R-T instability (Huang *et al.*, 2002). The positive electron density gradient region of the rapidly rising F layer bottomside becomes unstable due to density perturbations, leading to the growth of plasma bubble irregularities by the R-T instability mechanism. The plasma bubbles develop as flux tubes aligned vertically. The rising plasma depletions of large scale sizes with secondary irregularities also develop by cascading processes at the steepening density gradients of the bubbles (Abdu, 2001). The evening F layer height and the vertical plasma drift are due to the pre-reversal electric field enhancement that is controlled by the thermospheric zonal wind (eastward in the evening) and the longitudinal/local time gradient in the integrated E layer conductivity near sunset. According to Abdu (2001), the growth of R-T instability responsible for equatorial ionospheric irregularities is summarised by the exponential growth profile in equation 2.4.

$$A = A_o e^{\gamma t}, \tag{2.4}$$

where A_o is the initial instability and t is the time of instability growth. The growth rate γ in equation 2.4 can be expanded to give a generalised R-T instability growth rate when

chemical recombination is neglected as in equation 2.5.

$$\gamma \approx \underbrace{\frac{\Sigma_F}{\Sigma_F + \Sigma_F}}_{a} \left[\underbrace{\frac{E \times B}{B^2}}_{b} + \underbrace{U_n}_{c} + \underbrace{\frac{g}{\nu^{eff}}}_{d} \right] \underbrace{\frac{\partial N}{N \partial h}}_{e}, \tag{2.5}$$

where Σ_F is the conductance, h is the height above the earth, ν^{eff} is the effective ion and neutral collision frequency, U_n is the neutral wind velocity component perpendicular to the magnetic field and g is the gravitational acceleration.

Martins *et al.* (2005) points out that the five processes represented in equation 2.5 can be subdivided into two enabling conditions and three driving/suppressing effects, labelled a to e in equation 2.5. The post-sunset enabling effects occur when the F region and total (E + F) region Pedersen conductivity ratio (a) approaches unity. This increases the electron density gradient (e). The upward post-sunset E×B drifts (b) are believed to be the main driving mechanisms for generation of equatorial ionospheric irregularities (i.e. equatorial SF). The greatest growth rate (i.e. enhancing effect) occurs when the peak height of the ionosphere is high (i.e. when the ionosphere moves to high altitudes). This reduces the neutral and ion collision frequency, which in turn maximises (d) when the bottomside density gradient is sharp. Mid-latitude ionospheric changes can also be influenced by changes in the equatorial or high latitude ionosphere. It is therefore important to understand the neighbourhood of mid-latitude regions in order to trace the origin of mid-latitude irregularities. In this study, the upward post-sunset E×B drifts will be investigated to ascertain the drift velocity of the nighttime mid-latitude ionosphere.

2.4 Summary

The background information on the SF phenomenon, including factors which cause its variability have been discussed in this Chapter. The R-T instability mechanism, thought to be responsible for generating ionospheric irregularities has been explained. Ionosonde measurements and the interpretation of ionograms were also discussed.

Chapter 3

Scintillation and TEC

3.1 Scope

This Chapter reviews, in the context of the research presented in this thesis, the literature on ionospheric scintillation, TEC measurement and mapping, and the nature of irregularities that cause ionospheric scintillation in the L-band. The influence of the solar terminator on the growth of irregularities has also been explored.

3.2 The ionospheric scintillation phenomenon

The ionosphere contains free electrons stripped from atoms by solar extra UV (EUV) radiation. The ionosphere is the uppermost part of the atmosphere and lies along the signal path between the orbiting GPS satellites and the terrestrial users. The interaction of the GPS signals with the ionosphere results in the fading of the amplitude and fluctuation of the phase of the signals, collectively known as ionospheric scintillation. Ionospheric scintillation in the mid-latitudes are caused mostly by small scale irregularities in electron density ranging from a few meters to kilometres. Scintillation in the ionosphere is a function of solar activity, geomagnetic activity, time of the year, local time, and geographic location. Ionospheric scintillation in the equatorial latitudes is attributed mainly to the ionospheric equatorial anomaly, which is associated with the sharp gradients in the electron density within such a region. According to Kintner *et al.* (2007), ionospheric scintillation occurs mostly at the high and low latitudes with a much lower incidence in mid-latitudes. High latitude ionospheric irregularities have been associated with energetic particle precipitation, such as in the South Atlantic Magnetic Anomaly (SAMA) region. Mid-latitude scintillation increases during geomagnetically active periods. Low latitude ionospheric irregularities are attributed

to decreased ionospheric conductivities as a result of plasma bubbles, plasma drifts, neutral winds and pre-reversal enhancement of the equatorial eastward electric field (Du *et al.*, 2000).

When an irregularity appears in the ionosphere as evidenced at HF band by a SF occurrence, the calculated TEC derived from GPS observables at the L-band may show a fluctuation. An irregularity seen as SF may also be correlated with a quick variation in the received carrier-to-noise ratio ($\frac{C}{N_o}$) on GPS L-band signals. However, scintillation can also be observed in the frequency of cycle slips in the phase of a GPS signal. An increase in data loss and number of cycle slips often occurs when the signals traversing the ionosphere encounter irregularities causing scintillation. These effects become severe during the occurrence of intense ionospheric scintillation events in the equatorial or auroral regions. The presence of reflecting obstacles in the vicinity of the receiving antenna can cause multipath effects that may have the same result as scintillation associated with ionospheric irregularities.

A receiver's ability to cope with scintillation depends on the frequency of occurrence of scintillation, as well as on the radio frequency and the position (azimuth, elevation) of the observed satellite (Conker *et al.*, 2000). GPS receivers operate at a fixed frequency and frequent scintillation may not allow enough time for the receiver to recover from a cycle slip or loss of lock before the next scintillation causes loss of lock. Therefore, sufficiently intense signal fluctuations cause GPS receivers to stop tracking the signals from GPS satellites during loss of lock, which may increase navigation errors or even cause navigation failure (Kintner *et al.*, 2007). Scintillation makes acquisition or reacquisition of GPS satellite signals difficult. Radio communication systems are known to be seriously affected by ionospheric disturbances which in turn limit the ability of the receiver system to coherently integrate weak signals (Dierendonck *et al.*, 1993).

The equatorial anomaly is the region which lies approximately $\pm(10°\text{-}20°)$ north or south of the magnetic equator. This region corresponds to two belts of enhanced ionisation and has been identified as the most likely region for the source of ionospheric scintillation (Dubey *et al.*, 2005). Based on in situ and ground-based measurements, Wernik *et al.* (2004) observed that ionospheric irregularities are concentrated near the magnetic equator and are observable during the pre-midnight period. In addition, they can also be observed during the nighttime in auroral zones and at all local times in polar regions. According to Wernik *et al.* (2004), high latitude irregularity scale sizes range from hundreds of kilometres to a few centimetres. The authors also state that the structures are highly dynamic, with variable convective motion controlled by the interplanetary magnetic field (IMF). The strongest

scintillation activity at high latitudes corresponds to the auroral oval and the region above 80° geomagnetic latitude over the polar cap (Aarons, 1982). The study by Hajkowicz (1994) reveals that mid-latitude scintillation maximum occurrence is during summer and mainly at nighttime as mentioned in Chapter 1. Nighttime scintillation is caused by either TIDs (Hajkowicz *et al.*, 1981) or by SF (Hajkowicz, 1977) mainly in the F region. The daytime scintillation events are attributed to the presence of the Es layer (as stated before in Chapter 2).

3.2.1 Ionospheric scintillation measurements

Ionospheric irregularities that cause scintillation have been studied with several airborne, ground- and satellite-based HF techniques. These include coherent backscatter, in situ rocket and satellite measurements and scintillation techniques which measure radio signal perturbations (Radicella and Ezquer, 2002). Data from the International GPS Service (IGS) network, which was primarily designed for satellite orbit measurement and Earth rotation monitoring, can also be used for investigation of the ionosphere. GPS signals provide an excellent means of measuring scintillation effects (via ionospheric disturbance and TEC measurements) on a global basis, since they are continuously available and can be measured through many points of the ionosphere simultaneously (Dierendonck *et al.*, 1993). In GPS data, scintillation at L-band frequencies can be inferred from both dedicated scintillation receivers such as the Novatel GSV4004B GPS ionospheric scintillation and TEC monitor (GISTM) or dual frequency GPS receivers. A high rate of change of TEC (ROT) along a ray path from the GPS satellite to the receiver is commonly used to characterise scintillation. In addition, the derivative of ROT, (DROT) and their respective standard deviations $ROTI$ and DROTI have been used to quantify scintillation levels (Du *et al.*, 2000).

3.2.2 Scintillation and morphology of irregularities

The appropriate analysis of scintillation observations requires one to deduce the irregular plasma structure in the scattering medium from the diffracted intensity fluctuations at the observing plane (Rufenach, 1971). The irregular structure in the scattering medium imposes a random phase on the transmitted radio wave signals. According to Rufenach (1971), the relationship between the phase spectrum and spectrum of the intensity fluctuations for weak or single scattering reveals two definite Fresnel effects:
(i) the severe attenuation of the intensity fluctuations for irregularities of a scale size larger than the Fresnel zone radius (r_F), and (ii) a sinusoidal type of oscillation in the intensity spectrum for structures smaller than r_F. The r_F parameter pertains to both phase and

amplitude scintillation, and is expressed mathematically as

$$r_F = \sqrt{2r\lambda}, \tag{3.1}$$

where λ is the incident signal wavelength, and r is the distance from the irregularities to the receiver, both measured in metres (m).

The power spectral density of phase scintillation obeys an inverse power law relationship (Rino, 1979; Fremouw, 1978). The power spectral density of amplitude scintillation also follows a similar power law relationship for high fluctuation frequencies, but is heavily attenuated at low frequencies. Yeh and Liu (1982) state that the cut-off frequency of the amplitude scintillation power spectrum called the Fresnel cut-off frequency ($f_{cut-off}$) is given in Hertz (Hz) by

$$f_{cut-off} = \frac{v_p}{\sqrt{2r_F}}, \tag{3.2}$$

where v_p is the effective scan velocity in km/s and is a function of the velocity of the ionospheric pierce point (IPP) through the irregularity layer.

The IPP is the point at which the satellite signal ray path intersects the ionosphere at the irregularity height as shown in Figure 3.1. This is normally taken to be the height of the F2 layer peak which typically has values between 300 km and 400 km. It is important to note that $f_{cut-off}$ is also the frequency that corresponds to the peak of the amplitude scintillation power spectrum. The Fresnel filtering factor and the r_F are both needed to account for the low frequency cut-off in the amplitude scintillation power spectrum. Fresnel filtering is important because amplitude scintillation is produced mainly by diffraction effects, which are only significant when the irregularity scale size is of the order of the r_F (Rufenach, 1971). The r_F has typical values of $\sim$ 276 m at the GPS f1 (1575.4 MHz) frequency and $\sim$ 312 m at the GPS f2 (1227.6 MHz) frequency, assuming an irregularity height of 400km.

In addition, the HF phase variations associated with diffraction tend to be more pronounced when the irregularity size is of the order of the r_F. For much larger irregularities, the phase variations merely follow the in situ density profile. Smaller irregularities produce prolific HF phase variations, but at a level that is unlikely to affect GPS satellite measurements. In general, because the r_F at L-band frequencies is quite small, large density gradients are required in order to produce significant scintillation effects. This tends to restrict scintillation activity to the equatorial anomaly and polar regions where large density gradients are known to exist. Radicella and Ezquer (2002) state that weak mid-latitude and strong

low latitude scintillation are respectively caused by diffractive and refractive scattering from bubbles that are perpendicular to the line of sight. The refractive and diffractive scattering are as a result of irregularities of scale size larger than r_F and near the r_F respectively.

3.2.3 Amplitude scintillation

This phenomenon is mainly due to signal fading and enhancement caused by ionospheric small scale irregularities, which can be observed from the rapidly changing signal-to-noise ratio ($\frac{S}{N}$) time series measured by GPS receivers. Amplitude scintillation is quantified by the S_4 index, which is essentially a normalised standard deviation of the signal intensity measured over a time period (Datta-Barua *et al.*, 2003) and is mathematically expressed as

$$S_4 = \sqrt{\frac{\langle I^2 \rangle - \langle I \rangle^2}{\langle I \rangle^2}}, \tag{3.3}$$

where I is the mean incoming signal power in watts (W).
Davies (1990) and Radicella and Ezquer (2002) adopt another index as an approximate measure of amplitude scintillation, which is defined as:

$$SI = \frac{P_{max} - P_{min}}{P_{max} + P_{min}}, \tag{3.4}$$

where P is the received signal power in W.

Severe amplitude scintillation reduces the $\frac{S}{N}$ at the GPS receiver and this causes the received signal intensity to drop below the receiver's lock threshold. This forces the receiver to re-acquire the signal and leads to errors in both GPS carrier measurements and GPS code (or loss of code lock). The lock threshold is determined by the bandwidth of the GPS receiver system and depends on the receiver tracking channel. Wanninger (1993) states that a code-correlation can withstand lower signal levels than a squaring channel or a cross-correlation channel. The $\frac{S}{N}$ can be mathematically expressed as

$$\frac{S}{N} = \left(\frac{P_{signal}}{P_{noise}}\right) = \left(\frac{A_{signal}}{A_{noise}}\right)^2, \tag{3.5}$$

where P is the average power in W and A is the root mean square amplitude in volts (V). $\frac{S}{N}$ is usually expressed in decibels (dB) as

$$\frac{S}{N}(dB) = 10 \times log_{10}\left(\frac{P_{signal}}{P_{noise}}\right) = 20 \times log_{10}\left(\frac{A_{signal}}{A_{noise}}\right). \tag{3.6}$$

The ratio $\frac{C}{No}$ is the $\frac{S}{N}$ of a modulated signal and the higher this parameter value, the better the quality of reception. It is expressed in dB-Hz and mathematically defined as

$$\frac{C}{No} = \frac{C}{K_B T}, \tag{3.7}$$

where C is the received carrier power in W, K_B is the Boltzmann's constant in Joules per Kelvin (JK^{-1}), and T is the receiver system noise temperature in Kelvin (K).
According to Dubey *et al.* (2005), the nominal $\frac{C}{No}$ for the L1 band is ∼45 dB-Hz; below ∼ 24 dB-Hz, tracking of signals gets interrupted. The authors also state that the L2 signal is affected more than L1 by the decrease in the $\frac{C}{No}$, since its power is less than that of L1 by ∼6 dB.

3.2.4 Phase scintillation

This type of scintillation is a consequence of sudden changes in ionospheric diffraction and refraction effects. Ionospheric refraction normally produces slow changes in L_1 - L_2 phase differences while phase scintillation produces rapid changes. These phase changes can be of the order of > 0.5 cycles of L_2 which causes L_2 channels aided by L_1 tracking data to lose lock. Phase scintillation is known to complicate cycle slip detection and measurement since it can reach cycles of L_1 or L_2 signals between two epochs with a common epoch rate of ≤ 10 seconds (Wanninger, 1993). Phase scintillation is produced by ionospheric irregularities at small wave numbers with sizes near the r_F (equation 3.1). Phase variations are often quantified in terms of the sigma phi index (σ_ϕ) which is the standard deviation of the refractive component of the GPS signal phase deviation produced during transit through the ionosphere. It is mathematically expressed as follows

$$\sigma_\phi = \sqrt{\langle \phi^2 \rangle - \langle \phi \rangle^2}, \tag{3.8}$$

where ϕ is the signal phase in degrees or radians.
Phase scintillation can cause GPS receiver systems to lose lock on the signal due to rapid changes in the signal frequency. The apparent range rate errors can produce a Doppler shift change in GPS signals, and when this shift exceeds the bandwidth of the phase lock loop (PLL), it results in loss of phase lock.

3.2.5 TEC measurements

TEC measurements can be obtained from GISTM or determined by calculation from dual frequency GPS code or carrier phase measurements. The received codes from GPS satellites at the two frequencies (f1= 1575.42 MHz and f2 =1227.60 MHz) often show a differential bias due to different hardware paths inside the transmitter. According to Wanninger (1993), the phases also experience offsets as a result of unknown carrier phase ambiguities and differential equipment phase delays. Satellites are mostly observed along oblique signal paths which pierce the ionosphere at an assumed ionospheric shell height (i.e. IPP) which corresponds to the height typically associated with the peak electron density in the ionosphere ($\sim$ 350 km for this study). The TEC along the signal path (slant path) between the receiver and the GPS satellite, commonly referred to as slant TEC ($STEC$), is defined as.

$$STEC = \int_R^S N_e ds, \tag{3.9}$$

where TEC is measured in TEC Units (TECU) with 1 TECU = 10^{16} electrons per m^2, R and S stand for the receiver and satellite positions respectively in km. The line integral is assumed to include all the electrons in a column with a cross-section of 1 m^2 and extending from receiver to satellite.

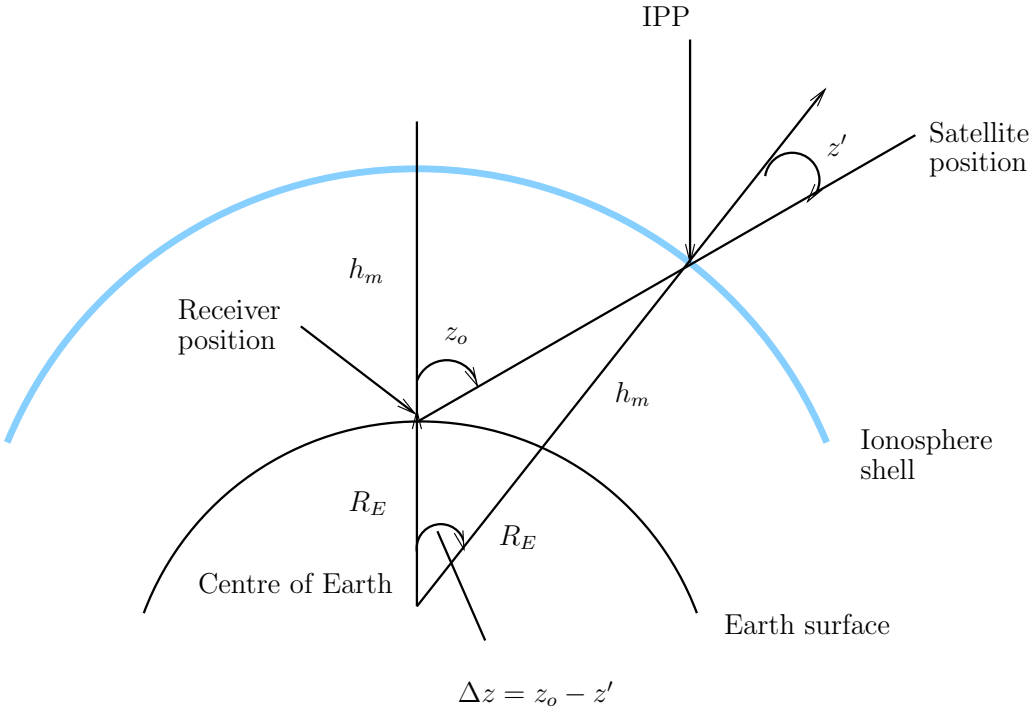

Figure 3.1: Schematic illustration of geometrical conversion from $STEC$ to vertical TEC (VTEC).

The $VTEC$ is modelled using a mapping function and the geographic position of the IPPs (Hoffmann-Wellenhof *et al.*, 1992) as follows

$$VTEC = STEC \times cos(z^{'}). \tag{3.10}$$

From the geometry of Figure 3.1, the following relation can be established.

$$sin(z^{'}) = \left(\frac{R_E}{R_E + h}\right) \times sin(z_o), \tag{3.11}$$

where R_E and h are the mean radius of the earth and height of the ionosphere respectively, both measured in km, and $z^{'}$ and z_o are zenith angles (both in degrees) at the IPP and observation site respectively. For a known satellite position, z_o can then be calculated and the approximate coordinates of the IPP can be determined. However, TEC is a difficult quantity to model since its variability is complex due to factors such as sunspot activity ($\sim$11-year cycle), seasonal and diurnal variations, the line of sight (elevation and azimuth) of the satellite and position of the observer (Hoffmann-Wellenhof *et al.*, 1992). Investigations by Forte and Radicella (2005) suggest that the actual effect of ionospheric scintillation on satellite navigation systems cannot be assessed by analysing experimental data (even if measured by GPS scintillation monitors) in the classical way. According to them this method of analysis deals with average scintillation activity which varies with geophysical conditions such as season and solar activity, but does not take into consideration particular navigation characteristics.

3.2.6 Geomagnetic storm events and ionospheric scintillation

Electric fields, thermospheric meridional winds, and high latitude particle precipitation are among others the physical mechanisms used to explain the ionosphere's response to geomagnetic storms observed at different latitudes (Mansilla, 2004). In this study global geomagnetic space weather indices such as disturbance storm time (Dst) and auroral electrojet (AE) were used to determine the correlation between magnetic storms and scintillation events. The condition of the Earth's magnetosphere is monitored by magnetometers which detect the rapid variations in the geomagnetic field resulting from the magnetosphere-ionosphere coupling effect of solar particle radiation. The Dst index is a geomagnetic index which monitors the global magnetic storm level. Dst is determined by obtaining the average of the horizontal component of the geomagnetic field from mid-latitude and equatorial magnetograms from all over the world.

Storm levels have been classified by various authors, but this study adopts a classification scheme used by Tsurutani *et al.* (2006). Tsurutani *et al.* (2006) categorised storms as minor/weak (-50 nT $<$ Dst $\leq$ -30 nT), moderate (-100 nT $<$ Dst $\leq$ -50 nT), intense (Dst $<$ -100 nT) and super (Dst $<$ -250 nT). Negative Dst values depict the presence of a geomagnetic storm or sub-storm, and the more negative the Dst value, the higher the intensity of the storm. These negative variations in the Dst index are as a result of the storm time ring current which flows around the Earth from east to west in the equatorial plane. The ring current results from the differential gradient and curvature drifts of electrons and protons in the near Earth region and its strength is related to the solar wind conditions. Large magnetic storms with extreme Dst indices cause prompt penetration of the mid-latitude and the equatorial ionosphere electric fields. This results in steep spatial TEC gradients and hence scintillation in GPS receivers. The AE index is derived from geomagnetic variations in the horizontal component observed at selected (10-13) observatories along the auroral zone in the northern hemisphere.

3.2.7 Travelling ionospheric disturbances (TIDs)

TIDs have been explained as a consequence of the interaction between atmospheric GWs in the thermosphere with the ionosphere (Hernández-Pajares *et al.*, 2006). The TIDs are wave-like structures associated with variations in the ionospheric electron density to the tune of several percent of TEC (Davies, 1990; Wanninger, 1993). Various techniques such as fixed-frequency observations, analysis of ionosonde traces and multi-frequency HF Doppler and incoherent scatter have been used to study TIDs (Davies, 1990; Kelley, 2009). These TIDs are categorised according to their characteristic scale sizes. Large scale disturbances (LSTIDs) with horizontal scale size $>$ 1000 km are thought to be generated by impulsive heating in the auroral oval and equatorwards propagation. This happens generally as a result of geomagnetic disturbances such as aurora and ionospheric storms. These disturbances produce an energy transfer toward lower latitudes in the form of thermospheric waves that in high altitudes, interact with the ions (Hernández-Pajares *et al.*, 2006). They are believed to have horizontal phase speeds and periods ranging from about 300 km/s to 1000 km/s and $\sim$30 minutes to $\sim$3 hours respectively (Wanninger, 1993).

Mesoscale (or medium scale) TIDs (MSTIDs), which have horizontal scale sizes of several hundreds of kilometres, are thought to be generated by atmospheric GWs. Atmospheric GWs are formed by a combination of the following: temperature-dependent recombination, wind effects like neutral winds or the solar terminator (Hernández-Pajares *et al.*, 2006). This class

of TID tends to have horizontal phase speeds of range ∼100 - ∼300 km/s and periods from ∼12 minutes to approximately one hour (Wanninger, 1993). MSTIDs are thought to be of tropospheric weather origin and due to orographic effects. They occur more frequently than LSTIDs. The MSTIDs can be detected in the time series of single station dual frequency GPS phase data. Lastly, intermediate scale structures of size 1-50 km are thought to be height variations of constant density contours and these can cause both range and frequency spreading of ionosonde returned echoes (Michael *et al.*, 2003).

The presence of ionospheric disturbances such as TIDs has a detrimental effect on the performance of precise navigation systems. This is because the slant differential ionospheric delays need to be interpolated with high precision in order to navigate with a few centimetres of error by fixing the carrier phase ambiguities in real time. Hernández-Pajares *et al.* (2006) state that during the ionospheric interpolation process, the TIDs can introduce a significant error within the networks with baselines from tens to hundreds of kilometres, significant distances compared to the MSTIDs wavelengths.

3.2.8 Solar terminator disturbances

The boundary between day and night (i.e. the solar terminator) represents a region of sharp change in the energy input from solar radiation, which consequently leads to strong gradients in the Earth's atmosphere and ionosphere (Hernández-Pajares *et al.*, 2006; Liu *et al.*, 2009). It is believed that as the Earth rotates, the solar terminator traverses through the atmosphere and such movement may generate atmospheric waves. Liu *et al.* (2009) state that the atmospheric irregularities and inhomogeneities are generated as a consequence of the atmospheric gas in the vicinity of the solar terminator attaining a non-equilibrium state. Terminator wave is indiscernible in the dawn side wind. Most wave structures are observed at night, with some extension to the sunlit region around solstices. The midnight density maximum seems to be closely connected to terminator wave structures, hence indicating a possible role of terminator waves in its formation (Liu *et al.*, 2009). According to Hernández-Pajares *et al.* (2006) the local time dependency of TIDs seems to be confined by the solar terminator.

3.3 Summary

The basic theory of the ionospheric scintillation phenomenon, TEC measurement and factors which influence the occurrence of the scintillation phenomenon were explained in this

Chapter. The spectral density of both amplitude and phase scintillation, and the effects of the Fresnel filtering factor on the morphology of the irregular plasma structures causing scintillation were explained. Some of the irregularities responsible for ionospheric scintillation (such as TIDs) are presented. Ionospheric scintillation is sometimes attributed to the R-T gravitational instability processes which operate on the steep upward gradient of the bottomside of the F region (see Chapter 2). The fact that it occurs particularly near the F2 layer makes it observable in ionosonde data through a spreading of the HF radar return in both altitude and frequency. This knowledge can be used to check for simultaneous occurrences of scintillation and SF phenomena. The study of the fluctuations in the signal intensity and phase is used to characterise the behaviour of the ionosphere.

Chapter 4

Data description and analysis

4.1 Scope

This Chapter describes the main data sets and their analyses for the investigation of the mechanisms responsible for the occurrence of mid-latitude SF and ionospheric scintillation.

4.2 Ionosonde data

The first data set comprises vertical incidence measurements obtained from ionograms recorded by the South African ionosonde network. Vertical sounding ionosondes make use of remote sensing by radio waves to study the behaviour and structure of the ionosphere. This technique has provided much of today's understanding of the ionosphere. The Hermanus (34.42°S, 19.22°E) digisonde (DPS-4D) is currently programmed to record at a time resolution of 15 minutes. The digisonde (DPS-4) at Grahamstown (33.32°S, 26.50°E) has a varying resolution of 15 and 30 minutes (see Figure 5.2 of Chapter 5). The two digisondes (DPS-4) at Madimbo (22.38°S, 30.88°E) and Louisvale (28.51°S, 21.24°E) record at 30 minute intervals. Both the DPS-4 and the DPS-4D are manufactured by the University of Massachusetts Lowell Center for Atmospheric Research in the United States. The ARTIST system is an automatic scaling programme which implements an algorithm characterised by high percentages of reliable autoscaled values given as output. It is only applicable to ionograms where polarisation tagging distinguishes between Ordinary (O) and Extraordinary (X) rays. In the past data from the South African ionosonde network was sent in real time to a central archiving centre in Grahamstown and made available to the global ionospheric community via various data resources including the Space Physics and Interactive Data Resource (SPIDR) and the Digital Ionosonde Database (DIDBase). Currently the

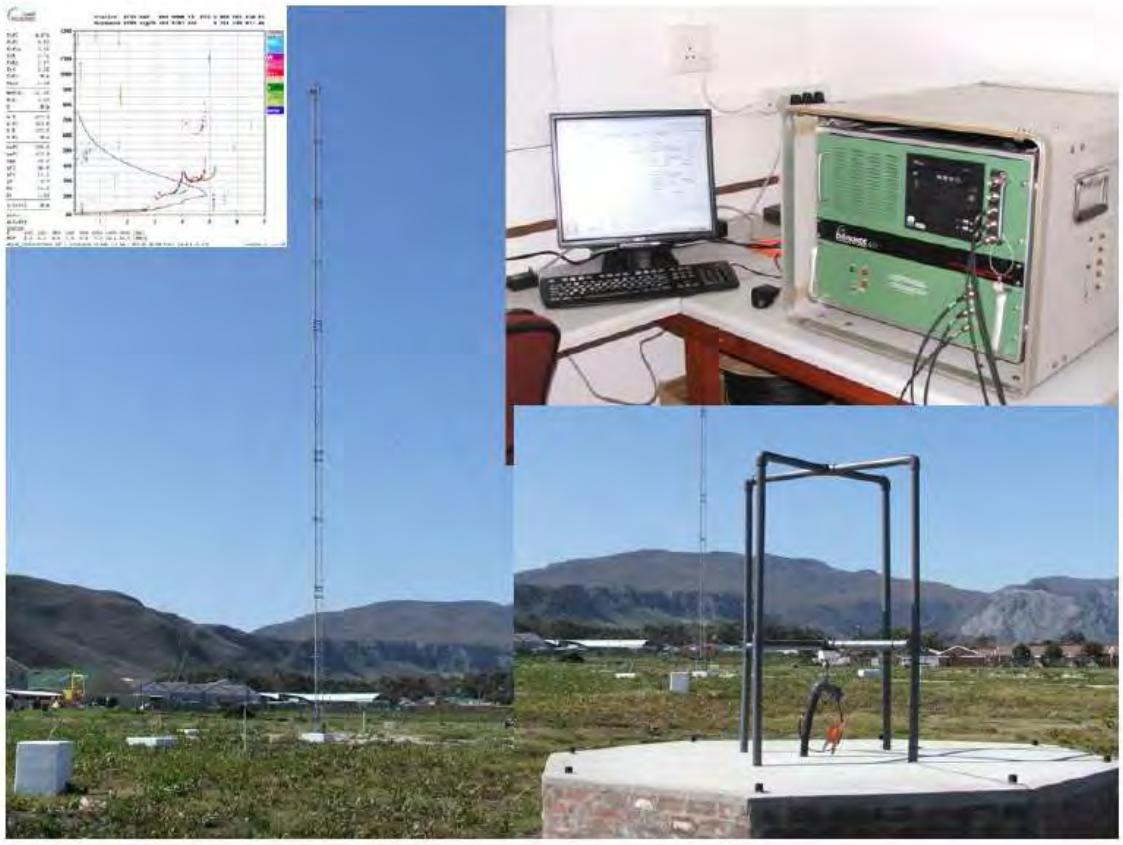

Figure 4.1: Hermanus DPS-4D ionosonde showing the transmitter (Tx), receiver (Rx) and the digisonde.

South African ionosonde data archiving centre is at South African National Space Agency (SANSA) in Hermanus. In this study ionosonde data was used to look for the occurrence of SF. Data was analysed to extract the ionospheric parameters required to identify mechanisms causing the occurrence of SF. The peak height of the F2 layer, hmF2, and the virtual height of the F layer, h'F, were the two parameters used in this study.

4.3 ACE data

The second data set was obtained from the Advanced Composition Explorer (ACE) satellite (Chiu *et al.*, 1998). The measurements were taken in the middle of every hour. The ACE satellite orbits around the Sun-Earth L1 libration point at $240R_E$ sunward of the Earth (Stone *et al.*, 1998). This satellite measures the velocity, particle composition, strength and orientation of the Interplanetary Magnetic Field (IMF) embedded in the solar wind (Stone *et al.*, 1998; McComas *et al.*, 1998; Chiu *et al.*, 1998). The ACE satellite carries several

instruments and those relevant to the work presented in this study are outlined below.

4.3.1 The SWEPAM instrument onboard the ACE

The Solar Wind Electron, Proton, and Alpha Monitor (SWEPAM) measures the solar wind plasma electron and ion fluxes (rates of particle flow) as functions of direction and energy. These sets of data provide detailed knowledge of the solar wind conditions and internal state every minute (McComas *et al.*, 1998). SWEPAM also provides real-time solar wind observations which are continuously transmitted to the ground for space weather purposes (Stone *et al.*, 1998; Chiu *et al.*, 1998). Electron and ion measurements are recorded by the ion and electron sensors onboard the ACE satellite, with an energy range of 0.26 to 36 KeV, and 1 to 1350 eV respectively. Both sensors use electrostatic analysers with fan-shaped fields-of-view and measure the energy per charge of each particle by bending their flight paths through the system. The fields-of-view are swept across all solar wind directions by the rotation of the spacecraft (Stone *et al.*, 1998; Chiu *et al.*, 1998).

SWEPAM observations provide the context for elemental and isotopic composition measurements made onboard the ACE satellite. These instruments in turn allow the direct examination of numerous solar wind phenomena such as CMEs, interplanetary shocks, and solar wind fine structure, with advanced 3-D plasma instrumentation (Stone *et al.*, 1998). They also provide an ideal data set for both heliospheric and magnetospheric multi-spacecraft studies. SWEPAM places the ACE satellite composition measurements in the context of low-speed streamer-belt flows, the high-speed solar wind from coronal holes, CMEs, the various types and strengths of interplanetary shocks, magnetic connection to the Earth's bow shock, and other solar wind structures. The ion data from this instrument was used in this study to investigate cases of increased or decreased ion number density and shock waves (i.e storms) during periods of SF. This facilitates the investigation of the correlation between ionisation/recombination and occurrence of SF irregularity.

4.3.2 The SWICS and SWIMS instruments

The Solar Wind Ion Composition Spectrometer (SWICS) and the Solar Wind Ion Mass Spectrometer (SWIMS) onboard the ACE satellite are optimised for measurements of the chemical and isotopic composition of solar and interstellar matter. SWICS determines the chemical and ionic charge composition of the solar wind, the temperatures and mean speeds of all major solar wind ions and resolves H and He isotopes of both solar and interstellar sources. SWICS measures the distribution functions of both the interstellar cloud and dust

cloud pick-up ions up to energies of 100 KeV/e (Stone *et al.*, 1998; Chiu *et al.*, 1998). SWIMS measures the chemical, isotopic, and charge state composition of the solar wind for every element between He and Ni. Each of the two instruments uses electrostatic analysis followed by a time-of-flight and, as required, an energy measurement. This instrument provided electric field (E-field) data for this study. A knowledge of E-field and other solar wind parameters (e.g. speed, ion number density) provides additional knowledge of the occurrence rate of geomagnetic storms, recombination or energetic particle precipitation in the ionosphere.

4.3.3 The ACE Magnetic Field (MAG) instrument

This instrument provides time-varying, large-scale structure information of the IMF near the LI point as derived from continuous measurements of the local field at the spacecraft. MAG measurements allow the effective interpretation of simultaneous ACE satellite observations and determination of the source location for solar wind thermal and energetic particles. This experiment consists of a pair of twin, boom-mounted, triaxial fluxgate magnetic sensors co-located from the centre of the spacecraft on opposing solar panels (Garrard *et al.*, 1998). The instrument provides data with between 3 to 6 $vectors^{-1}$ resolution for continuous coverage of the IMF (Smith *et al.*, 1998). Real-time observations with one-second resolution are provided continuously for near-instantaneous, world-wide dissemination in service to space weather studies (Chiu *et al.*, 1998). Magnetic field data from MAG was used to investigate the presence of solar wind shock waves to indicate sudden storm commencements (SSCs). Dst, IMF(Bz) and AE were used in this study to quantify the level of geomagnetic storms for the examination of the causes of SF and scintillation events.

4.4 GPS data

The third data set was obtained from selected GPS receivers distributed all over South Africa. The data used was recorded by standard dual frequency GPS receivers and GISTM receivers. Standard dual frequency GPS receiver observation data is stored in Receiver Independent Exchange (RINEX) format. This format stores the pseudoranges and carrier phases (L1 and L2) for each satellite. A network of dual frequency GPS receivers was established countrywide by various South African agencies, including the International GPS service (IGS), the Hartebeesthoek Radio Astronomy Observatory (HartRAO) and Electricity Supply Commission (ESKOM). The data from ESKOM is not meant for research purposes. The dual frequency GPS data sets used in this study are archived at HartRAO and the IGS

trignet GPS network. The map and table showing the location of the GPS stations and their coordinates are provided in Chapter 2. The GPS stations from which data was obtained in this study are distributed all over South Africa.

4.5 Data analysis and procedure

This section describes the necessary steps taken to process the data sets. In this study, patterns of events and variability of some parameters were looked for with both ionosonde and GPS data sets and any simultaneous occurrences observed on both data sets were investigated.

4.5.1 Ionosonde data analysis

Ionosonde data was loaded using the SAO Explorer software (Reinisch *et al.*, 2004), with which ionograms and their characteristics can be viewed and extracted. For this study hmF2 and h'F were extracted for the event analysis. These ionospheric characteristics for the days when SF was observed were plotted as a function of universal time (UT). The patterns and correlations between the events and any possible mechanisms triggering them were investigated. The total number of ionograms and those showing SF were recorded for each month and then used to compute the probability of SF occurrence. The monthly totals of ionograms showing SF occurrences were used to determine annual, diurnal and seasonal statistics.

Another parameter used in this study was derived from the time derivative of h'F (Vd = d(h'F)/dt) which is a measure of the ionospheric drift velocity. The perturbations in hmF2 (denoted α) and h'F (denoted β) were also derived (for some particular events) for identifying the degree of disturbance induced in the ionosphere. The data for these parameters was detrended using a two-day mean. The perturbations were calculated using the equations below.
α = hmF2 - $\overline{hmF2}$.
β = h'F - $\overline{h'F}$.

where $\overline{hmF2}$ and $\overline{h'F}$ are the mean values of the hmF2 and h'F respectively.

It should be noted that any number of days can be used to calculate the mean values, depending on the data reliability. The peak electron density of the F2 layer (NmF2), which is dependent on the foF2, was also used to investigate ionospheric phenomenon. The NmF2

was derived using the well-known equation, similar to equation 2.3 in Chapter 2:
$\mathrm{NmF2} = 1.24\times10^{10}\times(\mathrm{foF2})^2$.

4.5.2 Comparison of GPS_TEC and ASHA algorithms

In order to process GPS data, the Adjusted Spherical Harmonic Analysis (ASHA) and GPS_TEC analysis algorithms developed by Dr. Ben Opperman and Dr. Gopi Seemala ($http://seemala.blogspot.com/$) respectively, were implemented.
The ASHA model calculates the geographic locations of the IPPs using the thin-shell model. The code-and-phase-derived TEC is calculated and assimilates all phase-derived TEC measurements and associated IPP locations for all receivers and satellites. The model proceeds to calculate the standard deviation of all slant phase-derived TEC observations. The ASHA software uses Fourier series based on IPP longitude and latitude scaling to sun-fixed longitude and (adjusted) co-latitude. Spherical harmonic coefficients and satellite and receiver differential clock biases (DCBs) required to obtain time-and position-dependent estimates of the TEC are calculated by using a weighted least squares method. Therefore, the model uses a spherical harmonics filter to estimate the TEC above the receiver ($VTEC$). The details of the derivations and numerical approaches for this model are provided in **?**.

The GPS_TEC analysis algorithm also computes $STEC$ (at each IPP) and converts it to $VTEC$ (at each IPP), removes the outliers/jumps and then calculates the mean $VTEC$ as a measure of the TEC above the receiver. The mean $VTEC$ is derived by calculating the two-sigma iteration of the TEC values computed every 2 or 5 minutes from all satellites. The GPS_TEC algorithm uses Kalman filtering to estimate TEC from GPS data. The $VTEC$ output of these two algorithms is shown in Figure 5.1.

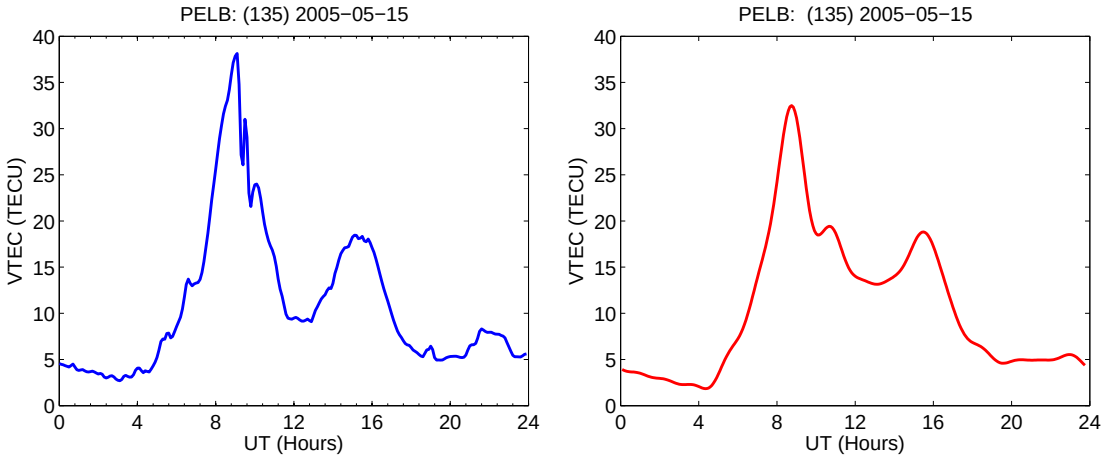

(a) (b)

Figure 4.2: $VTEC$ derived using (a) GPS_TEC and (b) ASHA algorithms for 15 May, 2005.

The $VTEC$ calculated using ASHA model is fairly smooth compared to $VTEC$ computed using GPS_TEC software. The difference in filters may be responsible for the presence and absence of small fluctuations in Figures 5.1 (a) and (b) respectively. Both results reflect the nature of the dynamics in the ionosphere, in terms of variability of TEC. It's clear from these results that the two algorithms do agree in determining any ionospheric disturbances in the ionosphere. In this study both algorithms were used extensively in the search for ionospheric phenomena associated with SF and scintillation.

4.5.3 Dual frequency GPS data analysis

This section offers an overview of the data and procedures for investigating the variability of TEC, the S_4-proxy scintillation index (S_{4p}), and $ROTI$. These ionospheric scintillation parameters were extracted from GPS observation files by means of the GPS_TEC algorithm. GPS satellites transmit their ephemeris (and other information) on two carrier frequencies (f1= 1575.42 MHz and f2 =1227.60 MHz) on the L-band for research purposes. The time-based pseudorange observables associated with f1 and f2 frequencies are denoted by P1 and P2 respectively. The GPS_TEC software calculates TEC with an elevation mask of $\gtrsim 20^{\circ}$, and applies satellite and receiver bias corrections according to equation 4.1. The software takes RINEX observation files with at least C1 (coarse/acquisition code transmitted on the f1), L1, L2, P2 observables as inputs. In the presence of $\frac{S}{N}$ observable S1, GPS_TEC derives a proxy for S_4 index (S_{4p}) at ten-minute intervals from 30 second samples of S1 ($http://seemala.blogspot.com/$).

The GPS_TEC programme also uses the RINEX navigation file of any IGS station available

for internet download. It calculates elevation and azimuth angles of the observed satellites which are then used for the $VTEC$ calculation. The differential code bias (DCB) files provided by the Centre for Orbit Determination in Europe (CODE) are also required. The GPS_TEC algorithm also reads satellite (P1-C1) biases and the (P1-P2) DCB biases, if available. In the absence of biases, it calculates the inter-frequency biases for different satellites visible to the receiver (though this is not very effective as it allows some room for TEC variability). The biases in the observed $STEC$ are accounted for by computation via the expression below.

$$(STEC)_{desired} = STEC + B_{Rx} + B_{Rich} + B_{sat}, \tag{4.1}$$

where B_{Rx}, B_{Rich} and B_{sat} are the receiver bias, receiver inter-channel bias and satellite biases respectively. The receiver biases are estimated by assuming that the nighttime TEC values are fairly constant. Biases are then evaluated by minimising the root mean square (rms) average error (of TEC values) obtained from different satellites at the same time ($http://seemala.blogspot.com/$).

The $VTEC$ derived from the ASHA algorithm was used to calculate the TEC perturbation as a measure of the disturbance of the ionospheric electron concentration. The GPS data for selected stations was processed to extract observation files. These observation files (sampled at 30 sesonds) were then fed as input for the ASHA software to calculate $VTEC$, which in turn was used to calculate $VTEC$ perturbation. The data for each GPS station for a number of quiet days before and after a SF event (or period) was used to calculate the background TEC (mean $VTEC$) of the data points for every 30 seconds in order to smooth out the quiet day data. This quiet day mean $VTEC$ ($\overline{VTEC}$) was then used in a MATLAB script to compute the $VTEC$ perturbation using the expression below.

$VTEC$ perturbation = $VTEC$ - $\overline{VTEC}$.

It should be noted here that the mean values for each row were calculated using a number of data points determined by the number of quiet days chosen.

4.5.4 $ROTI$ as S_4 amplitude scintillation proxy

In this study, dual frequency GPS receiver observables were used to determine $VTEC$ and $ROTI$ (rate of change of TEC index). These parameters were derived using the GPS_TEC software, to look for signatures of ionospheric irregularities. In the absence of measured L-band scintillation values, a proxy for the S_4 amplitude scintillation index (S_{4p}) is derived.

The S_{4p} parameter is derived from $ROTI$, which is defined as the standard deviation over a 5-minute period of ROT (rate of change of TEC) calculated from 30-second sampled GPS data (Pi *et al.*, 1997). Studies by Pi *et al.* (1997), Basu *et al.* (1999) and Beach and Kintner (1999) concluded that $ROTI$ measurements could be used as a proxy for assessing the presence of ionospheric scintillation. Beach and Kintner (1999) concluded that the S_4 scintillation index is roughly proportional to measures of TEC fluctuation for weak scintillation with $ROTI \approx$(2-5)$\times S_4$ rendering good expressions for their measurements. Similarly, Basu *et al.* (1999) found $ROTI \approx$(2-10)$\times S_4$ correlations using their data set. The quantitative relationship between $ROTI$ and S_4 varies considerably due to variations within the ionospheric projection of the satellite velocity and the ionospheric irregularity drift. The study by Basu *et al.* (1999) indicated that $ROTI$ is selective of Fresnel scale structures of 400 m at GPS frequencies.

In this study the approach of Du *et al.* (2000) was followed in quantifying S_{4p} related to $ROTI$ by an elevation-weighted coefficient (γ). γ is calculated from a function of a GPS satellite's motion relative to the ionosphere, which is assumed to be concentrated on an imaginary thin shell of 400 km above the Earth. The S_{4p} and $ROTI$ parameters are calculated using the following expressions:

$$S_{4p} = \gamma \times ROTI, \tag{4.2}$$

$$ROTI = \sqrt{\langle ROT^2 \rangle - \langle ROT \rangle^2}, \tag{4.3}$$

where

$$\gamma = 6.2135 \times 10^{-3} \left(\frac{v^2}{s} \right).$$

$$v^2 = \left(v_p^2 + v_d^2 - 2 v_p v_d cos\alpha \right) cos^2\varphi.$$

$$v_p = \frac{v_S(r_S + h)}{R_E + r_S}.$$

$$s = \frac{(r_S + h)cos(\varphi + \theta)}{cos\varphi}.$$

$$\varphi = sin^{-1}[rcos\frac{\theta}{r + h}].$$

with

R_E = Earth radius (6378 km),

h = assumed ionospheric height (350km),

θ = satellite elevation angle,

α = GPS orbital plane inclination (55°),
v_d = ion drift velocity (120 ms^{-1}),
v_p = velocity of the IPP moving at h ,
v_S = satellite orbital speed (3874 ms^{-1}),
r_S = satellite orbital altitude (20000 km).
The elevation-weighted coefficient (γ) selectively suppresses low elevation scintillation compared to high elevation scintillation.

GISTM data analysis

For calculation and analysis of ionospheric scintillation, the following GPS observables are required: L1, L2 (carrier phase in cycles on f1 and f2 respectively) and S1 (carrier noise level on the f1) in dB-Hz. The S1 parameter is the signal-to-noise ratio (C/No) on L1 and L2 observables which is extracted from the binary data files using the software TEQC (UNAVCO). The S1 parameter is sampled at an interval of 5 seconds. The GISTM measures phase and amplitude at a rate of 50 Hz for each visible satellite and computes TEC from combined L1 and L2 pseudorange and carrier phase measurements.

The ScintSoft algorithm (Python software) developed by Rory Meyer at the South African National Space Agency (SANSA) at Hermanus was also used in this study. The ScintSoft software reads and parses GISTM files and it was used to look for scintillation events. The parameters of interest were analysed using the ISM-read algorithm. A MATLAB programme ISM-read developed at the South African National Space Agency (SANSA), uses a customised programme called parseismr.exe (developed by AJ Systems, Silicon Valley) to extract the parameters of interest from the binary file. Thresholds of elevation (20°), S_4 (0.05) and σ_ϕ (0.20 radians) were applied to the data. Time-jumps larger than 2.00 minutes are suppressed, scintillation events below 20° elevation filtered. The corrected S_4 and σ_ϕ values were plotted to detect indications of amplitude and phase scintillation. Other parameters like C/No and $VTEC$ were also investigated for any ionospheric scintillation events.

4.6 Summary

The data sources used in this study and the corresponding algorithms used for data analysis are described. The formats of the GPS data and processing techniques used in the analysis are explained. The derivation of the $VTEC$ perturbation and ionospheric drift speed (Vd) as a mechanism of detecting the level of disturbance in the ionosphere are also explained. A

comparison of the main algorithms used in the processing and analysis of GPS data is made. The results and discussion of the processed data are presented in Chapter 5.

Chapter 5

Results and observations

5.1 SF events

This Chapter presents statistics of SF observed at Madimbo and Grahamstown ionosonde stations. SF as discussed in Chapter 2 is a well established phenomenon and its effects at high and equatorial latitudes have been studied in detail by several authors such as Davies (1990), Foppiano and Rodger (1994) and McKinnell *et al.* (2010). The cause and effect of mid-latitude SF particularly in the southern hemisphere has not been as effectively established compared to other latitudes. This Chapter offers an analysis of ionosonde, GISTM and dual frequency GPS data for SF and ionospheric scintillation events.

5.1.1 Classification of SF

SF is observed on ionograms when the pulses returned from the F region of the ionosphere are of longer duration than the transmitted signals. SF is generally identified in terms of the appearance of the Ordinary (O) and Extraordinary (X) ray traces on an ionogram. SF identification is usually independent of the physical mechanisms by which it forms. The mechanisms by which SF forms at mid-latitudes still remains speculative (Davies, 1990; Bhaneja *et al.*, 2009). For this study, SF was classified into frequency SF (FSF), range SF (RSF) and mixed SF (MSF) in a manner similar to that of Lambert (1988), Davies (1990) and Wang *et al.* (2008). FSF is characterised by diffuse echoes near foF2, thus making the foF2 parameter undefinable (Davies, 1990; Wang *et al.*, 2008, 2010). It occurs due to a range of densities at a given altitude that causes pulses of different carrier frequency to be reflected from that altitude. RSF is associated with the diffusiveness of the echoes near the horizontal part of the trace (Davies, 1990; Wang *et al.*, 2008) due to reflection at different altitudes at a given frequency. Both range and frequency spread can occur separately as FSF and RSF or

simultaneously giving rise to MSF (Bhaneja *et al.*, 2009). The three types of SF are shown in Figure 5.1 as well as an example of the Es phenomenon, which is outside the scope of this study. Ionosonde data from Madimbo (30.88°E, 22.38°S) and Grahamstown (26.50°E, 33.32°S) was extensively examined for SF events and correlated with outside events observed at Louisvale (21.24°E, 28.51°S).

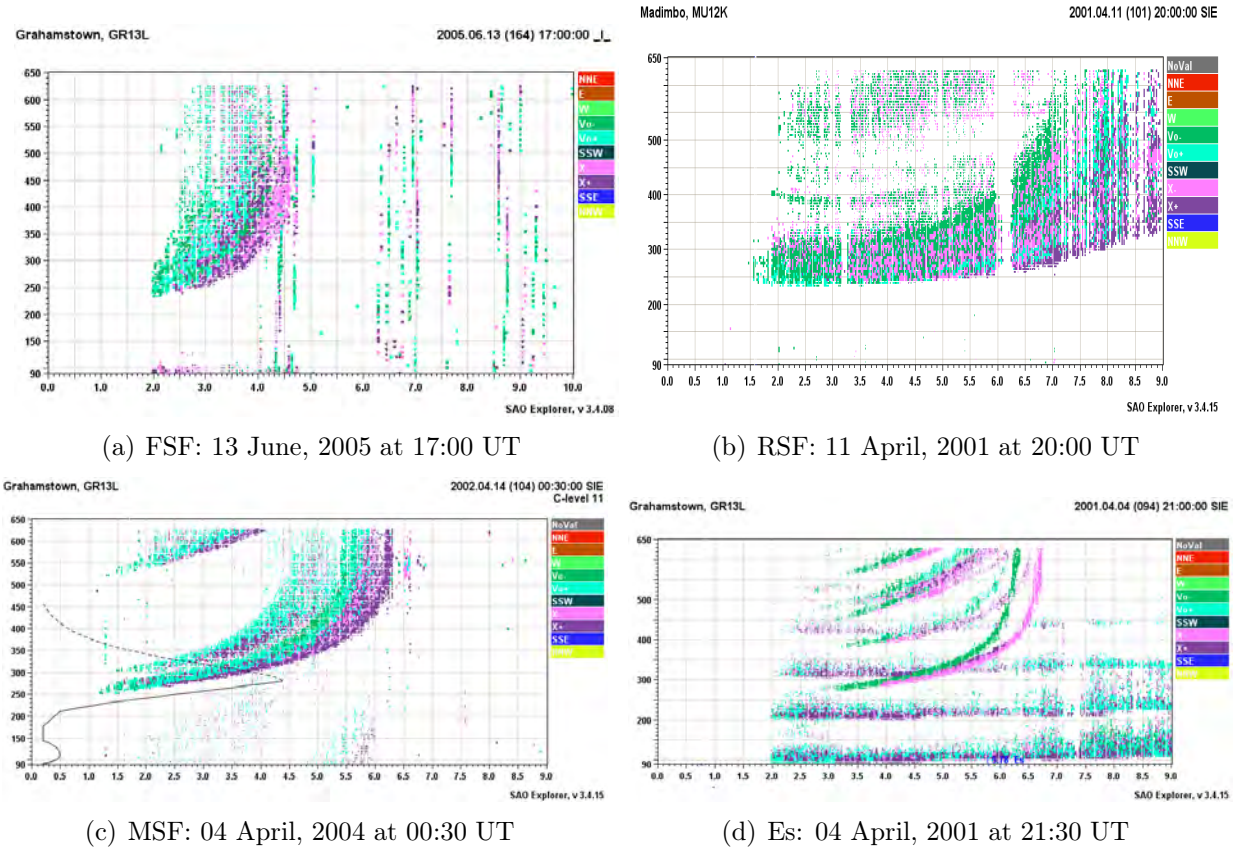

(a) FSF: 13 June, 2005 at 17:00 UT

(b) RSF: 11 April, 2001 at 20:00 UT

(c) MSF: 04 April, 2004 at 00:30 UT

(d) Es: 04 April, 2001 at 21:30 UT

Figure 5.1: Ionograms showing the appearance of the O and X ray traces during (a) FSF, (b) RSF and (c) MSF. (d) Occurrence of normal reflected echoes and Es at lower virtual heights ∼(90 - 350 km).

5.1.2 Annual SF statistics

This section presents the annual occurrence of SF and the availability of data in terms of the number of available ionograms. These ionograms were viewed with SAO Explorer (Reinisch *et al.*, 2004) to identify SF events. The number of ionograms showing SF was recorded for each type of SF. The statistics of observed SF events at Madimbo and Grahamstown were recorded for eight years (2001-2008) and are presented in Figures 5.2 and 5.3. The monthly percentage occurrence (i.e. probability) of the three types of SF was calculated using the

following formula:

$$\text{Probability} = \frac{\text{Sum of SF occurrences}}{\text{Total number of observed ionograms}} \times 100\% \tag{5.1}$$

The statistical analysis was based on the probability of SF occurrence and illustrates the trend of monthly, annual, seasonal and diurnal variability. The probability of SF occurrence is an important parameter in the prediction and modelling of SF (McKinnell *et al.*, 2010).

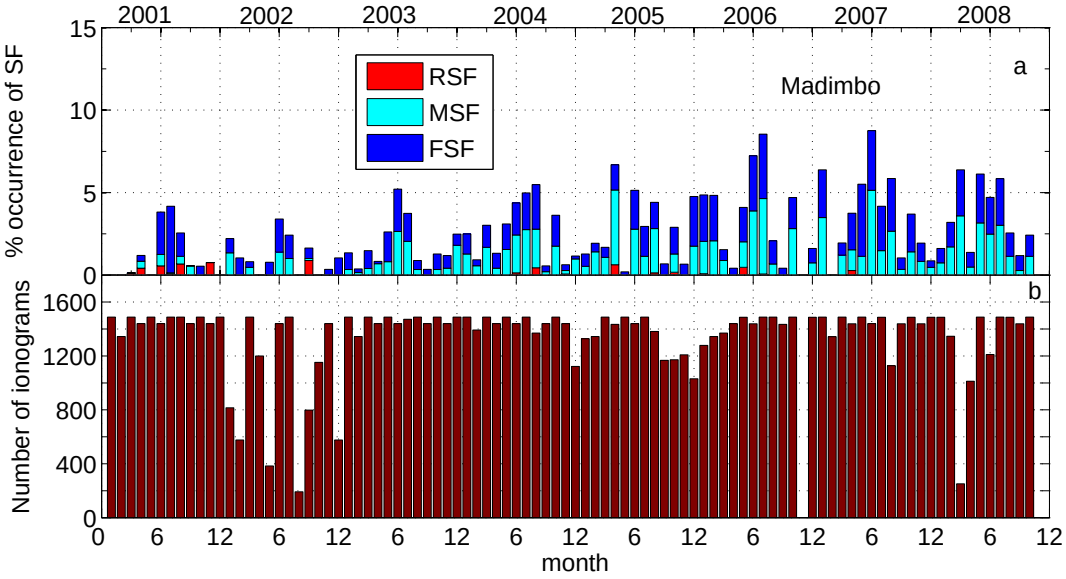

Figure 5.2: (a) Monthly probability of SF from 2001 to 2008 with sub-bars for each type of SF at Madimbo. (b) Monthly number of available ionograms. The months are numbered from 1 (for January) to 12 (for December), with years labelled above the graph.

Figure 5.2 (a) shows that RSF probability was very low for the observed period, but peaks occurred in 2002 (September ∼0.88%) and 2001 (November ∼0.76% and August ∼0.67%). MSF peaks were observed in 2007 (June 5.14%) and 2005 (April 4.53%), while the peaks for FSF occurred in 2007 (May 4.37%) and 2001 (July 4.03%). The annual peak of all types of SF occurrence at Madimbo was 4.0 % in 2001, increasing from 2002 to the maximum value of ∼8.0% in 2006 and 2007, and then decreasing in 2008. No SF events were observed during the summer of 2001 at Madimbo (Figure 5.2). Similar results for the annual probability of SF observed at Grahamstown is shown in Figure 5.3 below.

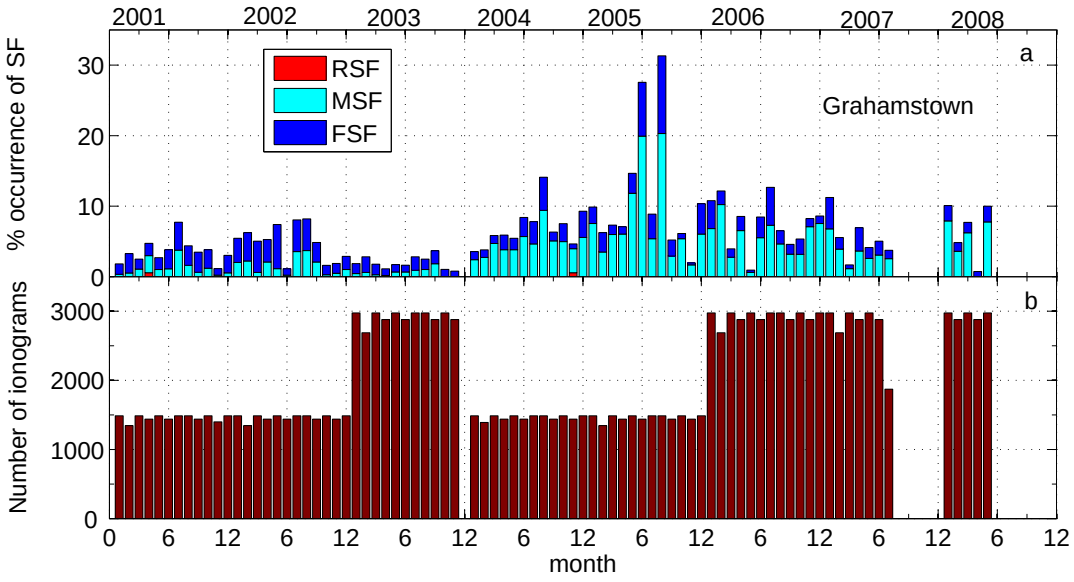

Figure 5.3: (a) Monthly probability of SF from 2001 to 2008 with sub-bars for each type of SF at Grahamstown. (b) Monthly number of available ionograms.

Figure 5.3 (a) shows that RSF at the Grahamstown station was observed only in 2001 (April 0.56% and November 0.56%). Both MSF and FSF reached their peaks in 2005 in the months of August (20.30%), and June (19.93%) respectively. The annual probability peak of all types of SF observed at Grahamstown is higher in 2005 (August 31.32%). It was observed in this study that at least MSF or FSF (or both) occurred on 80% of the nights for which there is reliable data at both stations. The absence of SF occurrence in Figure 5.3 means lack of data or unreliable data. This is evident in December 2006 at Madimbo (see Figure 5.2 (b)), and in December 2003, during August to December 2007 and during June to December in 2008 at Grahamstown (see Figure 5.3 (b)).

The important observation here is that MSF and RSF are the most dominant SF irregularities over South Africa, with much higher occurrences at Grahamstown than at Madimbo. Most of the atmospheric GWs in the ionosphere are generated in the lower atmosphere, depending on the ground conditions (Huang *et al.*, 2011). The difference in SF probability at these two stations could be attributed to the difference in the levels of atmospheric GW activities in the ionospheric F regions over the two stations. The different latitude locations of these two stations probably contribute to their differences in SF probability, since SF is latitude dependent.

Table 5.1 compares the annual probability of SF at Madimbo and Grahamstown ionosonde

stations.

Table 5.1: The probability of the three types of SF for two ionosonde stations.

MU12K					GR13L				
Year	RSF	MSF	FSF	Total	Year	RSF	MSF	FSF	Total
2001	0.22	0.18	0.75	1.15	2001	0.05	1.21	2.28	3.54
2002	0.75	0.47	0.06	1.28	2002	0.00	1.62	3.22	4.84
2003	0.00	0.83	0.99	1.82	2003	0.00	0.60	1.38	1.98
2004	0.05	1.35	1.27	2.67	2004	0.05	4.70	2.36	7.11
2005	0.08	1.45	1.25	2.78	2005	0.00	8.08	3.35	11.43
2006	0.06	1.63	1.86	3.55	2006	0.00	5.41	2.12	7.53
2007	0.02	1.61	2.01	3.64	2007	0.00	3.43	2.14	5.57
2008	0.00	1.64	1.69	3.33	2008	0.00	5.14	1.58	6.72

This table shows that RSF occurs less at Grahamstown (GR13L) than at Madimbo (MU12K), although the probability was the same for the two stations in 2004. MSF and FSF occurred more at Grahamstown than at Madimbo for all observed years. The most important feature derived from this table is that MSF and FSF are the dominant forms of ionospheric irregularity over South Africa.

Diurnal variation of SF

Ionospheric disturbances in the F region over two well-separated mid-latitude stations in South Africa were identified on ionograms by their spread echoes. Diurnal variation of mid-latitude SF over South Africa conducted by Lambert (1988) revealed a consistent minima in the probability of disturbance around sunrise and sunset. Disturbance probability was lowest during autumn and spring, while the winter level exceeded the summer level. Almost no SF was observed during the daytime in this study except the one occurrence in Figure 5.2 (a), hence diurnal variation was limited to nighttime (18:00 to 04:45 UT). The statistics for diurnal variation of SF were divided into seasons and the results for the two stations are presented in Figure 5.4.

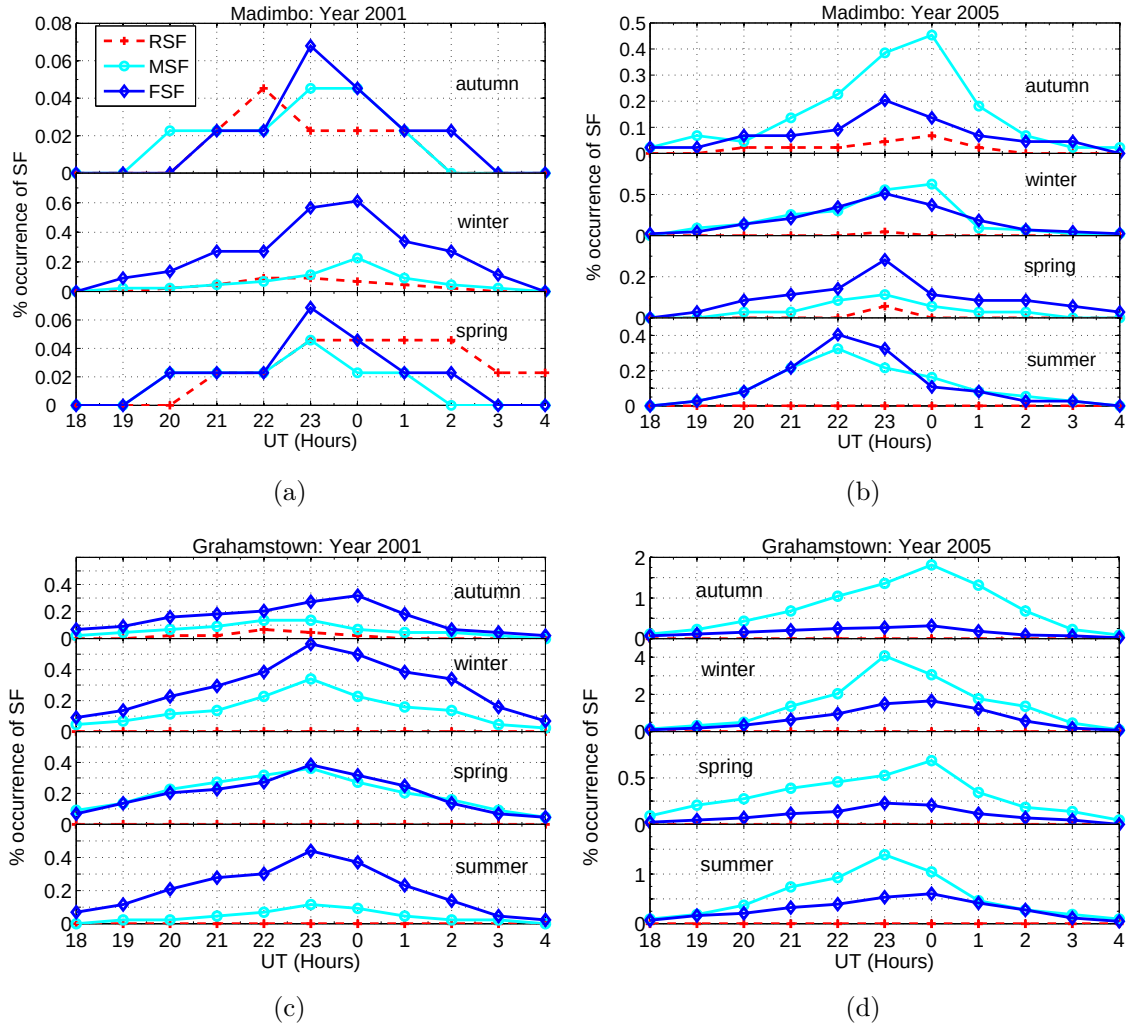

Figure 5.4: Diurnal variation of SF over Madimbo station for (a) 2001 and (b) 2005. Diurnal variation of SF over Grahamstown for (c) 2001 and (d) 2005. No SF was observed during summer 2001 at Madimbo ionosonde station.

Figure 5.4 (a) shows that there was a gradual increase in the probability of FSF during winter with a peak value at 00:00 UT and 23:00 UT during autumn and spring 2001 respectively. RSF and MSF occurrences remained low, although RSF occurrence dominated from 00:00 to 04:00 UT during spring 2001. This clearly shows that FSF and MSF are the dominant nighttime SF irregularities observed at Madimbo, except from 01:00 to 04:00 UT (spring) and at 22:00 UT (autumn) when RSF showed the highest probability in 2001. Meanwhile, FSF and MSF contributed predominantly to irregularities during summer (0.40%) and spring (0.30%), with peaks at 22:00 UT and 23:00 UT respectively in 2001 and 2005 (see Figure 5.4 (b)).

The observations at Grahamstown during 2001 imply that FSF followed by MSF dominated the irregular plasma densities responsible for the generation of SF (Figure 5.4 (c)). The probability of both FSF and MSF increased steadily to a peak value at 23:00 UT and dropped gradually towards 04:00 UT during all seasons (except in autumn when FSF peaked at 00:00 UT). The most prominent SF irregularity observed at Grahamstown during 2005 was the MSF followed by FSF (Figure 5.4 (d)). The highest probability of occurrence of these two types of SF was at 23:00 UT during winter and summer, and 00:00 UT during autumn and spring. These observations indicate that the diurnal variation of SF at Grahamstown peaks in winter. Generally, SF probability is highest between 23:00 UT and 00:00 UT for all seasons and types of SF during the two years chosen, except during autumn and spring (for RSF) in 2001 at Madimbo. Observations seem to reflect that the probability of SF is linked to the seasons as indicated in Chapter 2. Having characterised the diurnal pattern of SF, the seasonal trend of SF during the period 2001-2008 was investigated.

5.1.3 Seasonal variation of SF

In order to study seasonal variation, the SF observations were grouped as follows: autumn (March-May), winter (June-August), spring (September-November) and summer (December-February). The probability of the three types of SF were computed for each season (for Madimbo and Grahamstown) and the results are presented in Figure 5.5. As stated in Chapter 2, Lambert (1988) studied the seasonal variation of mid-latitude SF by comparing data from two Kel IPS-4A pulse ionosondes located at Johannesburg (26.07°S, 28.10°E) and Hermanus (34.42°S, 19.22°E), in South Africa. Lambert (1988) observed a seasonal maximum in winter, equinoctial minima, and a secondary maximum in summer. The statistical results also show that SF constituted 32% of the events, and disturbances producing sharply defined ionogram signatures contributed to 77% of the events, with some overlapping of types. The SF study by Huang *et al.* (2011) over Changchun (125.26°E, 43.83°N) and Urumqi (87.63°E, 43.75°N), both in China, revealed that the annual maxima of SF occurrence over the two stations are also in summer and winter. The seasonal SF pattern over South Africa according to the current study is illustrated in Figure 5.5.

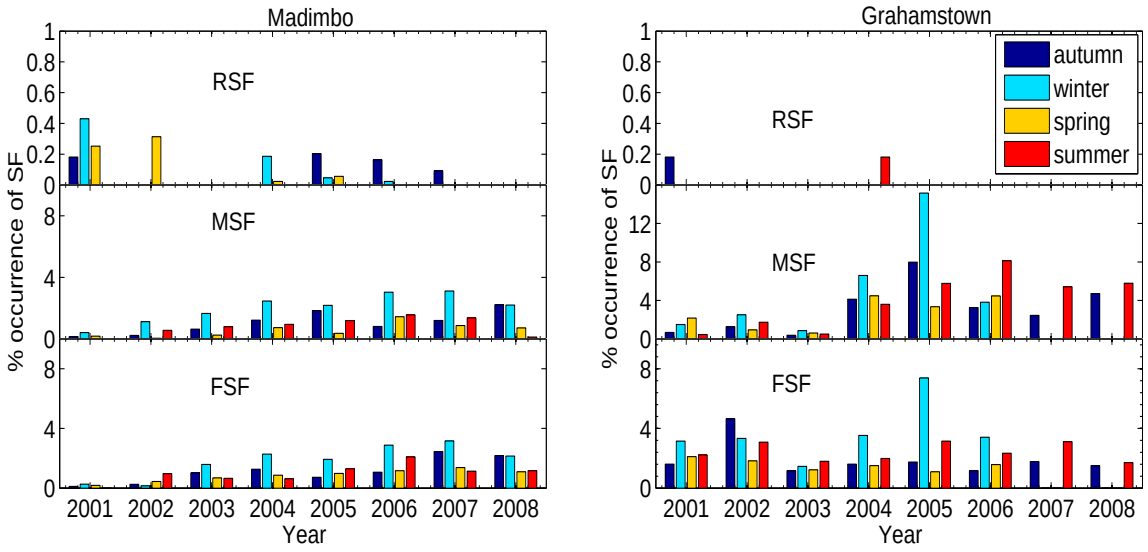

(a) (b)

Figure 5.5: The seasonal probability of the three types of SF from the peak of solar cycle 23 in 2001 to the minimum in 2008 observed at (a) Madimbo and (b) Grahamstown ionosonde stations. The scale for RSF is different because the probability of occurrence is small.

Figure 5.5 (a) shows that the seasonal peaks of RSF probability occurred during winter 2001 and spring 2002 at Madimbo. RSF was only observed during autumn 2001 and during spring 2004 at Grahamstown as shown in Figure 5.5 (b). The probability of MSF was higher at Grahamstown than at Madimbo during the observation period. The seasonal probability of MSF peaks during winter at Madimbo for all the observed years, except in 2008 when the probability decreased to the same value for both autumn and winter. The seasonal probability of this particular SF irregularity at Grahamstown had a random pattern, with the highest occurrence during winter 2005. The probability of FSF increased during winter from 2001 to 2007 and decreased in 2008 at Madimbo. The probability of FSF was still higher at Grahamstown than at Madimbo, with the highest probability during winter 2005, followed by a secondary summer peak in 2006. Therefore, MSF and FSF were the dominant seasonal SF irregularity structures observed from the two stations, with the peaks mainly during winter. These results indicating seasonal dependence of mid-latitude MSF and FSF are consistent with the results obtained by Lambert (1988) over this region. These results are also consistent with the nighttime local winter maximum occurrence of topside SF at mid-latitudes studied by Dyson (1968).

In addition to the above factors, SF occurrence is also known to be greatly influenced by solar activity. The current knowledge seems to favour the notion that the probability of SF

increases with a decrease in solar activity and vice versa. An investigation of the relationship between solar activity and SF over South Africa follows.

5.1.4 SF dependence on sunspot number

Sunspot number (SSN) as a measure of solar activity was used to investigate the correlation between solar activity and occurrence of SF. Wang *et al.* (2010) studied SF occurrence over Hainan station (geog. 19.5°N, 109.1°E, dip lat. 9.5°N) in Japan during the declining solar cycle 23 from March 2002 to February 2008. Their statistical results show that MSF and strong SF are the dominant irregularities over Hainan, with MSF occurring mainly during summer and low solar activity years. They found that strong SF is dominant during equinoxes and high solar activity years, with FSF being independent of SSN during each season. The comparison of the average monthly SSN (for the 8 years) with SF probability at Madimbo and Grahamstown ionosonde stations is presented in Figure 5.6.

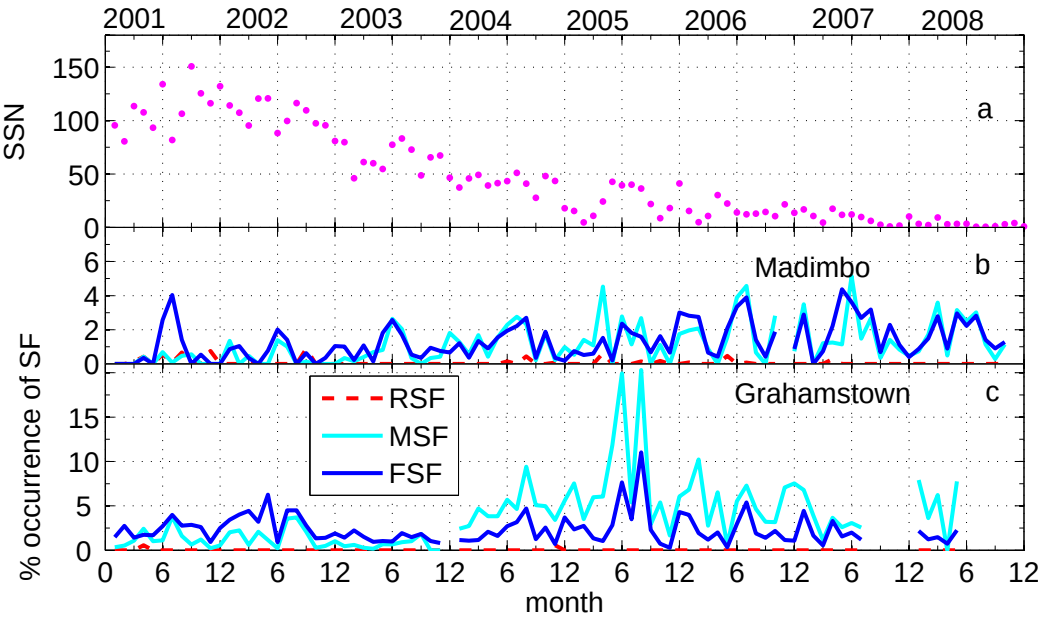

Figure 5.6: (a) The average SSN for each month of the year and the probability of the three types of SF observed at (b) Madimbo and (c) Grahamstown ionosonde stations.The months are numbered from 1 (for January) to 12 (for December).

It can be observed that the probability of both MSF and FSF showed peaks in 2005 during relatively low SSN (Figure 5.6 (b) and (c)). MSF and FSF were the dominant forms of SF irregularity observed over Madimbo and Grahamstown both during low and moderate solar activity. At Grahamstown, FSF showed higher probability up to 2004, after which, MSF

became the most dominant irregularity. The peak phase occurred in 2005, although a sharp anomalous decrease was observed in July 2005 at Grahamsown. At Madimbo FSF and MSF showed very low probability but approximately the same pattern for all the years, except 2001 when an anomalous FSF peak was observed at Madimbo. Thus higher FSF and MSF probabilities occurred during periods of low solar activity (i.e. low SSN) than high solar activity (i.e. high SSN). The results of the comparison of SF pattern with SSN for these two mid-latitude stations are consistent with the results obtained by Wang *et al.* (2010).

5.1.5 Scatter plots of SF occurrences

This section presents the results of the investigation into the correlation between the three types of SF and SSN. Correlation analysis done by Wang *et al.* (2010) showed that RSF and SSN are positively correlated during equinoxes and summer and have no relationship during winter. However, they found significant dependence of MSF on SSN during the summer and winter, but no relationship to SSN during the equinoxes. FSF was found to clearly increase with SSN during equinoxes and summer, but independent of SSN during the winter. The correlation between the three types of SF and SSN in this particular study are shown in Figures 5.7 and 5.9. The annual statistics for each type of SF for all the 8 years were combined to investigate the relationship between SSN and SF.

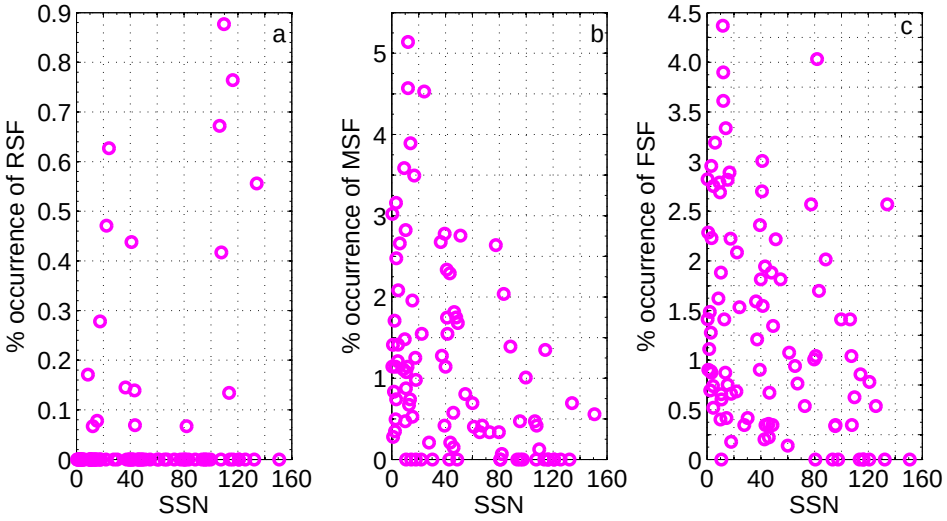

Figure 5.7: Scatter diagram for (a) RSF, (b) MSF and (c) FSF observed at Madimbo station during the period 2001-2008.

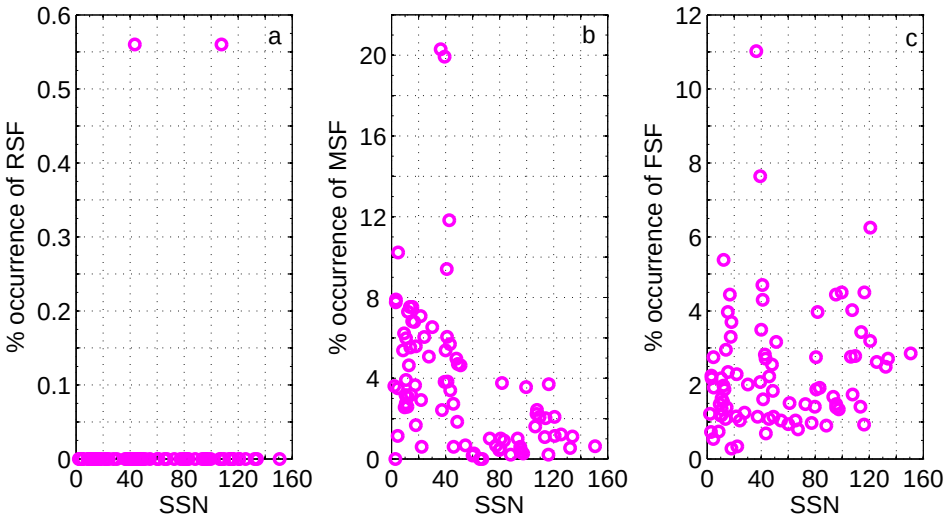

Figure 5.8: Scatter diagrams for (a) RSF, (b) MSF and (c) FSF observed at Grahamstown during the period 2001-2008.

The scatter plots in Figure 5.7 (b) and (c) show that the probability of both MSF and FSF increases with decreasing SSN, while in a few cases RSF occurrence increases with increasing SSN (see Figure 5.7 (a)). On the other hand, there was almost no (except for two cases) RSF at Grahamstown (Figure 5.8 (a)) during the period of available data, hence no conclusion about its correlation with SSN. The probability of MSF decreased with increasing SSN, although there were a few cases of outliers for SSN values ranging from 30 to 50 (Figure 5.8 (b)). Figure 5.8 (c) shows that the probability of FSF as a function of SSN is fairly random, with a few outlier cases for SSN values between 30 and 50. Therefore, this study suggests a weak negative correlation between SSN and probability of MSF at both stations. A weak positive correlation between SSN and RSF occurrence is suggested for Madimbo station only. No correlation between FSF and SSN is indicated for both Madimbo and Grahamstown stations.

After investigating the variability of SF over the South African region, this study further analysed some particular SF events to trace the origin and the nature of irregularities causing SF. The selected events fall within high (2001-2003), moderate (2004-2005) and low (2006-2008) solar activity periods. The selected SF events and an anomalous amplitude scintillation phenomenon are presented in the sections following.

5.2 SF events during high solar activity

5.2.1 11 April, 2001 SF event

The overhead observation of echoes causing the occurrence of SF may be observed from different ionospheric field stations simultaneously or independently. On this particular day SF was observed at Grahamstown, Madimbo and Louisvale (Figures 5.9, 5.11 and 5.10). This was one of the intense RSF events observed during the autumn of the solar maximum (2001). The sudden appearance and decay of the irregularity at all three stations suggests a TID related phenomenon, to be investigated in more detail.

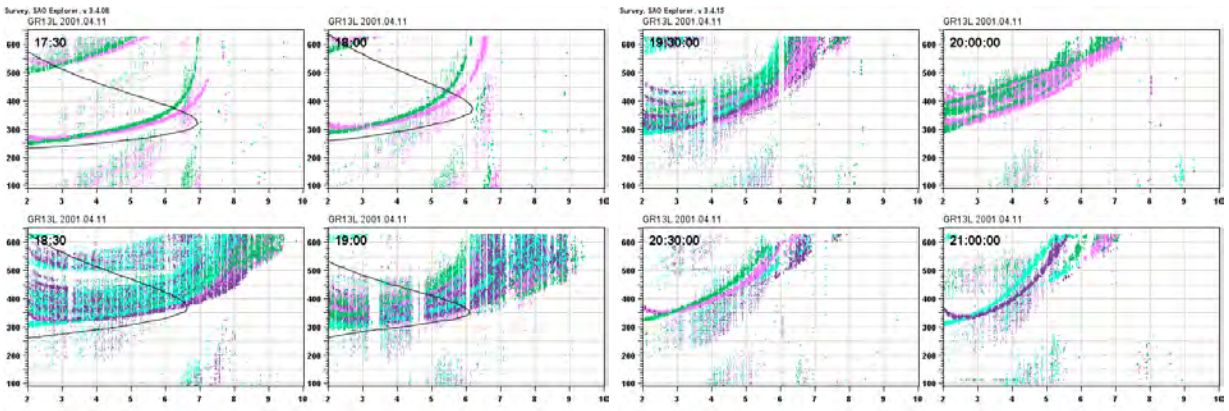

Figure 5.9: Grahamstown ionograms showing abrupt appearance of intense RSF at 18:30 UT on 11 April 2001, and gradual decrease until 21:00 UT.

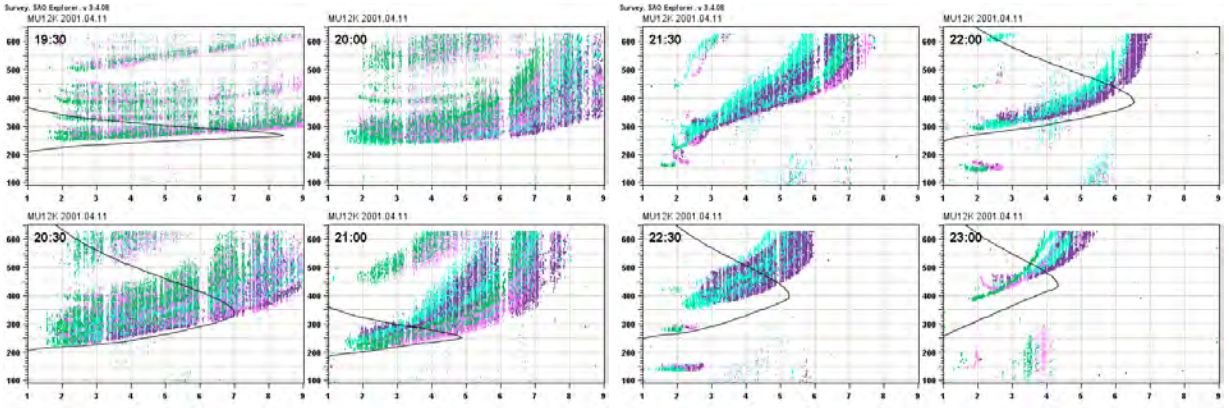

Figure 5.10: Madimbo ionograms for 11 April, 2001 showing the abrupt appearance of intense RSF at 19:30 UT and gradual disappearance towards 23:00 UT.

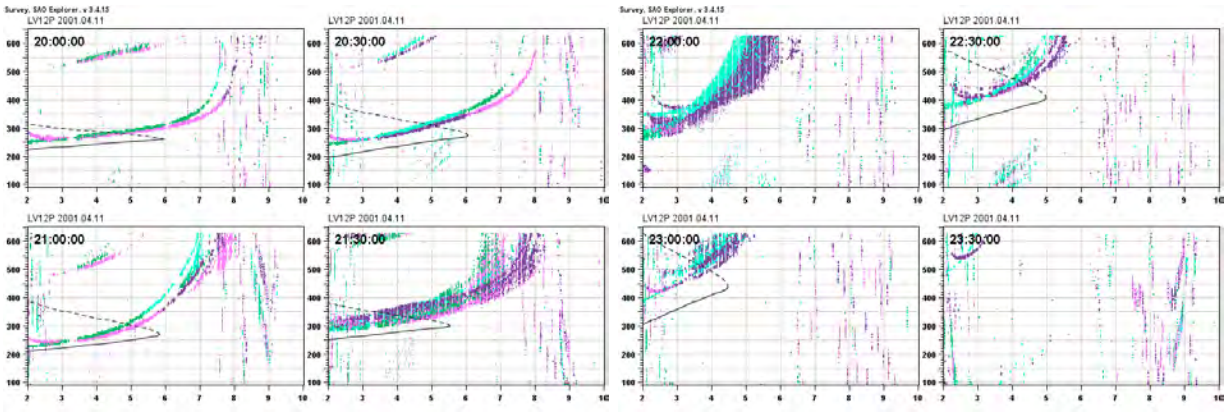

Figure 5.11: Louisvale ionograms showing abrupt appearance of RSF at 21:30 UT on 11 April, 2001 and gradual disappearance after 23:00 UT.

Figure 5.9 shows RSF observed at the Grahamstown station, which appeared suddenly with high intensity between 18:30 and 19:00 UT. A similar irregularity also appeared at Madimbo (see Figure 5.10) from 19:30 to 21:00 UT when the intensity at Grahamstown was diminishing. An irregularity structure identical to that observed at Grahamstown (at 19:30 UT) was observed at Louisvale from 21:00 to 22:00 UT on 11 April 2001 (Figure 5.11). The SF events observed at Grahamstown and Madimbo stations occurred within a frequency range of $\sim$ 1.5 and $\sim$ 9.0 MHz, while at Louisvale the event occurred within the range of $\sim$ 2.0 to $\sim$ 8.0 MHz (Figure 5.11). These events occur mostly at a virtual height within the range of $\sim$ 250 km to $\sim$ 600 km. The intensity of the RSF was strong between 18:30 and 22:30 UT and then decreased towards 00:00 UT, when the storm in Figure 5.14 shows a peak. These events are most likely attributed to plasma irregularities in the mid-latitude nighttime ionosphere as a consequence of a negative storm effect. The negative storm effect is characterised by decreased electron densities and structure changes in the ionosphere. According to Mansilla (2004), these decreases in electron density associated with changes in neutral composition, the ion convection pattern and changes in temperature are generated during geomagnetic storms at auroral latitudes. These ionospheric changes are then transported to lower latitudes by the perturbed thermospheric wind circulation produced by Joule heating and particle precipitation in the auroral region. These negative storm effects are believed to be dominated by increases in the molecular species resulting in increased recombination (Mansilla, 2004).

To understand the origin of the auroral activity, the solar particle condition was investigated by looking at the radio flux (F10.7), daily SSN (Rz), as well as electron and proton fluxes originating from the Sun. The data used was supplied by the Geostationary Oper-

ational Environmental Satellites (GOES) spacecraft (GOES-8). This spacecraft, formerly located at 75°W longitude (GOES East) was decommissioned on 05 May, 2004. Optical flares such as CMEs may be accompanied by X-ray, UV and radio bursts. The magnitude of an X-ray flare maximum is indicated by a class number with each class assigned according to the flux (E) measured by GOES. The major classes are defined as:

- C-class: $10^{-6} < \mathrm{E} < 10^{-5}$ Wm^{-2},
- M-class, with $10^{-5} < \mathrm{E} < 10^{-4}$ Wm^{-2},
- X-class: $\mathrm{E} > 10^{-4}$ Wm^{-2}.

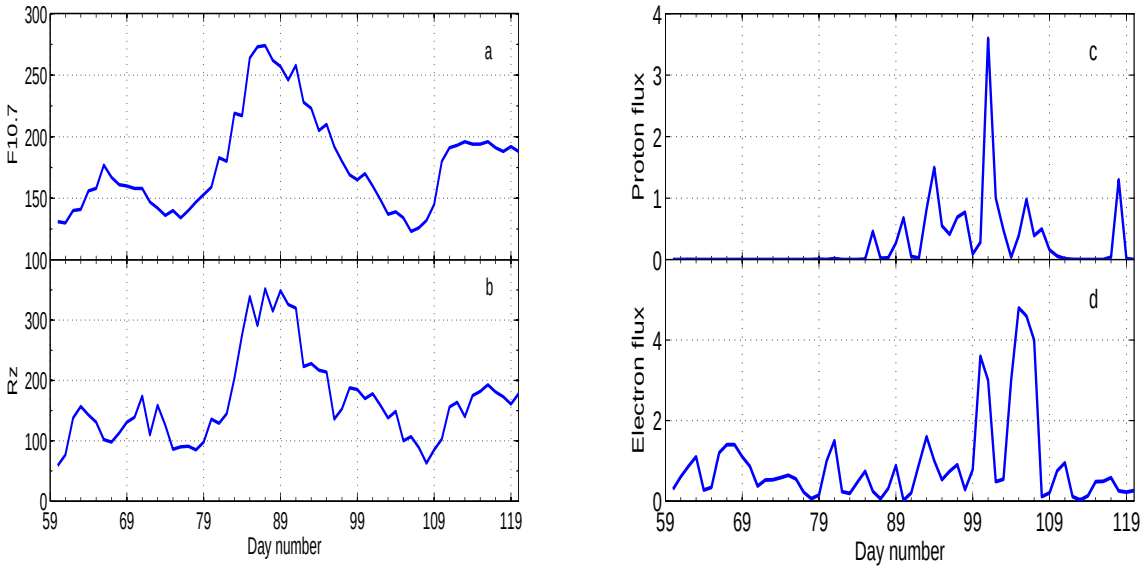

Figure 5.12: For day 59 to 119 of year 2001 (a) solar radio flux in units of $10^{-22}\mathrm{Wm}^{-2}\mathrm{Hz}^{-1}$. (b) The daily SSN. (c) The daily integrated particle fluxes (times 10^8) for protons of energy > 1.0 MeV in units of protons $\mathrm{cm}^{-2}\mathrm{day}^{-1}\mathrm{sr}^{-1}$. (d) The daily integrated electron fluxes (times 10^{10}) for electrons of energy > 0.6 MeV in units of electrons $\mathrm{cm}^{-2}\mathrm{day}^{-1}\mathrm{sr}^{-1}$. (Data source: $http://www.swpc.noaa.gov/ftpmenu/$).

The Space Weather Prediction Centre (SWPC) reported a high energy solar particle event which started on 10 April, 2001 at 08:50 UT and reached the Earth on this same day at 20:55 UT. This particular solar event is associated with the release of a halo CME on 10 April, 2001 at 05:30 UT caused by X2 flare activity on the same day at 05:26 UT ($http://www.swpc.noaa.gov/ftpdir/warehouse/$). Figure 5.12 shows that the radio flux and SSN were around their peak from day number 88 (29 March, 2001) to 99 (09 April, 2001), which is slightly earlier than this particular solar event. This event was followed by

low solar energetic particle fluxes at higher latitudes, probably due to precipitation of these particles at low latitudes, thus creating a deficiency of these particles. Most CMEs of the above-mentioned class result in geomagnetic storms once they hit the Earth.

To follow up on the effect of this solar event, the geomagnetic status and solar wind conditions were examined for this period using selected parameters. The variability of these parameters is presented in Figure 5.13.

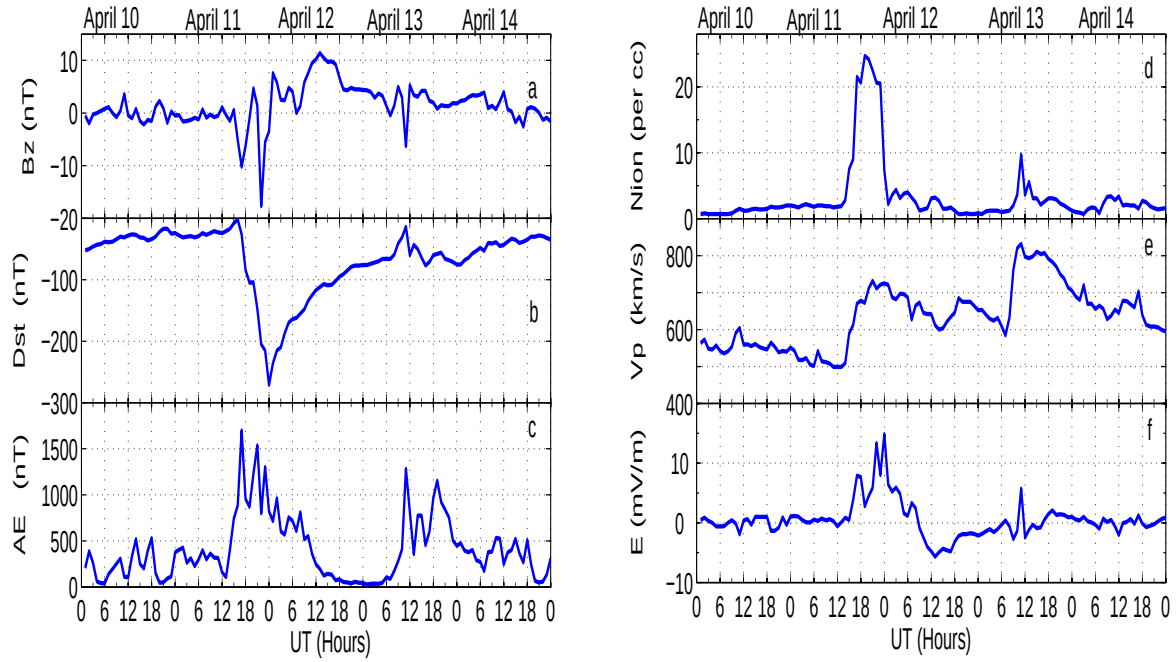

Figure 5.13: (a) Variability of IMF component (Bz). (b) Hourly Dst index for the storm period. (c) Hourly AE index as a measure of auroral activity. (d) Ion number density (Nion). (e) Plasma flow speed with a peak value of $>$ 800 km/s. (f) Electric field with sharp gradients on 11 April, 2001. (Data source: ACE website *http* : *//cdaweb.gsfc.nasa.gov/cdaweb/sp_phys/*).

High speed solar wind streams are believed to emanate from coronal holes on the Sun's corona and propagate into the solar wind and are associated with solar flares. CMEs directed towards the Earth reach the Earth as an interplanetary CME (ICME) (Tsurutani *et al.*, 2006). The shock wave of the travelling mass of solar energetic particles causes a geomagnetic storm that may disrupt the Earth's magnetosphere. This leads to compression of the Earth's magnetosphere on the dayside and extension of the nightside magnetic tail. Figure 5.13 (a), shows that three distinct solar wind shocks with southward magnetic field components (Bz) were observed by the ACE satellite from 11-13 April, 2001. The first, second and third shock waves arrived at $\sim$ 17:30 UT, $\sim$ 23:00 UT (both on 11 April, 2001), and

$\sim$ 11:00 UT on 13 April, 2001 respectively. The first shock wave marked the sudden storm commencement (SSC), while the second shock wave (strongest) initiated the main phase of the super-storm with a peak at 00:00 UT (minimum Dst $\sim$ -270 nT). The third shock wave initiated a sub-storm activity with a positive phase. Tsurutani *et al.* (2006) states that the main phases of magnetic storms are mainly caused by an injection of energetic particles into the magnetosphere by large scale intense magnetospheric dawn-to-dusk electric fields. The auroral electrojet (AE) index shows a prompt increase at the onset of interplanetary shocks. Figure 5.13 also shows clearly that from 12:00 UT (on 11 April, 2001) to 12:00 UT (on 12 April, 2001) and 08:00 to 00:00 UT (on 13 April, 2001) there are rapid fluctuations of auroral activity and solar wind dawn-to-dusk electric fields. During the period of higher auroral activity (12:00 to 00:00 UT) on 11 April, 2001, the ion number density increased by about 20 particles/cm^3, consistent with an increase in solar wind speed from about 500 km/s to $>$ 800 km/s.

Such sudden changes in solar wind speed and ionisation rates are mostly associated with the magnetic reconnection processes, which release enormous amounts of energy locked in the magnetotail into interplanetary space. During a strong geomagnetic storm, intense interplanetary convection electric fields lead to an energy influx into the magnetosphere-ionosphere system. This causes particles to be ejected from the tail into the ring current which in turn increases the total energy of the westward ring current around the Earth, thus prompting plasma density variations responsible for changes in the ionosphere (Davies, 1990; Mendillo, 2006). Perturbations of ionospheric density which occur at F region heights are associated with geomagnetic storms and vary with location, season, local time, solar activity and altitude. There was increased ion number density and rapid electric field fluctuation between $\sim$ 16:30 UT and $\sim$ 04:30 UT and between $\sim$ 06:00 UT and $\sim$ 12:00 UT on 11 and 13 April, 2001 respectively. This can be observed in Figures 5.13 (d) and (f) respectively. The increased ionisation reflected by the high ion number density is mostly likely due to an approaching CME, such that after the passage of the CME, the density decreases again.

Several research groups have attributed mid-latitude SF to locally generated instabilities within the bottomside of the F region (Earle *et al.*, 2010). The F region electric field drifts are believed to be caused by differences in the ionisation (Kelley *et al.*, 1979; Kumar *et al.*, 2008). Fejer (2003) studied low latitude ionospheric electric fields and currents by using incoherent scatter radar measurements from Arecibo (18°N, 67°W, dip latitude 30°N) and Jicamarca (11.9°S, 76.8°W, dip latitude 1°N). This author found that F2 region parameters (e.g. hmF2 and h'F) are often strongly disturbed during periods of enhanced geomagnetic

activity. The results show that the perturbations are consistent with the occurrence of strong prompt penetration electric fields reaching the magnetic equator, and can last for several hours after geomagnetic quieting. It is therefore necessary to understand this phenomenon in order to trace the mechanisms responsible for SF over the South African region. To investigate the ionosphere's response to the 11-13 April, 2001 storm, data which characterises the ionosphere, such as hmF2 and h'F was used. Data for SF events from Madimbo, Grahamstown and Louisvale was compared as shown in Figure 5.14.

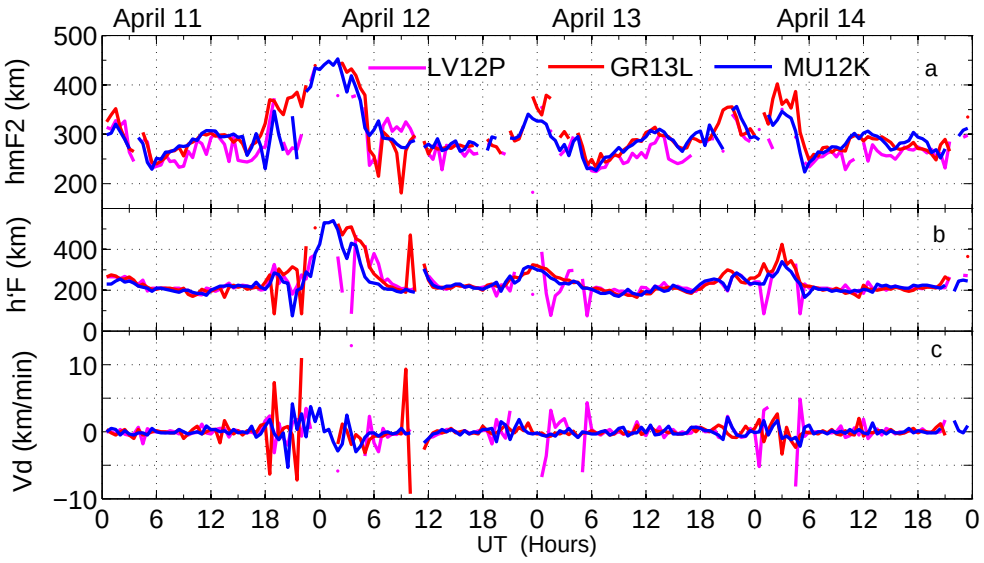

Figure 5.14: (a) hmF2 data for 11-14 April, 2001 from the three ionosonde stations. (b) F2 layer bottom height h'F variability. (c) The time derivative of the F2 layer bottom height (h'F). (Data source: SPIDR website *http* : *//spidr.ngdc.noaa.gov/spidr/*).

.

A geomagnetic storm is a phenomenon of solar wind or magnetospheric origin during which the ionospheric F2 layer becomes unstable, fragments, and may even disappear completely. The growth of ionospheric irregularities increases substantially during geomagnetic storms initiated by solar disturbances (Belehaki and Tsagouri, 2002; Hunsucker and Hargreaves, 2003; Buresova, 2005). Various features of a geomagnetic storm act at different heights of the ionosphere and neutral atmosphere. In the mid-latitude F2 region, the ionospheric response is attributed to the storm-induced changes in the neutral atmosphere, which are primarily a consequence of strong Joule heating in the auroral thermosphere (Fuller-Rowell *et al.*, 1994; Danilov and Lastovicka, 2001). A negative F region storm effect is related to atmospheric circulation that changes the composition of the neutral atmosphere, which in turn increases the effective electron loss rate (Mikhailov and Schlegel, 1998; Belehaki and Tsagouri, 2001; Kelley, 2009). The heating takes place below the F layer, implying that

the bottomside F2 layer is depleted, thus increasing the F2 layer height and consequently decreasing the electron densities. This can be observed in the increased hmF2 or h'F values (with high variability) at nighttime (18:00 to 06:00 UT) in Figure 5.14. The pre-midnight and post-midnight values of h'F are higher than the normal hmF2 (i.e. ∼400 km), which depict a nighttime enhancement of h'F. This effect is similar to that caused by GWs, where the F2 layer height may be increased by GWs generated by R-T instability. The peak values of hmF2 ($\geq$ 420 km) and h'F ($\geq$ 450 km) from $\sim$ 18:00 UT (on 11 April, 2001) to 06:00 UT (on 12 April, 2001) coincide with the main and recovery phases of the super-storm. The hmF2 and h'F values before and after the storm are very low compared to those during the geomagnetic storm, which implies an enhancement in the F2 layer density. This particular enhancement could be associated with the irregularity responsible for the increased SF events observed at Madimbo, Grahamstown and Louisvale on 11 April, 2001. The peak value of hmF2 and minimum of h'F between $\sim$ 18:00 UT (on 11 April, 2001) and $\sim$ 06:00 UT (on 12 April, 2001) shows a delayed response of the ionosphere over Grahamstown compared to Madimbo. The shift between the peaks may be attributed to TIDs moving from higher to lower latitudes, driven by GWs.

It is well-known that ionospheric irregularities can be observed at both HF and L-bands using several instruments. Ionospheric delay depends on the frequency, which makes TEC estimates from the carrier phases and P-code group delays of dual frequency GPS signals possible. However, the accuracy of ionospheric measurements generally depends on the determination of the inter-frequency bias between L1 and L2 signals for both the receiver and the satellite. These two biases are major factors with respect to the difficulties in the determination of absolute TEC values from GPS observations (Yamamoto *et al.*, 2000). Figure 5.14 (c) also shows the turbulent nature of the ionosphere, for example from 18:00 to 12:00UT (11-12 April, 2001). The maximum drift speed (Vd) of the F region ionosphere estimated for this interval is $\sim$ 83 m/s, which is slow. This probably implies that the ionosphere over South Africa did not experience serious oscillatory motions during this storm period.

To follow up on the response of the South African ionosphere to the 11-13 April, 2001 storm at L-band, the derived $VTEC$ for each of the available stations was investigated. The first step was to compare the mean $VTEC$ for the quiet days with the $VTEC$ for disturbed days as shown in Figure 5.15.

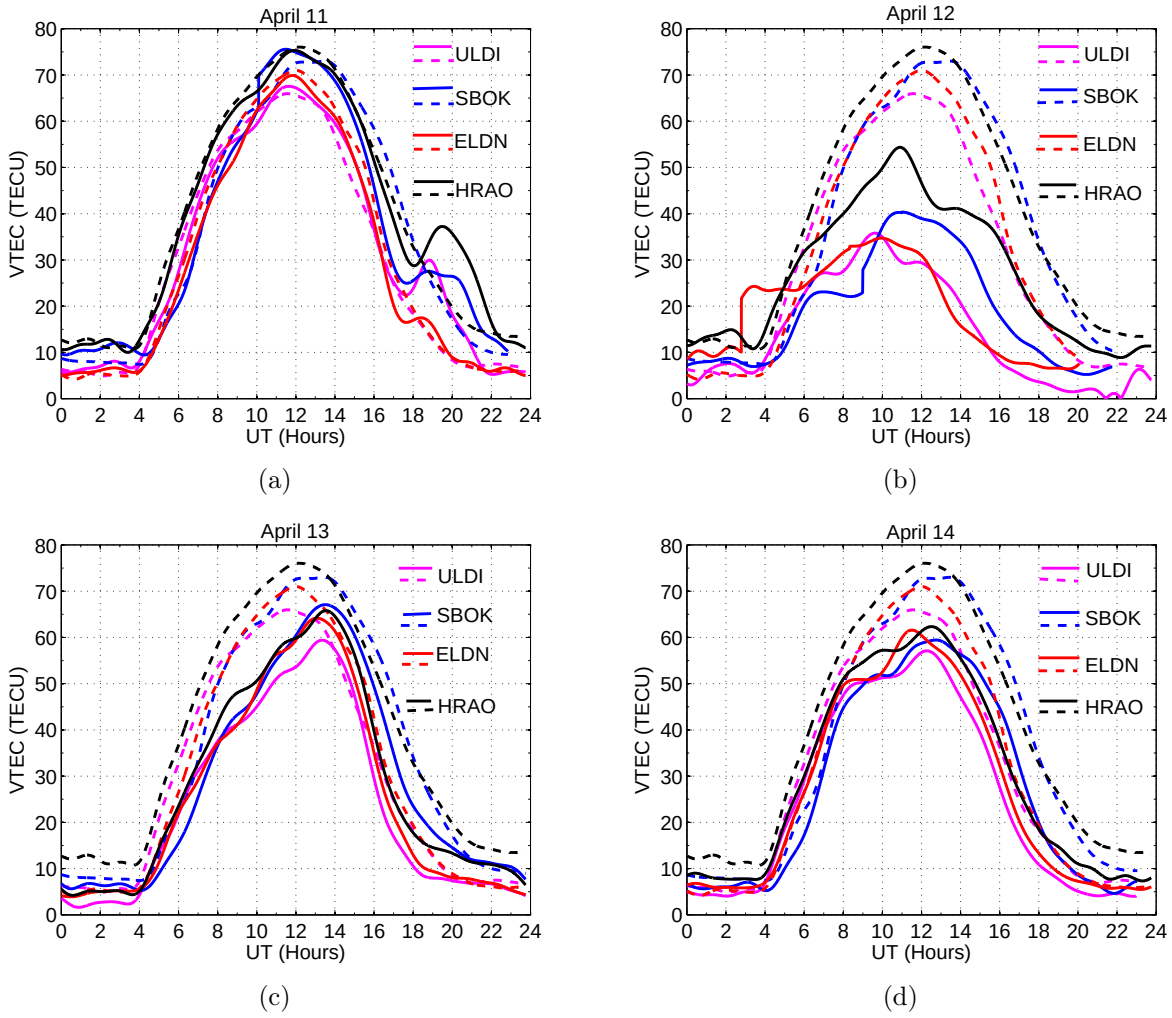

Figure 5.15: Variability of the $VTEC$ (solid lines) and the mean $VTEC$ (dashed lines) for the four stations.

The 11-13 April, 2001 storm event affected the ionosphere over South Africa in such a way that the TEC variation shows both negative and positive value phases during pre- and post-midnight hours. The mean $VTEC$ shows a smooth quiet day variation for all the stations. Figure 5.15 (a) shows that TEC depletion occurred from $\sim$ 17:00 to $\sim$ 18:00 UT, followed by TEC enhancement. The magnitudes of the TEC depletion and enhancement vary from one station to another, with higher values at HartRAO (HRAO) and Ulundi (ULDI), and the lowest at East London (ELDN). The negative storm effect on the South African ionosphere can be observed in Figure 5.15 (b), where the TEC values are lower than the mean values. The departure of the disturbed day $VTEC$ from the quiet day values on 12 April, 2001 has a magnitude of $\geq$ 20 TECU at all the stations. For observations at mid-latitudes the sub-storm effects tend to show a time delay, observable through the shifted peaks in Figures 5.14 (a) and 5.15 (a). The ionosphere went through a recovery phase but slightly lower TEC values

were registered on 14 April, 2001 (Figure 5.15 (d)). Foster and Rideout (1997) state, in a similar study, that during the initial hours of a geomagnetic disturbance, a positive phase enhancement of ionospheric density and TEC often occurs at mid- and low latitudes. The TEC changes in Figure 5.15 were characterised by smooth nighttime increases spanning a few minutes after the depletion. The effect of a geomagnetic storm on the derived GPS TEC at low latitudes at Varanasi (Geomagnetic lat 14.92° N, geomagnetic long 154° E) during the period May 2007 to April 2008 was investigated by Kumar and Singh (1982). This study found that TEC increased during the main phase of the storm during March 2008, while in the case of the November 2007 storm, TEC decreased during the main phase of the storm, but increased during the recovery phase of the storm.

Mendillo (2006) states that mid-latitude TEC enhancement serves as a source of populating the plumes of storm-enhanced density that are eroded by disturbance electric fields in the plasmasphere boundary layer. Storm- enhanced density occurs when low latitude cold plasma is transported sunward (towards noon) at the inner edge of the convection electric field. Two types of disturbance electric fields (i.e. prompt penetration zonal and disturbance dynamo electric fields) were identified by Kumar and Singh (1982) at the low latitudes. The prompt penetration electric fields are produced both during the southward turning of the IMF(Bz) and during the terminating phase of a storm when IMF(Bz) turns northward. Disturbance dynamo electric fields are produced due to increases in radiation and consequent Joule heating of the high latitude plasma (Blanc and Richmond, 1980). Kumar and Singh (1982) add that this additional heating may launch equatorward winds, which in turn generate disturbance dynamo fields.

The nature of the TEC variability in Figure 5.15 led to the investigation of the perturbations during the storm event. The perturbations in the mid-latitude ionosphere can also be observed on $VTEC$. The TEC perturbations associated with the strong geomagnetic storm of 11-13 April, 2001 have been studied. The method for derivation of the $VTEC$ perturbation is described in Chapter 4 and the results during 11-13 April, 2001 period are shown in Figure 5.16.

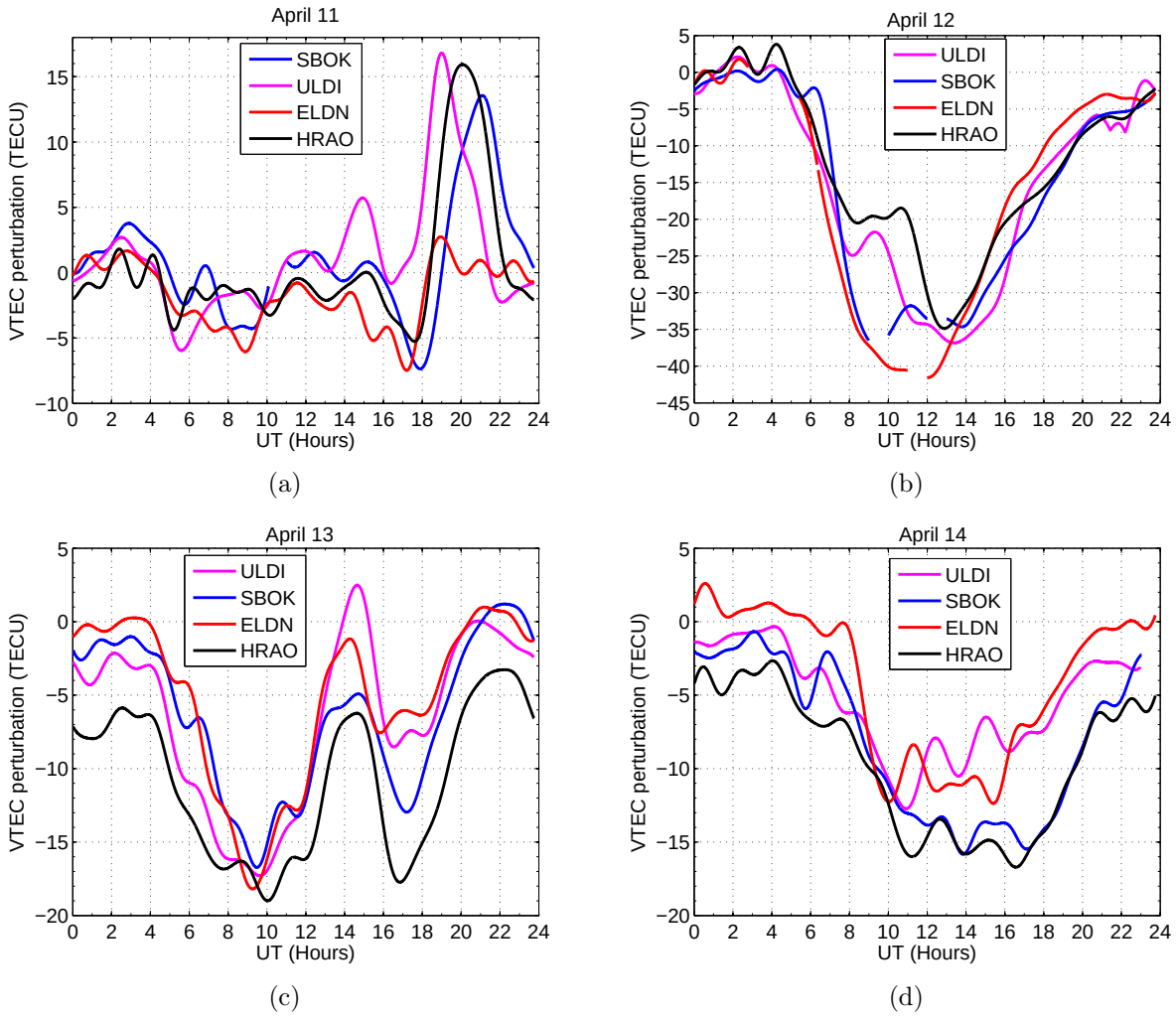

Figure 5.16: Derived $VTEC$ perturbation for the selected GPS stations during SF period.

The perturbations in the $VTEC$ for Ulundi (ULDI), Springbok (SBOK), East London (ELDN) and HartRAO (HRAO) indicate that the ionosphere was very unstable. The instability is caused by the variability in the nature of the irregularities affecting the GPS signals. The maxima and minima between adjacent stations are shifted, with the greatest amplitude enhancement between $\sim$ 19:00 and 22:00 UT (Figure 5.16 (a)). There is TEC depletion from $\sim$ 15:00 to 18:00 UT, after which TEC increased. This is typical behaviour for the main phase of the storm (Figure 5.13). A perturbation trough probably due to TEC depletion (i.e. negative storm effect) in the ionosphere is evident in Figures 5.16 (b) and (c) from $\sim$ 06:00-19:00 UT and $\sim$ 04:00-13:00 UT (also 15:00-19:00 UT) respectively. This may have hindered measurements of hmF2 and h'F at Louisvale and Grahamstown during this period (Figure 5.14). The perturbations in the $VTEC$ observed in Figure 5.16 (c) reveal two minima, between 08:00 and 11:00 UT and 16:00 and 19:00 UT. The ionosphere continued

to recover from the negative storm effect with variability in the perturbation until 14 April, 2001 (Figure 5.16 (d)).

The relationship between GPS TEC perturbation components and geomagnetic field variations was investigated by Yamamoto *et al.* (2000) at Chofu (35.65°N, 139.54°E), Tokyo. Their study revealed an increase in the amplitude of the TEC variation during the first 24 hours of a storm and then a decrease to below its normal diurnal value during the recovery for one or two days. Yamamoto *et al.* (2000) also found that during a negative phase of the TEC variation, the perturbation amplitude of TEC is much lower in summer than in winter.

There is a characteristic time delay observed at the different latitudes during the nighttime enhancement on 11 April, 2001 (Figures 5.16). This can be observed by particularly considering the stations East London and HartRAO, which are approximately on the same longitude so that we separate latitude variations from time variation in the TEC. This is a typical feature of travelling atmospheric disturbances (TADs) which manifest in the ionosphere as TIDs. The TADs are generated by auroral sub-storm activity which causes enhanced thermospheric pressure gradients, that launch GWs responsible for large scale ionospheric disturbances propagating from high to mid-latitudes (Prölss, 1993; Pi *et al.*, 1993; Mikhailov *et al.*, 1995; Ho *et al.*, 1998). The equatorward propagating waves (Kelley, 2009) can cause an uplifting of the F2 layer by pushing the ionospheric plasma along magnetic field lines to higher altitudes where recombination is much lower, which in turn leads to plasma density enhancement (Prölss, 1993; Ho *et al.*, 1998; Jakowski *et al.*, 1999).

5.2.2 15-16 November, 2001 SF event

A mid-latitude SF study was carried out by Soicher *et al.* (1997) using data from a European vertical sounding station in Spain (40.6°N, 0.6°E) for geomagnetically active and quiet periods. These authors observed SF during disturbed periods, most frequently at dawn. The SF event on 15-16 November, 2001 is an example of intense MSF during a minor storm and high solar activity. The irregularity responsible for such a SF occurrence appeared suddenly and strongly at 23:00 UT (on 15 November, 2001) and then decreased in intensity until 04:00 UT (on 16 November, 2001).

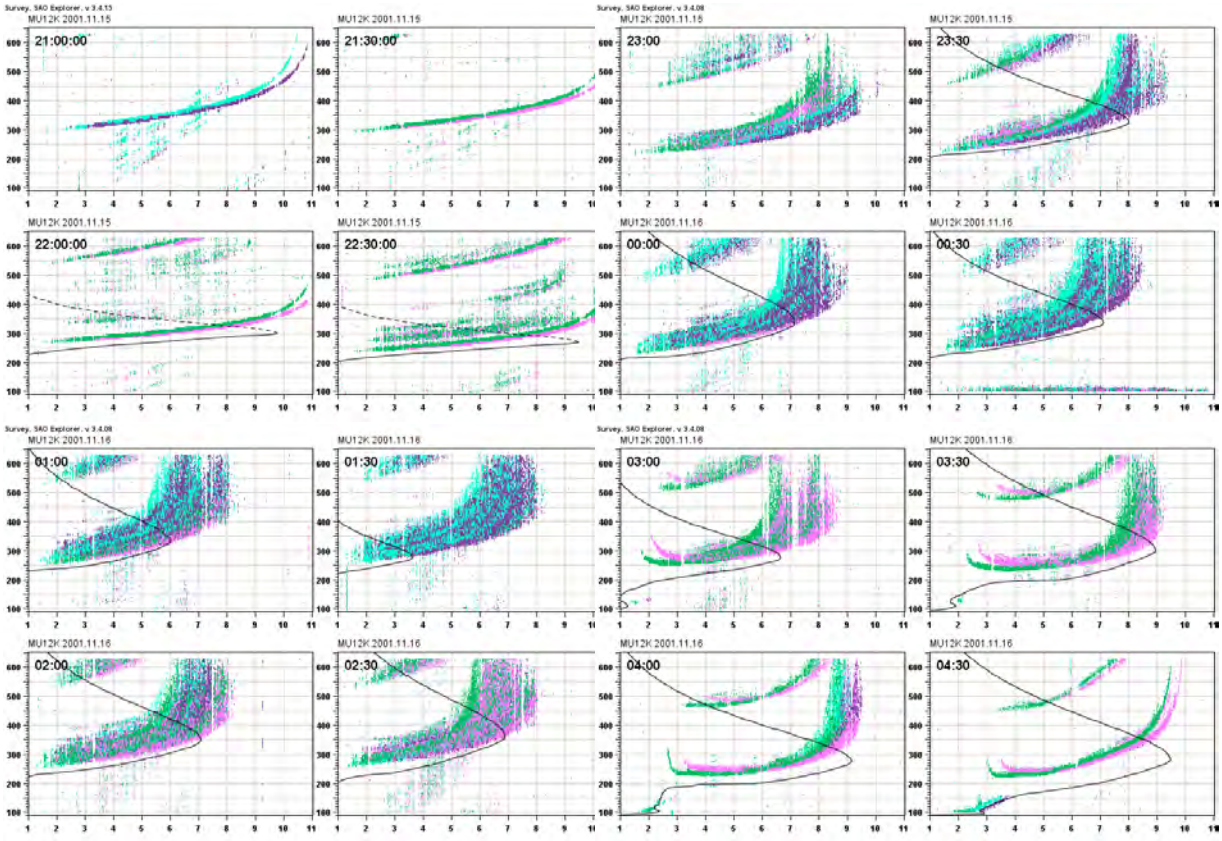

Figure 5.17: Madimbo ionograms showing the nighttime occurrence of intense MSF for the period 15-16 November, 2001.

In Figure 5.17 the onset of the MSF event follows the arrival of strong shock waves at $\sim$ 18:00 UT, as observed by the ACE spacecraft on 15 November, 2001. This could have been a consequence of the southward turning of Bz (Figure 5.18). The response of the ionosphere to the changes induced by the sub-storm may have led to the long-lasting intense MSF event observed at Madimbo. An investigation into the geomagnetic and solar wind conditions during this SF event follows.

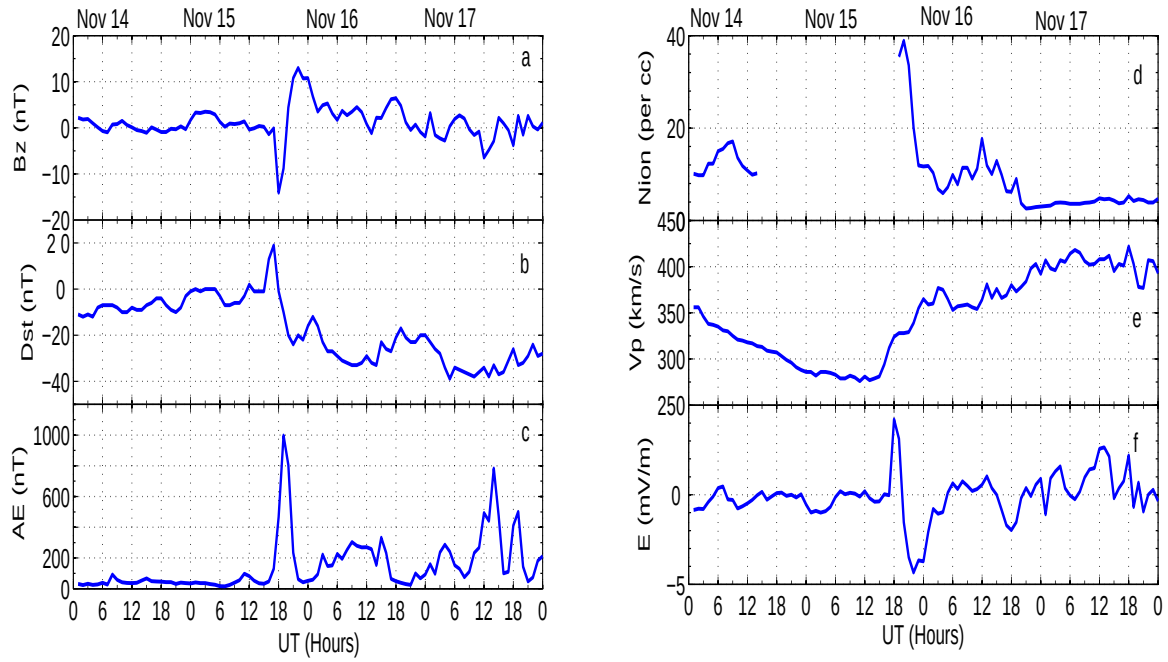

Figure 5.18: Variation of (a) IMF (Bz), (b) hourly Dst index, (c) hourly AE index for 15-16 November, 2001. (d) Fluctuating ion number density (Nion). (e) Variability of solar wind speed. (f) Electric field variability during increasing ionisation. (Data source: ACE website).

The frequency range $\sim$ 1.5 to $\sim$ 9.0 MHz of the SF occurrences in Figure 5.17 are consistent with the SF events on 11 April, 2001. No SF events were observed at Grahamstown and Louisvale ionosonde stations during 15-16 November, 2001. There was a sub-storm with a positive phase of maximum Dst $\sim$ + 20 nT and a negative phase of minimum Dst $\sim$ -40 nT. The positive phase was initiated by the southward turning of Bz slightly before 18:00 UT on 15 November, 2001. The southward Bz led to an increased intensity of the eastward auroral current (i.e. increased auroral activity), probably as a result of the injection of energetic particles which eventually penetrate the low latitudes through the field lines. During the positive phase the geomagnetic field is compressed on the dayside by the solar wind, causing an enhanced magnetopause current (hence Dst $>$ 0). A Dst change of $\sim$ 60 nT between the two storm phases is sufficient to influence particle influx into interplanetary space.

There was increased ionisation rate at $\sim$ 18:00 UT as shown in Figure 5.18 (d). This may have been caused by the ionospheric response to the interplanetary shocks or pressure pulses which lead to a sudden injection of energetic particles into the inner magnetosphere. The interplanetary shocks led to changes in the magnetic and electric fields which accelerated the injection of energetic particles into the inner magnetosphere. It is a well established fact that a highly fluctuating solar wind speed and southward IMF (Bz) during magnetic sub-

storms generate electric forces, which in turn increase the number of particles penetrating the inner magnetosphere. The disruption of the Earth's magnetic field by the solar wind causes changes in the F2 region ionospheric ionisation and recombination rates.

The ionospheric response to the above minor storm (with a few sub-storm activities) was also investigated using Madimbo and Grahamstown ionosonde data. The time derivative of h'F for these two stations was also investigated. Figure 5.19 illustrates the variability of these three parameters.

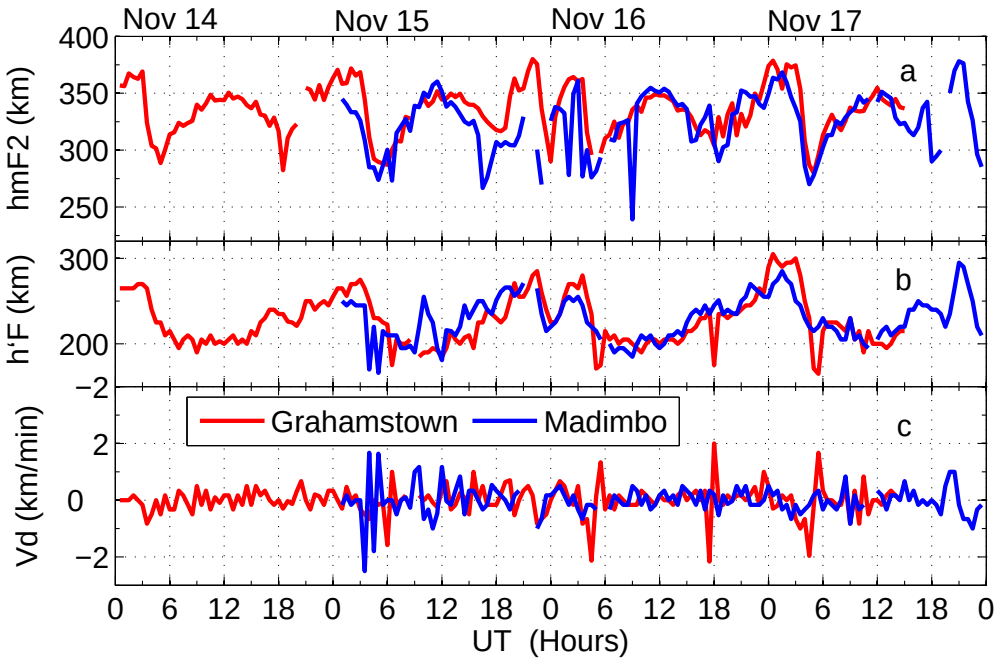

Figure 5.19: Variability of (a) hmF2 and (b) h'F from 14-17 November, 2001 recorded at Madimbo and Grahamstown ionosonde stations. (c) The time derivative of F2 layer bottom height (Vd). (Data source: SPIDR website).

Figure 5.19 shows that the occurrence of intense SF irregularities can obstruct the effective measurement of ionospheric characteristics such as hmF2 and h'F. The nighttime values of hmF2 and h'F are slightly higher at Grahamstown than at Madimbo. Mid-latitude, being an intermediate region between equatorial and high latitudes, can be affected by changes in these two regions. Wang *et al.* (2008) carried out an analysis of the seasonal dependence of SF over Hainan Observatory in China. These authors suggested that equatorial topside plasma bubble irregularities are the origin of the strong MSF they observed at low latitudes. SF events as illustrated in Figure 5.17 also imply that the irregularities responsible for the development of MSF events vary in intensity over time. These irregularity structures

build up and remained strong in intensity between 23:00 UT and 02:30 UT. The intensity decreased and disappeared gradually towards 04:00 UT, which is common for SF at mid-latitudes. SF with decaying intensity may also be attributed to composition changes in the neutral wind density. The difference between the hmF2 and h'F parameters at Madimbo and Grahamstown may be attributed to the difference in composition of the neutral wind over these two stations. This is because neutral winds depend on ion drag which is influenced by the local geomagnetic configuration (Huang *et al.*, 2011). The highest drift speed of the F2 layer computed for Figure 5.19 (c) using the procedure described in Chapter 4 is $\sim$ 35 m/s, which is relatively slow.

Further investigation into the mechanism(s) responsible for this particular SF event was undertaken using dual frequency GPS data. The technique of derived $VTEC$ perturbation was applied to the data from Springbok (SBOK), HartRAO (HRAO), Bloemfontein (BFTN) and Pretoria (PRET). Figure 5.20 shows the results.

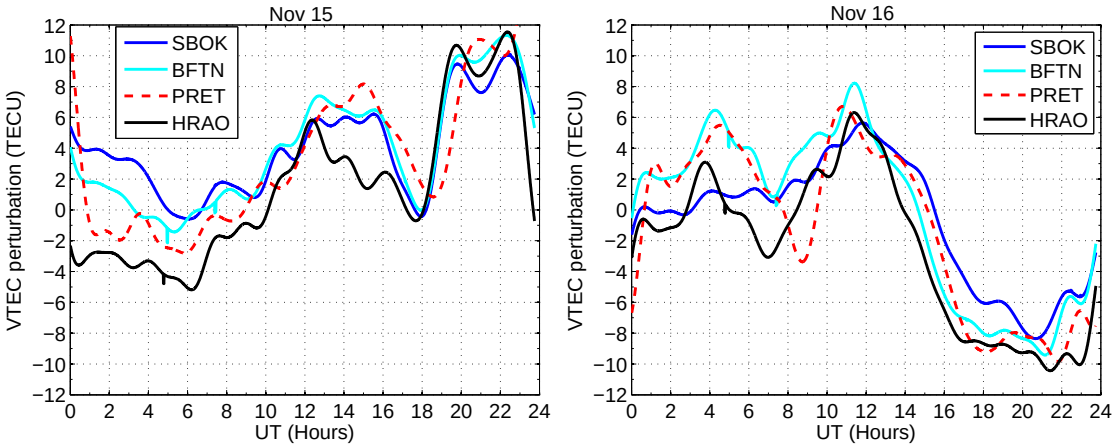

Figure 5.20: Derived $VTEC$ perturbation for the stations with reliable data during the 15-16 November, 2001 SF event.

The variability pattern of the $VTEC$ perturbation on the two days when SF was observed at Madimbo (Figure 5.17) is similar to the pattern of hmF2 and h'F (Figure 5.18). The most distinguishing features of the ionospheric disturbance are the maxima and minima of the $VTEC$ perturbation over the four stations (Figure 5.20). This can be observed from $\sim$ 16:00 to 19:00 UT (on 15 November, 2001) and $\sim$ 06:00 to 10:00 UT (on 16 November, 2001). The nighttime enhancement of the $VTEC$ perturbation is evident in the sudden increase in the perturbed $VTEC$ between $\sim$ 18:00 and $\sim$23:00 UT (on 15 November, 2001). This particular observation is consistent with the northward polarity change of the IMF(Bz)

in Figure 5.18 (a), accompanied by increased auroral activity and rapid variability in the penetrating electric fields.

According to Altadill *et al.* (2004), the atmospheric GWs, which are mainly driven by Joule heating produced by electric currents, energetic particle precipitation and mechanical forces in the auroral ionosphere, can generate disturbances in the ionosphere. The sources of atmospheric GW disturbances in the lower and middle atmosphere are attributed to regions of turbulence and wind shear. A variety of studies such as those by Somsikov (1995) and Galushiko *et al.* (1998) reveal the moving solar terminator as a source of such disturbances. Therefore, the sudden nighttime enhancement observed on 15 November, 2001 may be attributed to the moving solar terminator, as explained in Chapter 3. It is now well-known that the auroral electrojet enhancement, as observed in Figure 5.18 (c), is one of the main causes of TIDs. The AE index characterises the auroral activities and provides a measure of the Joule heating in auroral source regions which is related to the generation of GWs and hence TIDs.

5.3 SF events during moderate solar activity

This section discusses one of the SF events observed during a period of moderate solar activity. It was previously mentioned that both MSF and FSF probabilities at Grahamstown were highest in 2005. The discussion of an investigation into the cause(s) of the high SF occurrence during this moderate solar activity period at Grahamstown then follows.

5.3.1 18-20 February, 2005 SF event

The SF event from 18-20 February, 2005 is one of the long-lasting FSF events observed at Grahamstown during a summer period. There was no SF observed at Madimbo and Louisvale for this particular period.

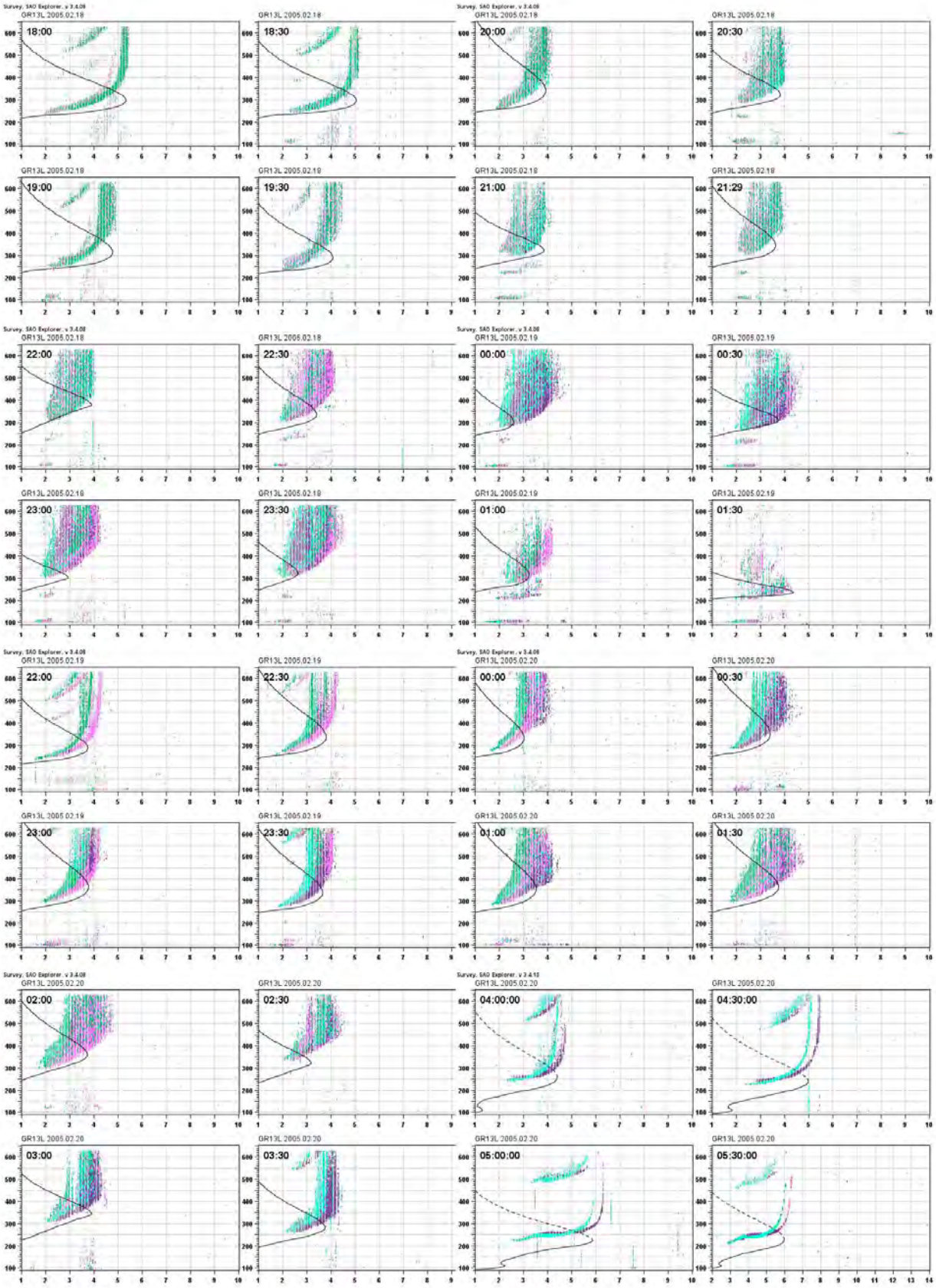

Figure 5.21: Growth and decay of FSF observed at Grahamstown station from 18-20 February, 2005.

The irregular structure that caused this SF started building up at 18:00 UT and intensified towards midnight on 18 February, 2005. Distinct FSF irregularity can be observed from 18:00 UT on 18 February, 2005, which then decreased in intensity on 19 February, 2005 from 01:00 UT until 22:00 UT, before building up again. This type of FSF covering the frequency range of 2 to 4 MHz may be attributed to the occurrence of sub-storms during the recovery phase of the minor storm in Figure 5.22. Although not often, SF is known to occur one or two days after a geomagnetic storm or sub-storm activity.

The geomagnetic and solar wind conditions for the period 18-20 February, 2005 were investigated. The results are illustrated in Figure 5.22.

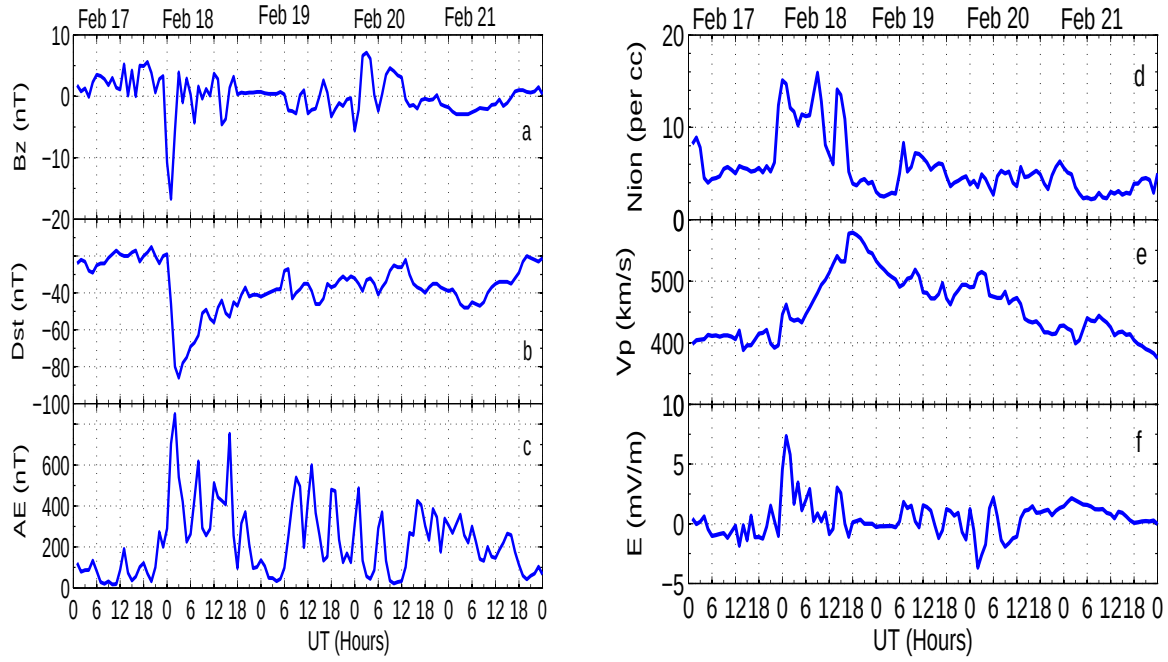

Figure 5.22: (a) Variability of the IMF (Bz) from 17-21 February, 2005. (b) Hourly Dst index showing storm and sub-storm activities. (d) Variation of ion number density. (e) Plasma flow speed with a peak value of $\sim$ 580 km/s. (c) Variability of the electric field. (Data source: ACE website).

A strong solar wind shock wave arrived at 00:00 UT on 18 February, 2005. This was caused by the sudden southward change in the direction of Bz and initiated the storm and sub-storm activity with a long-lasting recovery phase. This moderate storm with minimum Dst of $\sim$ -80 nT during post-midnight on 18 February, 2005 was accompanied by a sudden increase in electric field and ion number density. Therefore, the southward Bz implies that reconnection took place due to dayside compression of the magnetosphere of the Earth, thus allowing solar wind particles to penetrate the Earth's magnetic field. Throughout the rest of the

moderate storm period, ionisation decreased (i.e negative storm effect). Figures 5.22 (d), (e) and (f), show a sharp increase in ion number density, plasma flow speed and electric field from $\sim$ 18:00 UT (on 18 February, 2005) to 18:00 UT (on 19 February, 2005). The ACE satellite observed a moderate increase in auroral activity as in Figure 5.22 (c) from $\sim$ 00:00 UT to 18:00 UT on 18 February, 2005, with high fluctuations evident until 00:00 UT on 21 February, 2005. These nighttime changes evidenced by the variability of the parameters in Figure 5.22 are consistent with the occurrence of nighttime SF events as in Figure 5.21 It is an established fact that during geomagnetic disturbances, the electric fields and particle populations which characterise the auroral region expand equatorward and their effects are observed at sub-auroral latitudes (Foster and Rich, 1997). Mid-latitude ionospheric dynamics is known to be dominated by the inner magnetosphere and neutral winds (Kintner *et al.*, 2007). The intense electric fields drive and induce equatorward neutral winds through collisions by producing a rapid convection of ionospheric plasma at high latitudes (Yizengaw *et al.*, 2005). These electric fields then find their way to middle and lower latitudes along the magnetic field lines, thus causing changes in the mid-latitude ionosphere. Mansilla (2004) studied the ionospheric response to a strong geomagnetic storm on 13 March, 1989 at middle and middle-low latitudes in different longitudinal sectors. This author observed both positive and negative ionospheric storm effects, with a fluctuating increase (i.e. positive storm effect) of ionisation during the initial stage of the main phase of the moderate storm at low latitudes.

The study of the characteristics of irregularities during disturbed days gives insight into the role of electric fields of magnetospheric origin. According to Fejer and Scherliess (1998), an important parameter responsible for the growth of ionospheric plasma instabilities after sunset is the equatorial upward vertical plasma drift which is driven by the F layer dynamo zonal (eastward) electric field, known as the pre-reversal electric field. Rezende *et al.* (2010) showed that scintillation depends on the vertical drift velocity of the plasma. Therefore it was important to investigate the role of plasma drift. Ionospheric digisonde data for the base height (h'F) was used to compute the time derivative of h'F given by d(h'F)/dt as a measure of the vertical drift velocity. The variability of hmF2, h'F and the time derivative of h'F (denoted by Vd) is shown in Figure 5.23.
During geomagnetic storms, direct post-sunset penetration of eastward magnetospheric electric fields can amplify the pre-reversal electric field, thereby enhancing the process that triggers irregularities. Earle *et al.* (2010) state that mid-latitude SF events are generally attributed to TIDs and gravity wave-driven mesoscale (10-100 km) density perturbations. These authors also state that small scale wave perturbations in such regions are too weak and get filtered out in the lower thermosphere. These irregular plasma structures develop

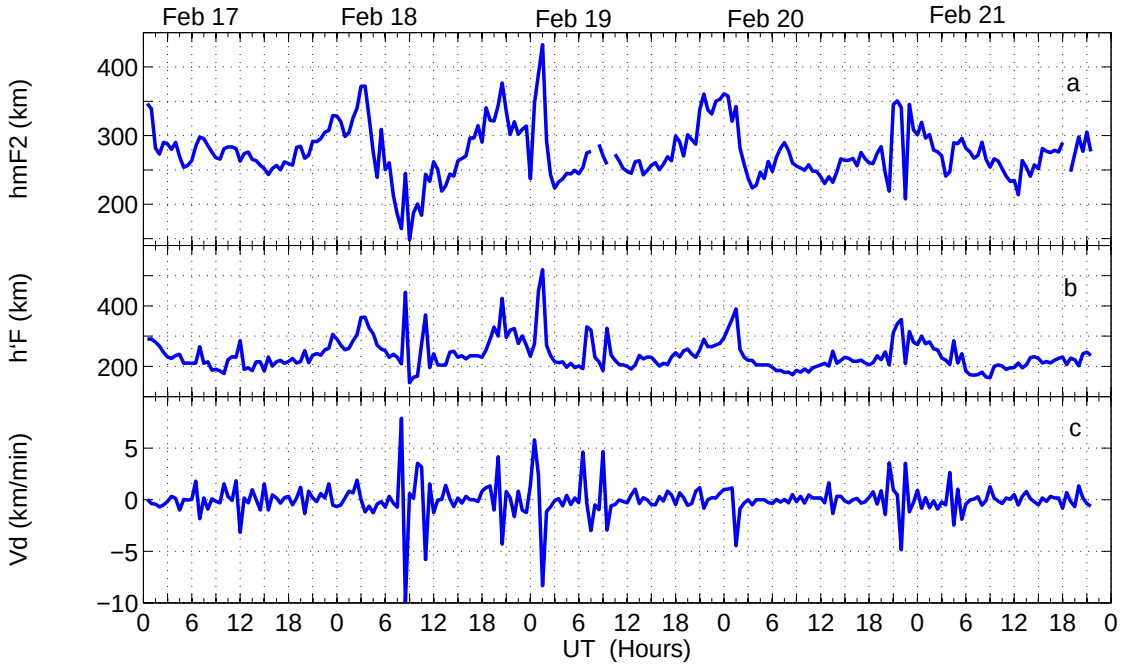

Figure 5.23: Time variation of (a) hmF2 and (b) h'F during 17-21 February, 2005 for Grahamstown ionosonde station. (c) The time derivative (Vd) of the bottomside virtual height.

as a result of instability processes and cause energy to cascade from larger to smaller scales (Earle *et al.*, 2010). This implies that SF irregularities are sometimes generated locally in the F region. Both negative and positive storm effects occurred slightly before or after midnight throughout the recovery phase of the moderate storm of 18-21 February, 2005. This can be observed from the rapid fluctuations in the bottomside F layer drifts (Figure 5.23 (c)). These nighttime variations are likely to generate density perturbations that may cause SF occurrence. A plasma drift velocity of $\sim$ 80 m/s was calculated around pre-midnight and post-midnight for 19-21 February, 2005. The same value was also obtained for 18 February, 2005 at around 12:00 UT. This implies that the plasma is likely to generate irregularities faster at night than during the day, which would then favour frequent nighttime SF occurrence. This behaviour of the mid-latitude ionosphere is analogous to equatorial E×B drifts.

The effect of the moderate storm on GPS signals over South Africa was examined to complement to the ionosonde study. The idea was to find out whether ionospheric disturbance caused by such moderate storm activity is observable at GPS frequencies. The results are shown in Figure 5.24.

Figure 5.24 shows that the ionosphere was turbulent on both quiet and disturbed days. The variability of $VTEC$ perturbation on a quiet day (Figure 5.24 (a)) is similar to that of dis-

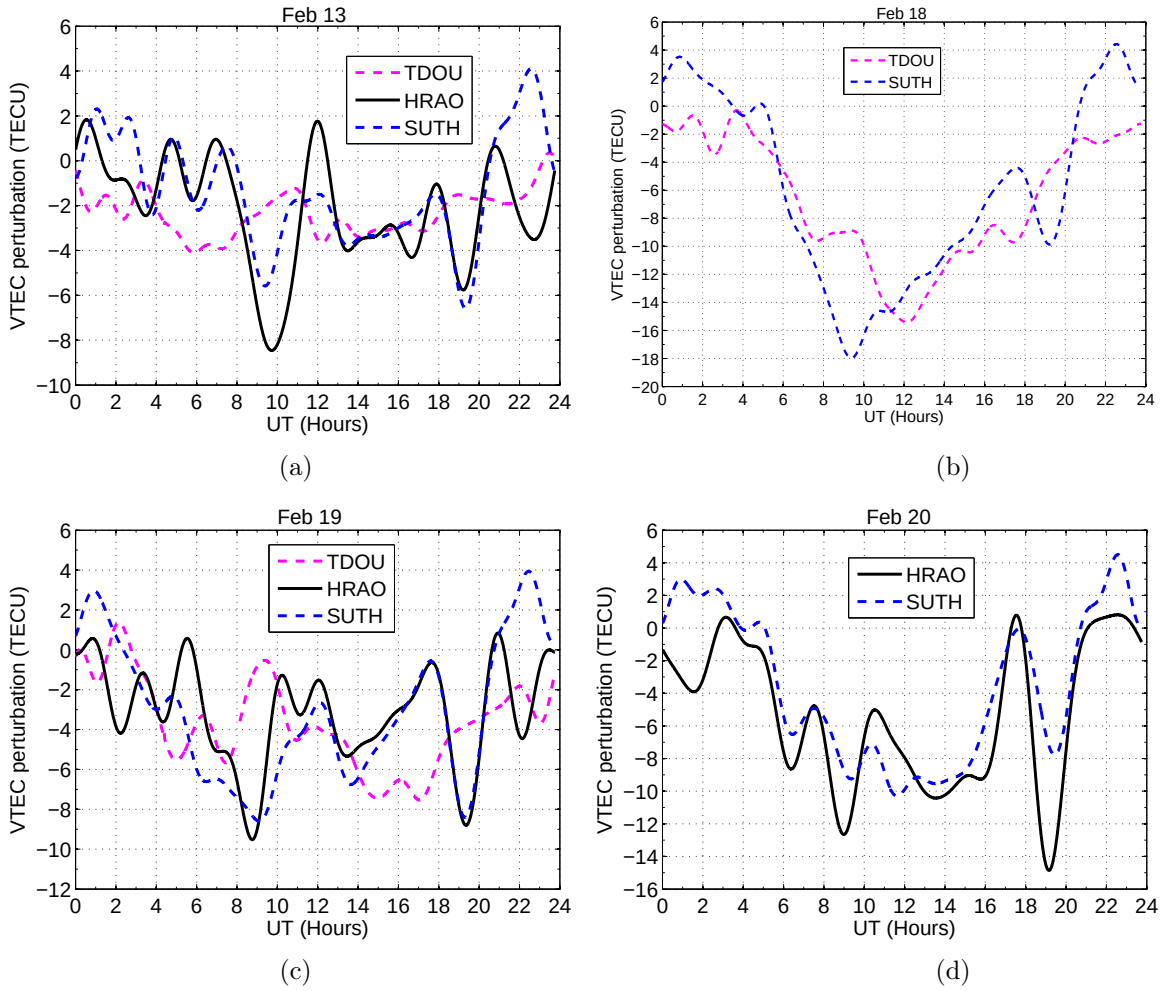

Figure 5.24: (a) The derived $VTEC$ perturbation for (a) a quiet day, and (b), (c) and (d) for disturbed days at the stations with available data.

turbed days (18-20 February, 2005). The minima of $VTEC$ perturbation at $\sim$ 18:00 UT are common to both quiet and disturbed days. The depletions and nighttime (20:00-23:00 UT) enhancements of $VTEC$ perturbation may be attributed to the disturbance dynamo electric field (Kumar and Singh, 1982) and the solar terminator effect. The solar terminator is a daily phenomenon and TIDs as a result of this process are independent of geomagnetic storms. The effect of penetration electric fields produced during the southward turning of the IMF (Bz) and during the terminating phase of a sub-storm when IMF (Bz) turns northward are both evident in Figure 5.22 (a). The disturbance dynamo electric fields produced by increases in radiation and the consequent Joule heating of the high latitude plasma seems to have an effect, as observed in Figure 5.22 (c). As mentioned previously, this additional heating may launch equatorward winds, which in turn generate disturbance dynamo fields Kumar and Singh (1982).

One of the objectives of this study is to trace simultaneous occurrence of SF and scintillation on GPS radio signals. Due to the absence of S_4 scintillation data, the S_{4p} parameter was used as a proxy for the S_4 index when looking for irregularity phenomena that could be associated with SF or scintillation. The cases where S_{4p} stays above the noise level (i.e $S_{4p} > 0.2$ TECU/min) were considered to be a significant disturbance of the ionosphere, capable of causing SF or scintillation.

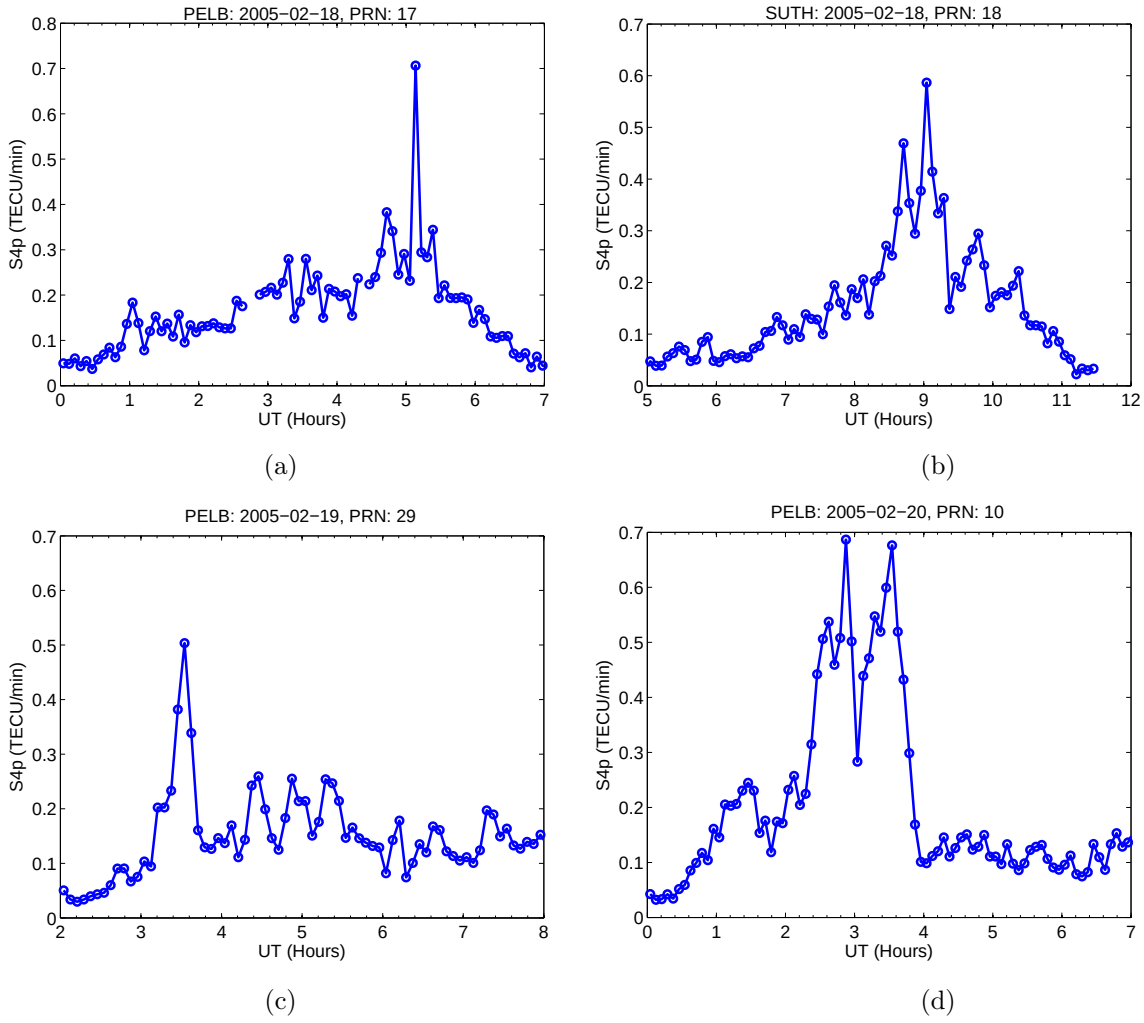

Figure 5.25: Variability of S_{4p} during the period of SF occurrence for two stations tracking different satellites.

Figure 5.25 shows a cross-section of the S_{4p} analysis for the visible satellites from 18-20 February, 2005. The GPS receiver at Port Elizabeth (PELB) was used as a reference due to its proximity to the Grahamstown ionosonde (GR13L) station. The gaps on satellite 17 at Port Elizabeth between $\sim$ 02:30 and 03:00 UT were caused as a result of the satellite being below the elevation mask (i.e. 20°), thus recording no data. A short period of a sharp peak in S_{4p} can be observed in Figure 5.25 (a) from 05:00 to 06:00 UT and in Figure 5.25 (c) between 03:00 and 04:00 UT. A sharp increase and decrease in the S_{4p} from 08:30 to 09:30 UT (Figure 5.25 (b)), and from 02:00 to 04:00 UT (Figure 5.25 (d)) can also be observed at Sutherland (SUTH) and Port Elizabeth respectively. The variability of S_{4p} in Figures 5.25 (b) and (d) reflect the fluctuations of the signal intensity during these intervals. These characteristic signal intensity fluctuations may be attributed to scintillation-related irregularity that may have been caused by wave-like structures generated in the auroral latitudes. The abrupt increase at 05:00 UT on 18 February, 2005 at Port Elizabeth may be attributed to a short period of irregularity induced by the southward turning of IMF (Bz) during the main storm phase. The latter causes daytime upward E×B plasma drifts. Rapid decrease of S_{4p} from $\sim$ 0.7 TECU/min to $\sim$ 0.3 TECU/min at $\sim$ 03:00 UT on 20 February, 2005, observed at Port Elizabeth coincides with the northward polarity change of Bz in Figure 5.22 (a). This is consistent with the observation of Kumar and Singh (1982) about the prompt penetration fields.

5.4 SF events during low solar activity

The period of low solar activity chosen for this study was 2006-2008. The nighttime SF (i.e. MSF and FSF) occurrence is very high during periods of low solar activity (Figure 5.6).

5.4.1 24-25 September, 2006 SF event

The event of 24-25 September, 2006 is an example of the increase in the intensity of SF during solar minimum (during spring). The resolution of the Grahamstown ionosonde station data during this particular observation period was 15 minutes, adequate to capture the SF irregularity phenomenon.

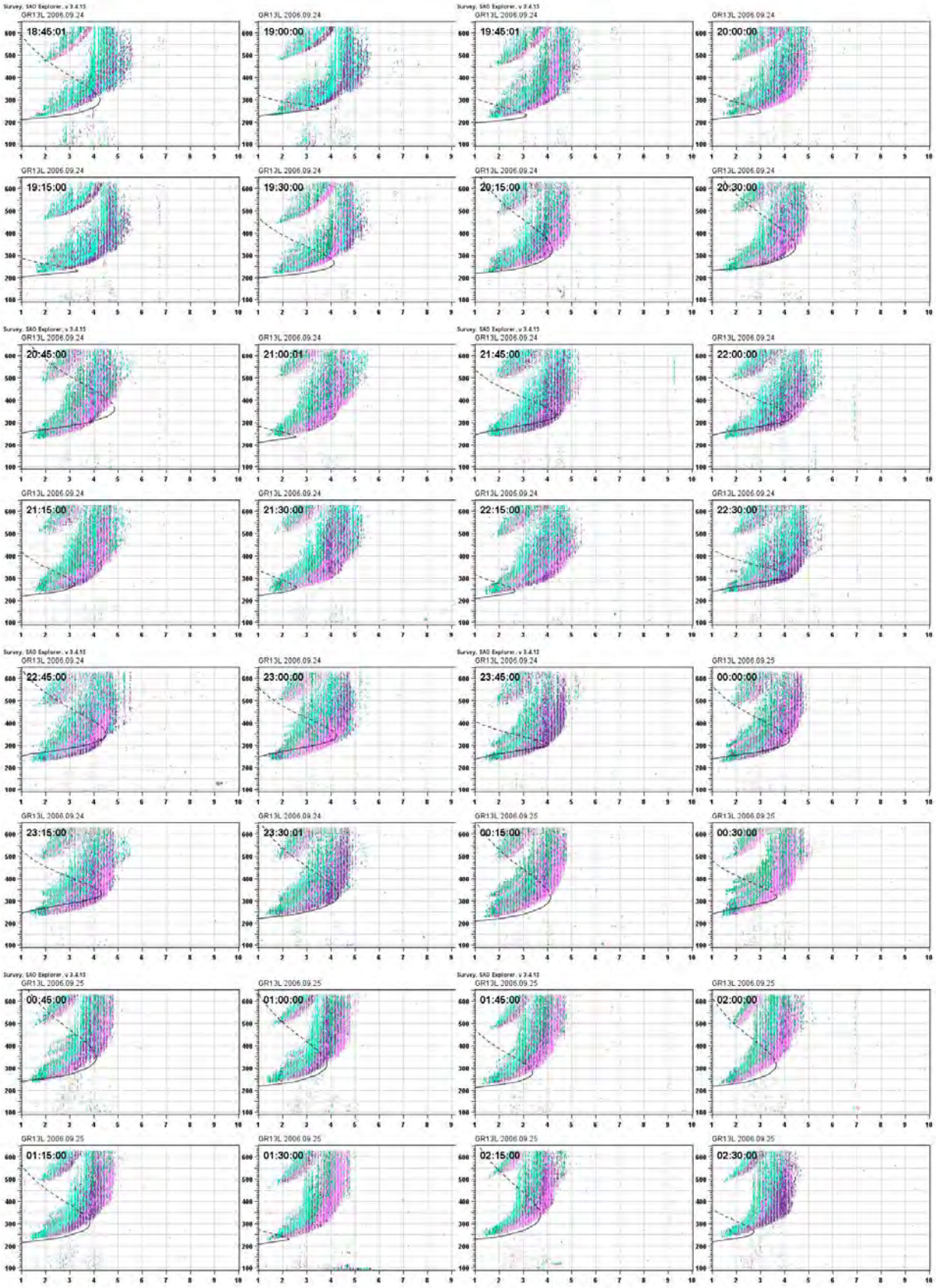

Figure 5.26: FSF observed at Grahamstown station for the period 24-25 September, 2006.

The occurrence of SF during this minor storm period (see Figure 5.27) started building on 24 September, 2006 at 17:45 UT. The intensity of SF increased from 18:45 UT to 03:30 UT on 25 September, 2006, and then decreased gradually until 04:30 UT. This happened on both days from sunset throughout the night hours (18:00-04:45 UT). The reflections due to density gradients in the scattering medium occurred at virtual heights between 200 km and 300 km. The investigation into the cause of such a long-lasting mid-latitude SF on the ionosphere is shown in Figure 5.27.

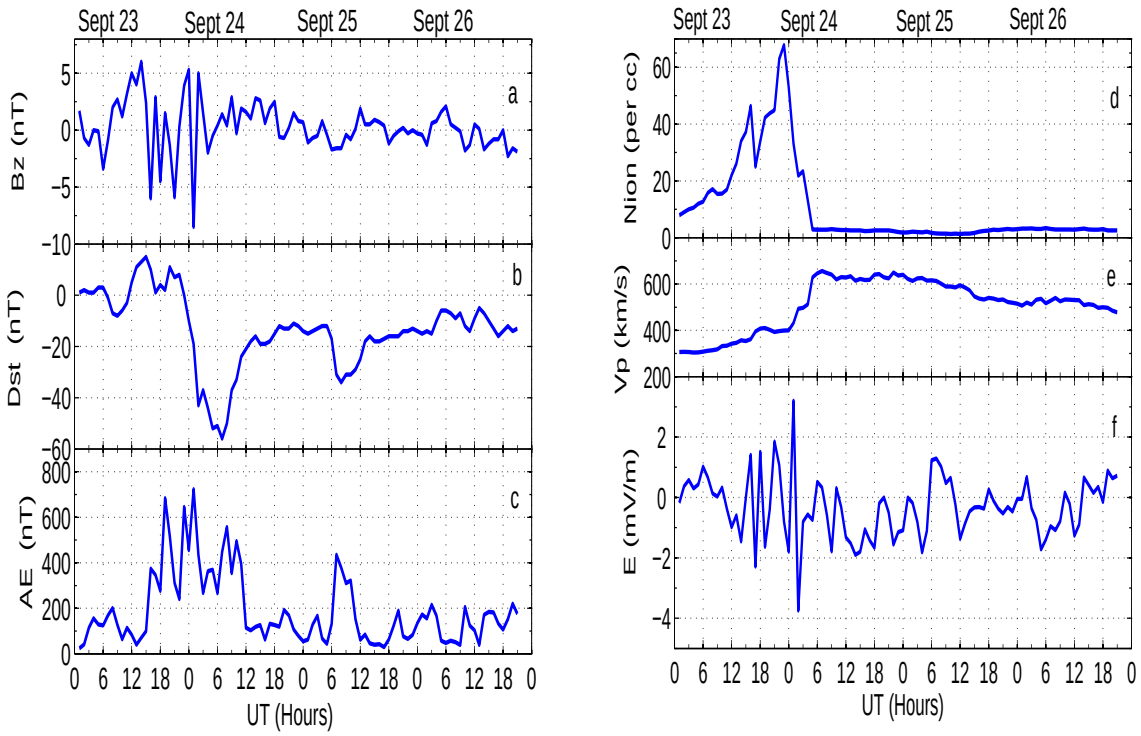

Figure 5.27: Variability of (a) IMF Bz, (b) hourly Dst index, (c) hourly AE index (d) ion number density, (e) plasma flow speed and (f) electric field; for 23-26 September, 2009.

The main phase of the moderate storm in Figure 5.27 (b), preceded by small positive phase (at $\sim$ 12:00 UT on 23 September, 2006) may be a consequence of increased auroral activity from 12:00 UT (on 23 September, 2006) to 12:00 UT (on 24 September, 2006) as seen in Figure 5.27 (c). The expansion phase of the moderate storm started at $\sim$ 21:00 UT on 23 September, 2006 when IMF (Bz) turned southward after which several shock waves approached the magnetosphere of the Earth. The moderate storm showed a minimum Dst of -56 nT at 09:30 UT on 24 September, 2006, during which the solar wind speed and auroral activity increased. The high solar wind speed at 06:00 UT was coincident with a serious decrease in ion number density which remained very low for the rest of the moderate storm period. This may have been caused by increased ion loss rates. The loss rate is mostly as-

sociated with a reconnection process which may have injected charged clouds or high speed streams of particles towards the Earth. Thus, geomagnetic disturbances are associated with large energy inputs into the upper atmosphere in the form of enhanced electric fields and currents (reflected in the increased AE index), and energetic particle precipitation. The electric fields that transport the plasma are caused by the polarising effect of the thermospheric winds. Rapid reversals of the IMF (Bz) from steadily southward to northward during sub-storm activity (e.g. from 06:00 UT to 12:00 UT on 25 September, 2006) are often associated with anomalous reversals of the zonal electric field component at the equator (Kelley *et al.*, 1979). The ion number density increased during the time frame 00:00 to $\sim$ 15:30 UT, then decreased at $\sim$ 17:30 UT, and increased again to the peak ($\sim$ 68 ions/cm^3) at 23:30 UT on 23 September, 2006 after which a rapid decrease to $\sim$ 2 ions/cm^3 occurred. The increased variability in ion number density is consistent with the sub-storm activity, which occurred at 06:00-12:00 UT and the positive storm phase at about 12:00 to 18:00 UT. The latter was initiated by rapid south-north polarity changes in the IMF (Bz) on 23 September, 2006.

After investigating the storm and solar wind conditions for this period of SF occurrence, the hmF2 and h'F ionosonde data was also investigated. The purpose was to confirm the suggested causes of the SF observed. The hmF2 and h'F data during the SF period was compared with data for a selected quiet day and repeated for each of four disturbed days. The results are presented in Figure 5.28.

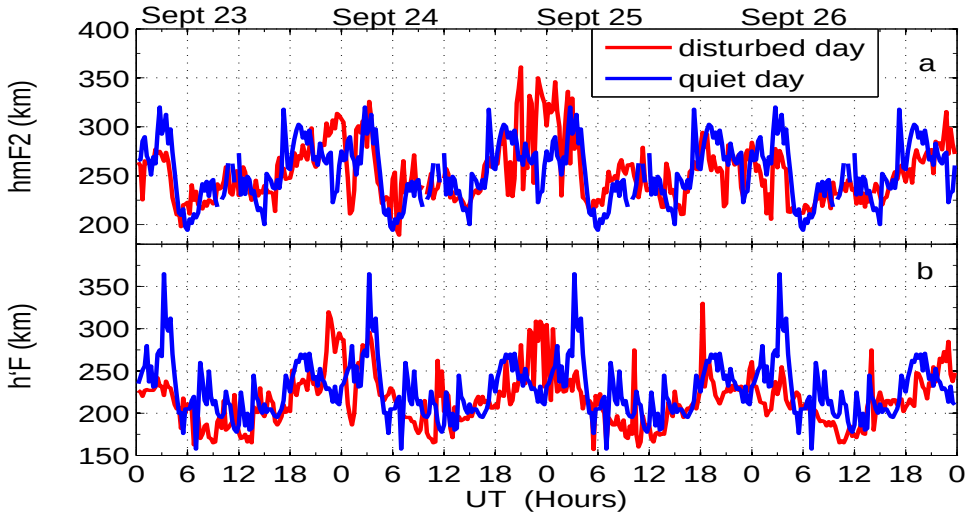

Figure 5.28: Comparison of (a) hmF2 and (b) h'F on disturbed days (23-26 September, 2006) with quiet day (background) data of 01 September, 2006 at Grahamstown. (Data source: SPIDR website).

Figure 5.28 illustrates the variability of hmF2 observed at the Grahamstown ionosonde sta-

tion. The hmF2 shows a larger variability around nighttime (e.g. 00:00 UT) than during daytime. According to Sethi *et al.* (2004), the maximum values of hmF2 around midnight are caused by an increase of upward drifts produced by meridional winds in the neutral air. Close to sunrise, the ionisation begins to intensify and the electron concentration near hmF2 increases at a rate dependent upon the production rate. This consequently causes the hmF2 to shift downwards due to rapid production of ionisation in the lower F region. During the daytime, both the concentration of atomic oxygen and loss coefficient increase proportionally to the molecular components, due to temperature increases, resulting in higher altitudes of hmF2 (Davies, 1990; Sethi *et al.*, 2004). Therefore, the increase of hmF2 from morning to afternoon is explained by the increase in the temperature. Decrease in the evening rate of ion formation is accompanied by a transitional period during which the height of hmF2 increases to its nighttime value (Sethi *et al.*, 2004). This entire process is enhanced by a change in the direction of the thermospheric winds, since an upward drift causes an additional uplift of the layer. The drift rate increases towards midnight, resulting in a rise in the F2 layer around midnight. Therefore, E×B drifts and thermospheric winds play a pivotal role in the daytime and nighttime profiles of hmF2 at mid-latitude regions. The hmF2 enhancement was highest during the recovery phase of the moderate storm in the pre- and post-midnight period of 24 September, 2006 and 25 September, 2006 respectively. Figure 5.27 (d) shows that this period was marked by very low (almost zero) ion number densities which imply a high rate of loss of ions.

The enhancements of hmF2 observed using ionosonde data were further investigated using the derived $VTEC$ perturbation. The GPS receiver at Grahamstown is co-located with the Grahamstown ionosonde with which this SF event was observed. The aim here was to examine the effects of this moderate storm on the mid-latitude ionosphere over South Africa in the L-band GPS frequencies. The stations selected here have either almost the same latitude (Grahamstown (GRHM) and East London (ELDN)) or longitude (Grahamstown, Aliwal North (ANTH) and Bloemfontein (BFTN)). In Figure 5.29 the left and right panels illustrate the longitudinal and latitudinal variations of the $VTEC$ perturbation respectively, with Grahamstown as the reference GPS station.

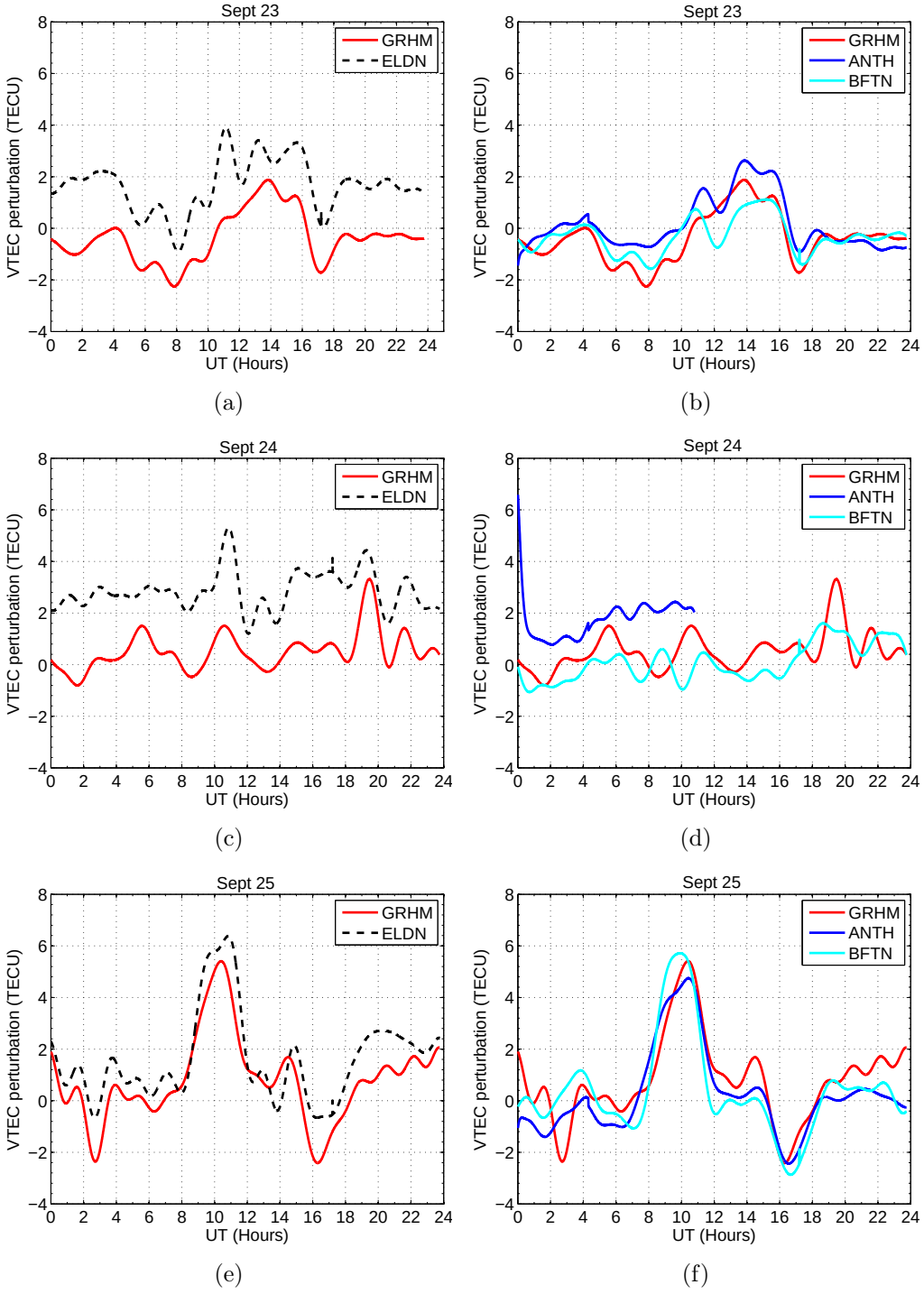

Figure 5.29: Comparison of the derived $VTEC$ perturbation for selected stations to investigate longitudinal (left panel) and latitudinal (right panel) dependence.

Figure 5.29 (a) shows that at Grahamstown and East London the electron density in the ionosphere was highly variable, and more depressed at Grahamstown than at East London. Figure 5.29 (b) shows that the $VTEC$ perturbation is slightly lower for Grahamstown than

the other two stations (Aliwal North and Bloemfontein). Prominent minima are observable in both cases at $\sim$ 08:00 UT, $\sim$ 12:00 UT (except Grahamstown) and $\sim$ 17:00 UT. The rapid oscillatory motions observed on 23 September, 2006 (more evident in Figure 5.29 (a)) may be attributed to the effects of the shocks on the magnetosphere shown in Figure 5.27 (a). During this period the electric field in Figure 5.27 (f) rapidly changes direction from east to west and vice versa. The eastward electric fields result in an uplift of the ionosphere, while the opposite westward fields pull the ionosphere downwards, thus setting the ionosphere into oscillatory motion of varying amplitude. The $VTEC$ perturbation in Figures 5.29 (c) and 5.29 (d) both reveal that the ionosphere experienced oscillatory motion on this day. The effects, for example, of the westward (i.e. 01:00 to 03:00 UT) and eastward (i.e. 08:00 to 12:00 UT) electric fields can be observed in the decreased and enhanced $VTEC$ perturbation respectively (Figure 5.27 (f)). A similar effect can be observed between 17:00 and 19:00 UT. Some shifts occur between either adjacent maxima or minima, for example between 05:00 and 12:30 UT on 23 September, 2006 in Figure 5.29 (b).

The fact that the ionosphere has to respond to the composition of the thermosphere affects the rate at which ions and electrons recombine. During a geomagnetic storm the energy input at high latitudes produces waves and changes in thermospheric winds and composition which in turn produces both increases (i.e. positive storm effect) and decreases (i.e. negative storm effect) in the electron concentration. Therefore, the increased auroral activity which led to the onset of the main phase of the moderate storm on 23 September, 2006 (Figure 5.27) may be the most likely cause of the wave-like structures in Figure 5.29. These observations may imply that the moderate storm and sub-storm activities reflected in Figure 5.27 generated TIDs as a result of atmospheric GWs from auroral regions. These TIDs propagated through the mid-latitude ionosphere and induced changes in the electron density.

5.4.2 22-23 May, 2008 SF event

The increased occurrence of MSF and FSF during low solar activity and winter has been established. An example of such MSF and FSF occurrence is shown in Figure 5.30. The low intensity SF in Figure 5.30 actually started on 22 May, 2008 at 00:15 UT, and the intensity increased from 17:30 UT to 23:15 UT and decreased until 23:45 UT on 23 May, 2008. It should be noted that the occurrence of FSF may sometimes change to MSF as the signals traverse the ionosphere through different scattering media.

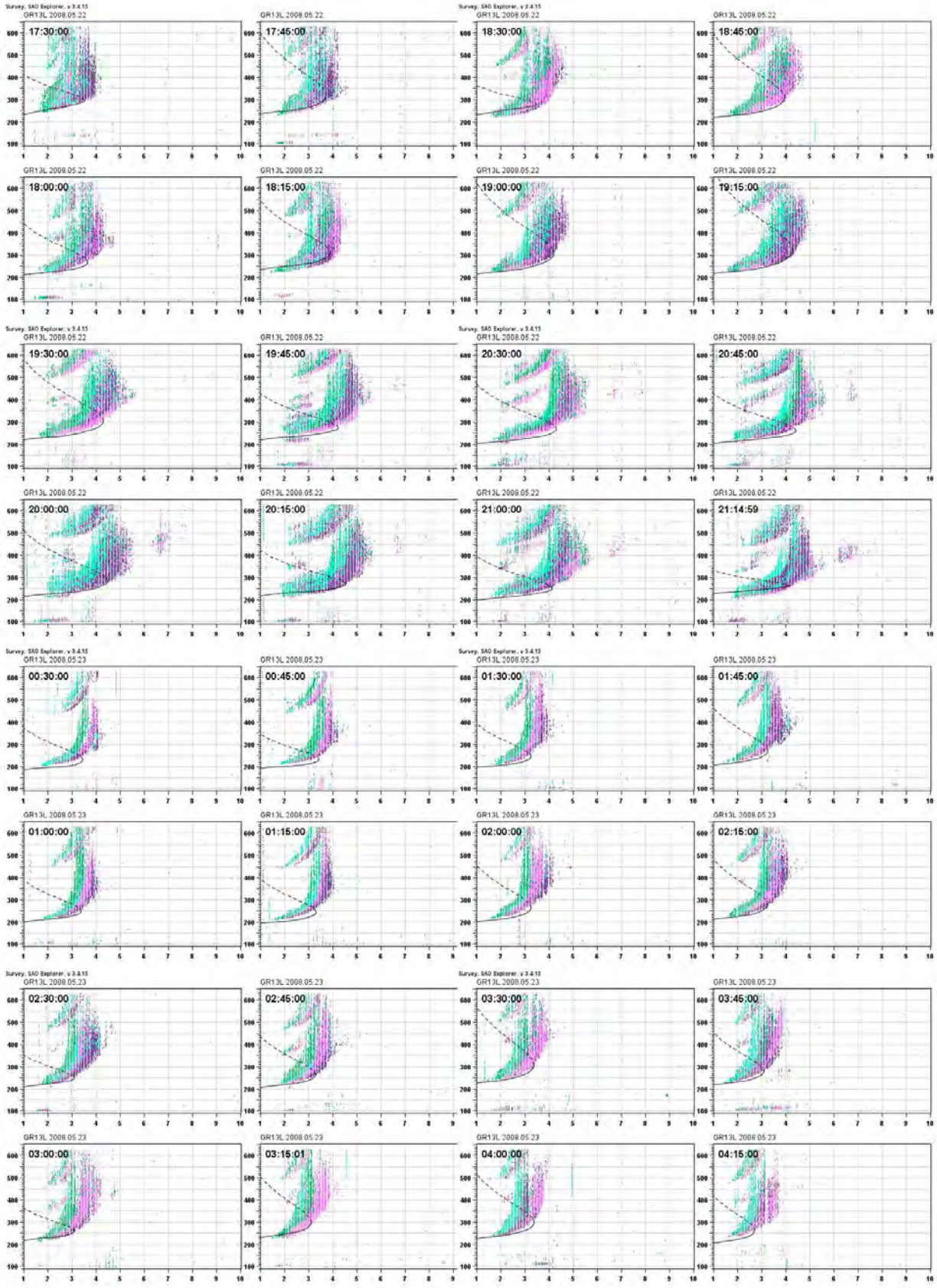

Figure 5.30: Nighttime MSF and FSF observed at Grahamstown station during 22-23 May, 2008.

The SF period of 22-23 May, 2008 was generally quiet, although minor sub-storms occurred during this period (Figure 5.31). Most of the SF events mentioned in this study are associated with storms of higher intensity. The SF event of 22-23 May, 2008 demonstrates that weak storm environments favour the growth of SF irregularities in mid-latitude regions.

The geomagnetic and solar wind parameters of interest for this study were plotted and shown in Figure 5.31. The reason for this is to check for impulses on the magnetosphere due to pressure force and shock waves. Sometimes changes in the ionosphere may occur during quiet conditions resulting from a significant Bz polarity change.

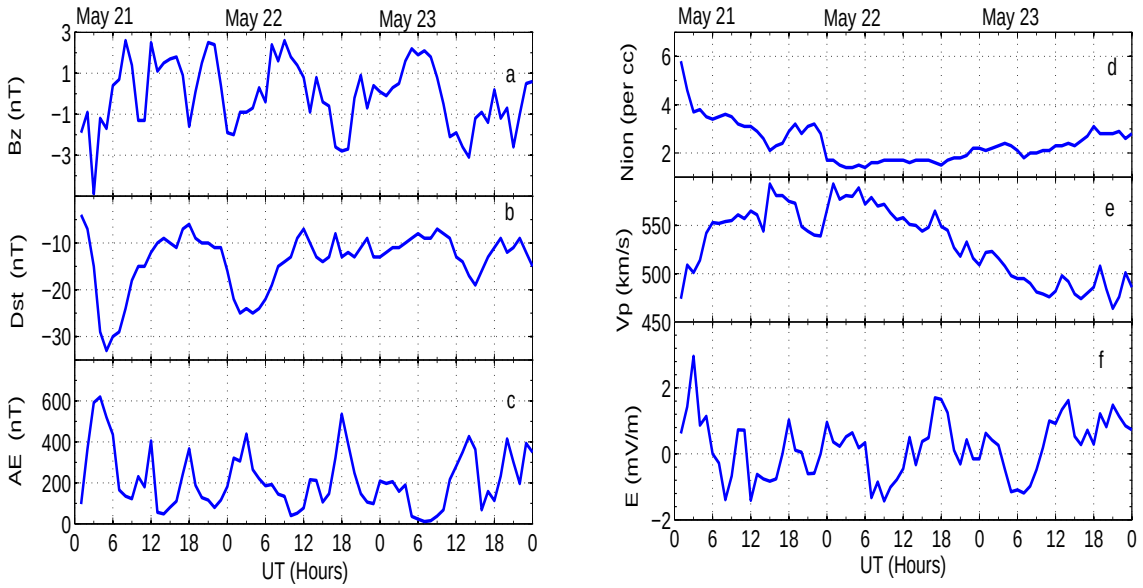

Figure 5.31: Variability of (a) IMF (Bz), (b) hourly Dst index, (c) AE, (d) ion number density, (e) plasma flow speed and (f) electric field during 21-23 May, 2008.

Figure 5.31 (a) shows that IMF (Bz) alternated between south and north with a small magnitude (|Bz|< 5 nT) throughout these three days. This resulted in a varying but relatively small Dst value, between 0 and -33 nT. The AE index shown in Figure 5.31 (c) reached a maximum of 620 nT during a northward sustained Bz. During geomagnetically quiet conditions, auroral activity (and hence Joule heating) is small. The peak of the main phase of the minor sub-storm occurred at $\sim$ 04:30 UT and was initiated by a shock wave at $\sim$ 03:00 UT on 21 May, 2008. The peak of the storm was accompanied by a combination of auroral and solar wind electric field activities. Figure 5.31 shows that every southward turning of Bz is accompanied by increased auroral activity and electric field. On average, an increase in solar wind speed during this minor sub-storm was accompanied by a decrease in ion number density and vice versa. It is believed that during such quiet conditions, ions from the solar

wind, and especially from the ionosphere, fill the magnetosphere with plasma (Davies, 1990). Therefore, the decrease in ion number density could be attributed to increased ion loss rates as the ions from the solar wind plasma are injected into the magnetosphere.

The variability of hmF2 and h'F for three consecutive days (21-23 May, 2008) was examined and the result is shown in Figure 5.32.

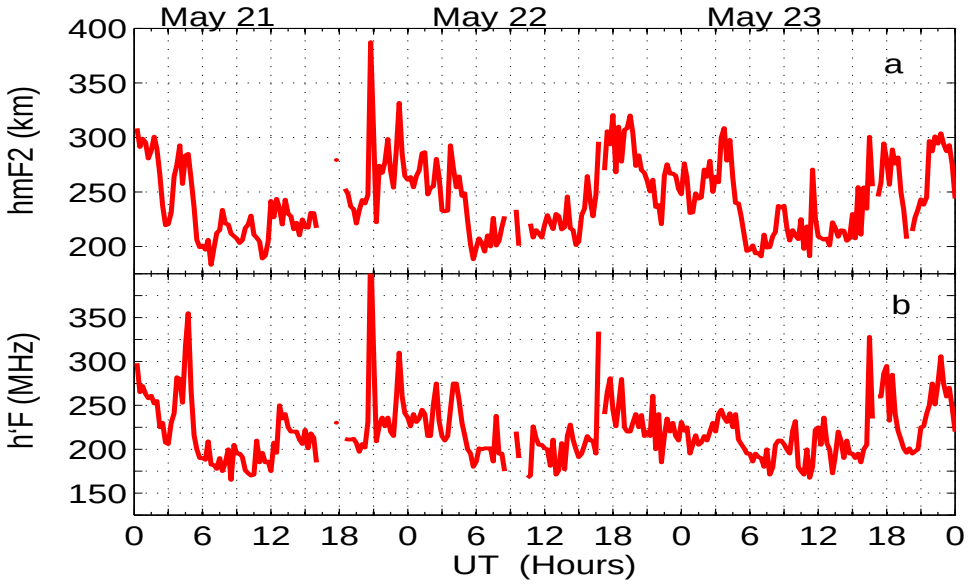

Figure 5.32: Variability of (a) hmF2 and (b) h'F at Grahamstown from 21-23 May, 2008. (Data source: SPIDR website).

Figure 5.32 shows no evidence of significant disturbance in the ionosphere over South Africa during this period, as observed in the HF band. Throughout these three days hmF2 and h'F departed from their monthly average values of 350 and 200 km respectively during the low level pre- and post-midnight period. The decrease in atomic oxygen concentration is primarily responsible for the hmF2 decrease below the monthly median value of $\sim$ 300 m. The hmF2 decrease results from a strong decrease in the electron concentration above an h'F of $\sim$ 250 km due to the upward plasma transfer under the E$\times$B drift. The increase or decrease of daytime electron density under quiet geomagnetic conditions is attributed to the free electron lifetime changes as the plasma moves into different loss regions.

The cause of SF during quiet solar activity and geomagnetic conditions was researched using GPS TEC data. The variability of the TEC perturbation for the period 21-23 May, 2008 for different (available) stations located on either approximately the same longitude or latitude was examined. The idea of using $VTEC$ perturbation fluctuations to observe the effects of

minor sub-storms has been exploited by Unnikrishnan *et al.* (2005). The TEC perturbation enhancements obtained in their study have magnitudes ≥25 TECU on geomagnetically disturbed days compared to the quiet day values. The approach used for the derivation of the $VTEC$ perturbation in this study is quite different from the one used by Unnikrishnan *et al.* (2005). The use of the mean $VTEC$ ($\overline{VTEC}$) for at least two days before and after the disturbed days yields good results (Figures 5.33 and 5.34). This pattern of $VTEC$ perturbation is a good indicator of any type(s) of disturbance(s) induced in the ionosphere.

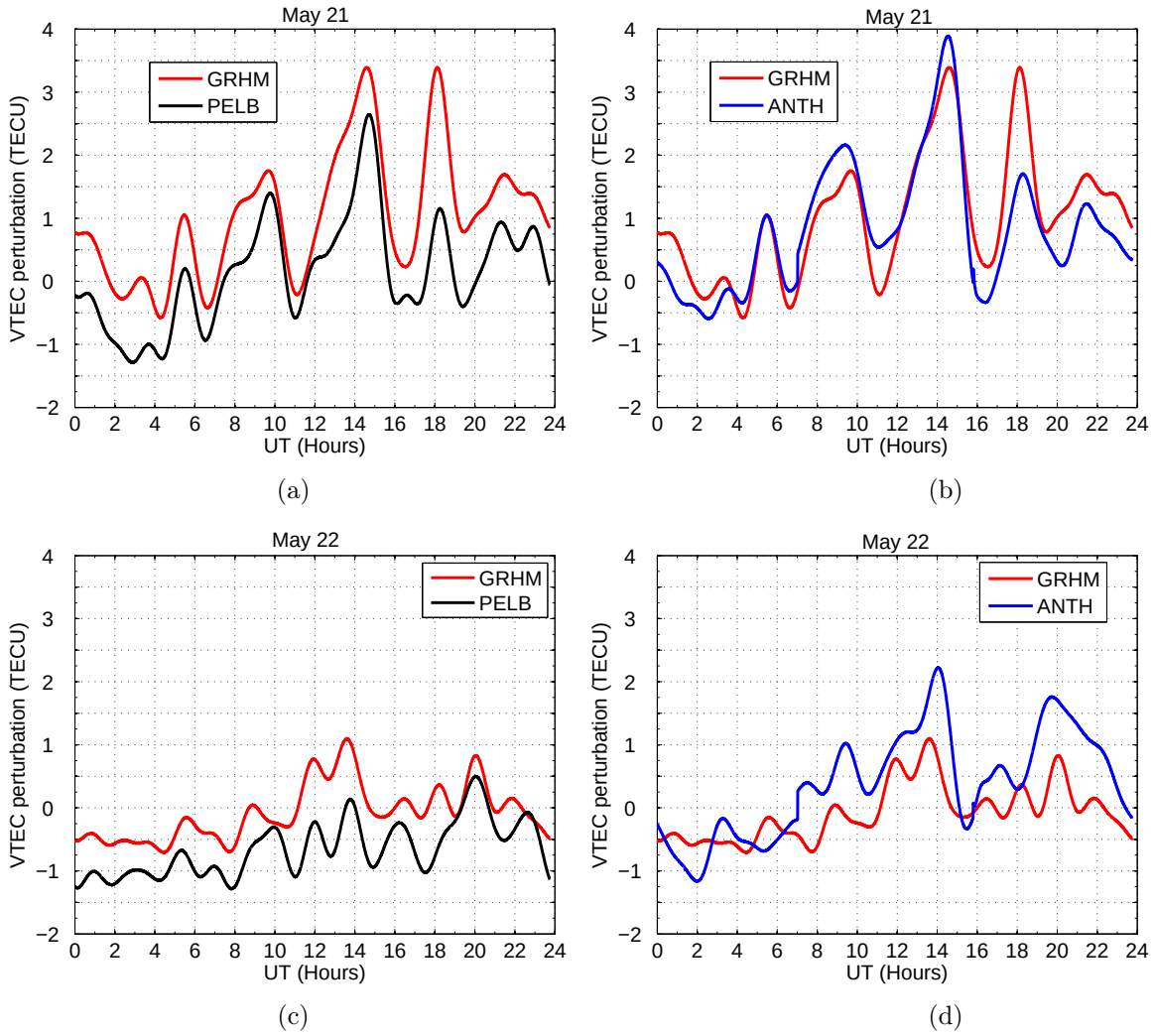

Figure 5.33: The derived $VTEC$ perturbation at Grahamstown and Port Elizabeth (left panel) and at Grahamstown and Aliwal North (right panel), for 21 and 22 May, 2008.

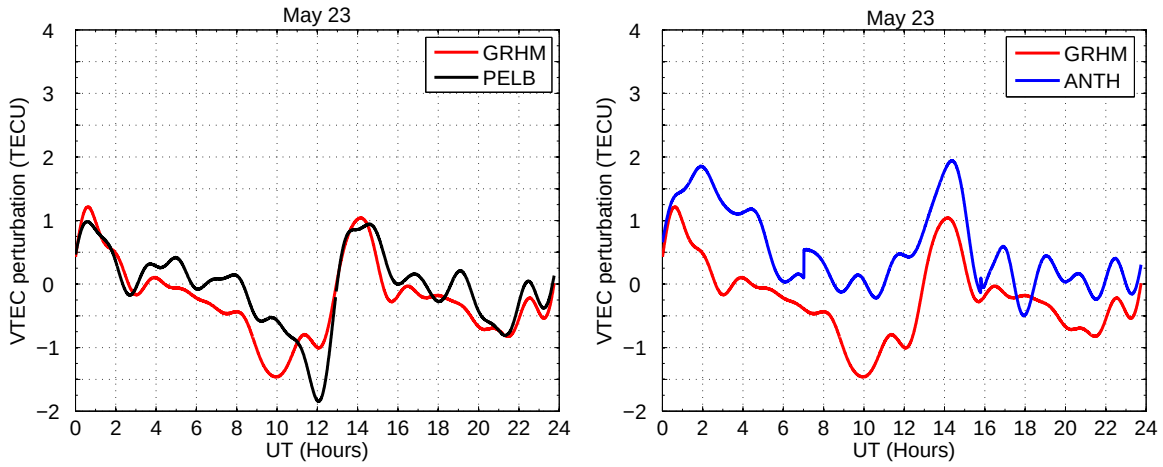

(a) (b)

Figure 5.34: The derived $VTEC$ perturbation at Grahamstown and Port Elizabeth (left panel) and at Grahamstown and Aliwal North (right panel), for 23 May, 2008.

The relationship between atmospheric GWs and TIDs has been documented in detail by authors such as Davies (1990) and Kelley (2009). The occurrence of TIDs is generally attributed to the passage of atmospheric GWs in the ionosphere. These TIDs are generated from the high latitudes and during their passage, ions are forced along the field lines by the neutral air winds driven by the pressure wave. Figure 5.33 shows rapid fluctuation of the low amplitude $VTEC$ perturbation in both the longitudinal and latitudinal sectors. The amplitude of the perturbed $VTEC$ is slightly higher on 21 May, 2008, with peaks at $\sim$ 15:00 UT and $\sim$ 18:00 UT (Figures 5.33 (a) and (b)). The wave-like oscillations of the $VTEC$ perturbation is evident on 22 May, 2008, in particular see Figure 5.33 (c), although the amplitude of the oscillations is lower on this day than the previous day. The perturbation shows peaks at $\sim$14:00 UT and $\sim$20:00 UT on 22 May, 2008 (which are slightly higher at Aliwal North). Meanwhile, on 23 May, 2008, the perturbation is also variable and oscillatory in nature. The minimum perturbation occurred at Port Elizabeth around 12:00 UT (Figure 5.34 (a)), while the perturbation at Aliwal North is slightly higher (with a peak at $\sim$14:00 UT) than that at the reference station (Grahamstown), observable in Figure 5.34 (b).

The overall picture indicates that the dynamics of the ionosphere during this period was governed by TIDs, probably driven by waves. Figure 5.31 shows that both Bz and AE are highly variable during this period. The variability of the perturbed $VTEC$ is consistent with that of the east-west auroral electric fields. Therefore, the rapid variation of the positive electric fields (associated with an uplift of the ionosphere) and negative electric fields (associated with a depression of the ionosphere) may be the source of TIDs that make the

ionosphere turbulent. The shifts in the maxima or minima can be observed in the longitudinal sector (i.e. between Grahamstown and Aliwal North) at $\sim$ 14:00 UT and $\sim$ 20:00 UT in Figures 5.33 (b) and (d). These longitudinal and latitudinal variations of $VTEC$ perturbation may be explained in terms of ion production. Ion production at lower altitudes increases TEC as the F region peak height is raised, while the electric fields perpendicular to the magnetic field redistribute the plasma in latitude and longitude (Mendillo, 2006; Foster and Rideout, 1997). This could be the main reason for the latitudinal and longitudinal variation of $VTEC$ observed in Figures 5.33 and 5.34.

5.5 Ionospheric scintillation results

Ionospheric scintillation can be observed in ionosonde data through the spreading of the F region returned signals (i.e. SF). In GPS data, ionospheric scintillation at L-band frequencies can be inferred from a high rate of change of TEC along a ray path from the GPS satellite to the receiver via the ionosphere. One of the objectives of this study was to investigate simultaneous occurrence of ionospheric irregularities over South Africa using co-located instruments. This was possible with the ionosonde, GISTM, and dual frequency GPS receivers, all located at Hermanus.

5.5.1 Anomalous amplitude scintillation on 30 September, 2010

The mid-latitude ionosphere is generally regarded as scintillation environment less active than the high and low latitudes, particularly at L-band frequencies. Scintillation events were identified by plotting the scintillation parameters along ray paths of all visible satellites for a particular day. Any events of interest were selected and then analysed further.

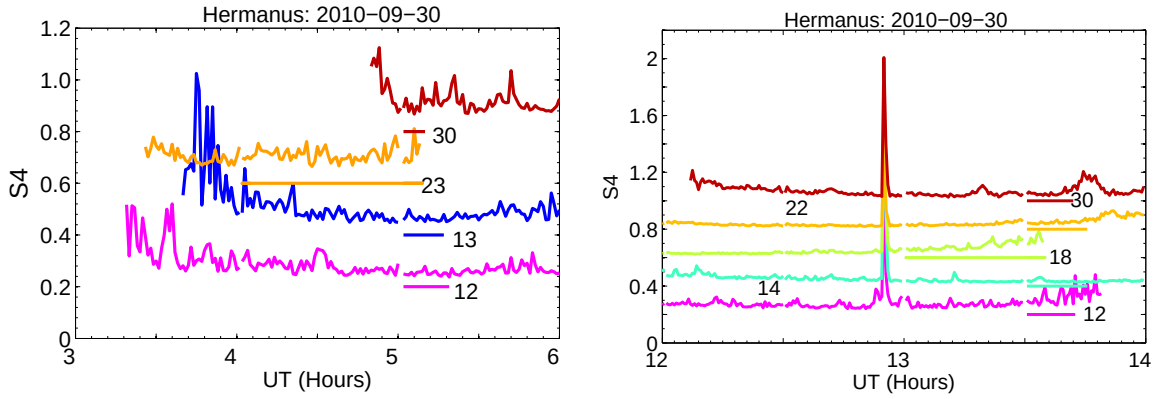

(a) (b)

Figure 5.35: Variation of S_4 index with time for selected satellites as observed from Hermanus GISTM receiver.

The sudden increase of S_4 index at $\sim$ 12:48 UT occurred on all satellites simultaneously, with essentially the same temporal profile. This suggests that some noise entered the antenna, rather than modulation due to irregularities along the satellite-receiver lines of sight (which would differ for each satellite). The effect of multipath can be observed in Figure 5.35 (a) on satellites 12 and 13 between 03:00 and 04:00 UT. Data gaps for short periods can be observed at $\sim$ 05:00 UT in Figure 5.35 (a), and at $\sim$ 13:00 UT and 13:30 UT in Figure 5.35 (b). Figure 5.35 (b) shows a sharp increase in the S_4 index on satellites 12 and 30 between 12:48 and 12:52 UT. Scintillation, being a random process, occurs at different times for the different satellites, which have different locations at any given time. The occurrence of the peak between 12:48 and 12:52 UT is then unlikely to be a scintillation phenomenon. Therefore, the peaks in Figures 5.35 (a) and (b) are most likely associated with a multipath effect and man-made noise of an unknown source. It is important to note that this phenomenon is a localised case which needs to be resolved before conclusions can be drawn about the event. According to Kintner *et al.* (2007), GPS observations of irregularities show that they may be distributed over the entire sky for at least two hours. It is well known that multipath signal interference can be misinterpreted as scintillation. The easiest way to distinguish between true scintillation and multipath is to check for the day to day repeatability of the fluctuations. Multipath tends to repeat from day to day because it is a function of relative satellite-receiver positioning, which nominally repeats every 24 sidereal hours (Kintner *et al.*, 2007). This idea was employed in this study, but the results show that these events (or peaks) were not repeated on a day to day basis.

An investigation of the signal-to-noise ratio ($\frac{C}{No}$) was carried out for the period of the event in Figure 5.35 (b). The results show that only pseudo-random numbers (PRNs) or satellites

12 and 30 showed a sharp decrease in the signal power (i.e $\frac{C}{No}$), coincident with the sharp peaks observed in Figure 5.35 (b).

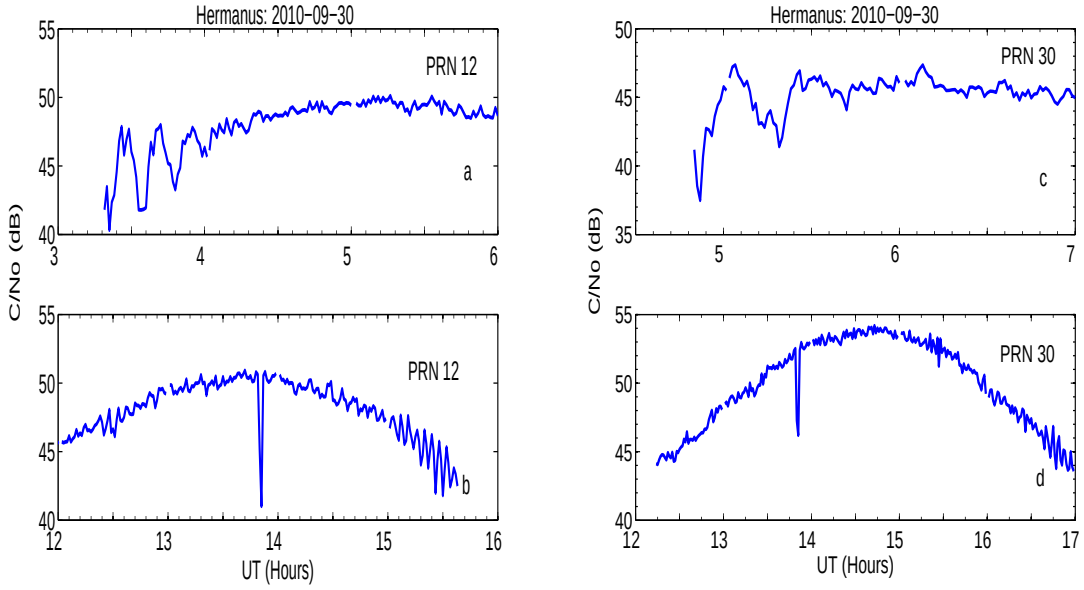

Figure 5.36: The $\frac{C}{No}$ for selected satellites from Hermanus GISTM on 30 September, 2010.

The dependence of L-band ionospheric scintillation on solar activity limits the monitoring of irregularities with GPS during solar minimum. The cases presented here are valid for only the signals coming from satellites with an elevation angle higher than 20°. Amplitude scintillation directly affects the ratio $\frac{C}{No}$ of signals in a GPS receiver and the noise levels in code and phase measurements. The nominal ratio $\frac{C}{No}$ for the L1 signal is about 45 dB-Hz, and tracking may be lost when the above ratio for the signal drops below 24 dB-Hz, depending on the receiver-specific tracking loop. Figure 5.36 shows the ratio $\frac{C}{No}$ of PRNs 12 and 30 recorded during the anomalous scintillation event. The fluctuation in the ratio $\frac{C}{No}$ in Figures 5.36 (b) and (d) is $\geq$5 dB-Hz. According to Kintner *et al.* (2007), GPS signals are vulnerable to ionospheric irregularities and scintillate with amplitude fluctuations exceeding 20 dB. The fluctuating nature of the ratio $\frac{C}{No}$ at the beginning and at the end of the path on PRNs 12 and 30 in Figure 5.36 (a) and (c) are due to the multipath effect when the satellite is close to the horizon. A very sharp decrease in the ratio $\frac{C}{No}$ on PRNs 12 and 30 at $\sim$ 13:48 UT resembles the sharp increase in the S_4 index in Figure 5.35 (b). However, the decrease in the ratio $\frac{C}{No}$ on these satellites were observed an hour after the detection of the increase in the S_4 index.

An attempt was made to follow up on the above scenario by analysing the $VTEC$ observed

at various dual frequency GPS receiver stations as shown in Figure 5.37. Since this particular day was geomagnetically quiet, the ionospheric variability was investigated in more datail.

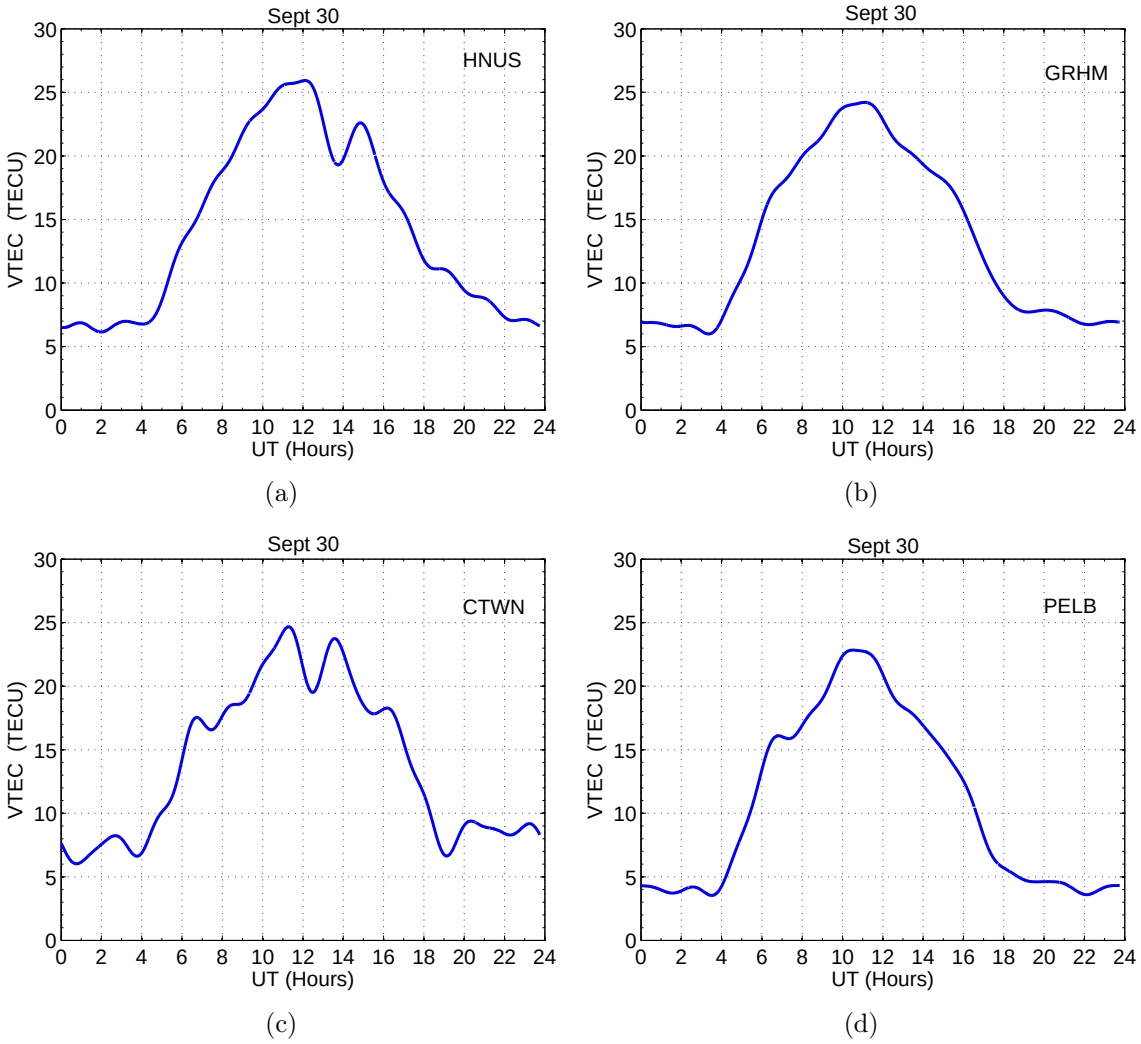

Figure 5.37: Variability of $VTEC$ at selected GPS stations on 30 September, 2010 as derived from the ASHA model.

The $VTEC$ values in Figures 5.37 (b) and (d) show a normal diurnal TEC pattern. A dip and double maxima in the $VTEC$ are evident in Figures 5.37 (a) and (c) at Hermanus (HNUS) and Cape Town (CTWN) between 13:27 and 13:38 UT respectively. These dips in the $VTEC$ were followed after $\sim$ 11 minutes by the sharp increase in the S_4 index, as in Figure 5.35. Another reason for this phenomenon may be the depletions in the ionosphere. The dips are also shifted, probably due to differences in the latitude and longitude of these stations. The daytime double maxima in the ionospheric TEC at middle and lower latitudes were studied by Pi *et al.* (1993). Pi *et al.* (1993) state that these twin peaks are related to sub-storm signatures, observable in both auroral electrojet and ring current variations.

These authors demonstrated that the diurnal double peaks in TEC can be created by a combined effect of E × B drift and altitude-dependent F region chemical loss. The latter suggestion of these authors may apply to the observed double peaks in Figure 5.37, since the element of a sub-storm is not applicable.

At this stage, there is no clear ionospheric phenomenon that can be associated with the observation from the GISTM data and other instruments. Further analysis was carried out using derived S_{4p} for some satellites to check any correlation with the S_4 and the results are shown below.

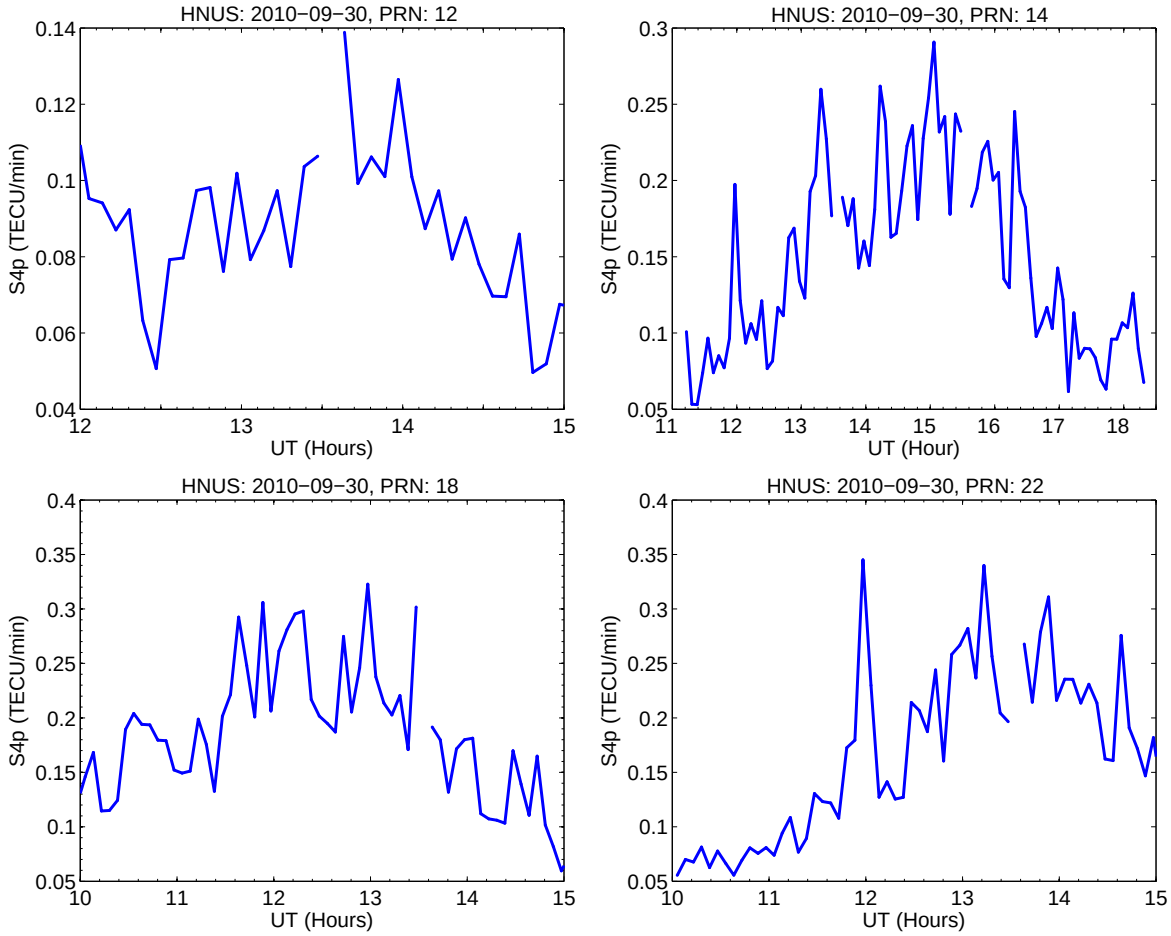

Figure 5.38: S_{4p} as derived from the GPS_TEC algorithm for satellites 12, 14, 18 and 22 on 30 September, 2010.

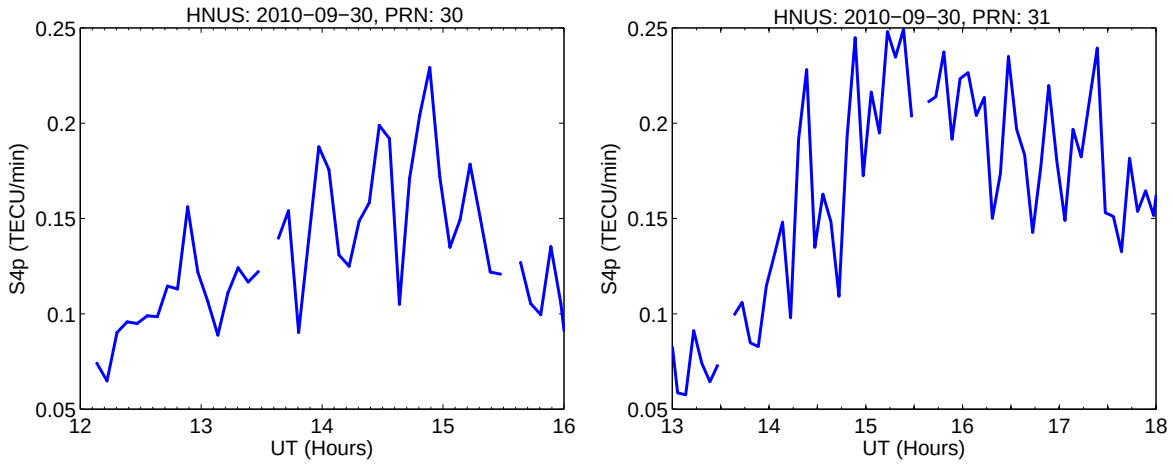

Figure 5.39: S_{4p} as derived from the GPS_TEC algorithm for satellites 30 and 31 on 30 September, 2010.

The S_{4p} for the satellites shows sharp peaks in Figures 5.38 and 5.39. Further investigation showed that serious data outages occurred on PRNs 12, 14, 18, 22, 30 and 31 between 13:27 and 13:38 UT. This suggests that the data outages observed in Figures 5.38 and 5.39, and which are also observable in Figure 5.35, may have been caused by short period power blackouts. The exact cause of these data gaps could not be established. According to the review of GPS scintillation by Kintner *et al.* (2007), scintillation at mid-latitudes are rare and are mainly associated with magnetic storms near solar maximum. The geomagnetic and solar wind conditions on this particular day were quiet.

An investigation of the ionosonde data was conducted by analysing the peak electron density for this day. The data from Grahamstown and Hermanus ionosondes was corrupted and ionograms could not be viewed. Therefore, the data used in Figure 5.40 was downloaded from the SPIDR website. No SF was observed on this particular day from Madimbo and Louisvale. The data for the hmF2 and h'F parameters was used to derive their respective perturbations α and β using the method described in Chapter 4. The data for these two parameters was detrended using a two-day mean obtained using the method described in Chapter 4.

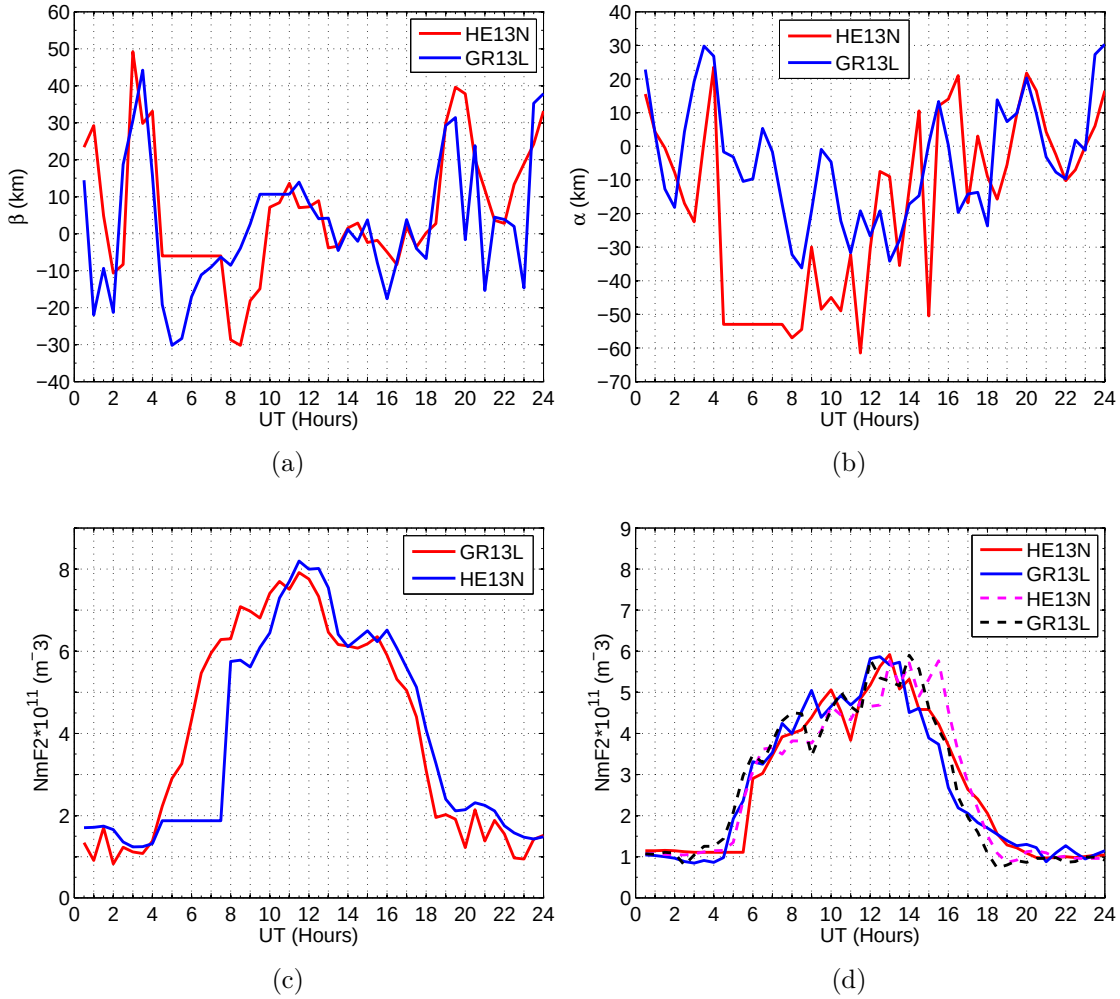

Figure 5.40: Perturbations in (a) hmF2 and (b) h'F derived from data for Grahamstown and Hermanus on 30 September, 2010. Peak electron density on (c) 30 September, 2010 and (d) 02 September, 2010 (solid lines) and 30 September, 2010 (dashed lines)

Figure 5.40 (a) and (b) both reflect that the ionosphere was slightly turbulent on this particular day as observed by these ionosondes. The variability of the perturbation in hmF2 is very high during the nighttime and low during the day. Meanwhile the variability in h'F perturbation occurs almost throughout the daytime and nighttime on this day. Figure 5.40 (c) shows that the peak electron density pattern at Grahamstown is close to the expected diurnal pattern. On the other hand, the electron density pattern at Hermanus increased sharply between 07:00 and 08:00 UT. Another unusual pattern at Hermanus occurred between 04:30 UT and 07:30 UT when the peak electron density remained constant. The most interesting feature in Figure 5.40 (c) is the small dip in the peak electron density between 13:00 and 14:00 UT, which is consistent with the L-band GPS measurements. The value of the peak electron density is lower in Figure 5.40 (d) by a factor of ~ 2.0 as compared

to that in Figure 5.40 (c). However, it was not possible to draw any conclusions about the anomalous amplitude scintillation from these observations.

5.6 Summary

Three types of SF were described, as well as their diurnal, seasonal and annual patterns, and relationship to solar activity. The results reveal MSF and FSF as the dominant forms of SF irregularity over South Africa. The F layer height changes and perturbations in the hmF2 and h'F (i.e. α and β) were examined to look for mechanisms that trigger SF and scintillation. The geomagnetic and solar wind conditions during the periods of SF and scintillation events were analysed. The parameters of interest were Dst, IMF (Bz), AE, ion number density (Nion), solar wind speed (Vp) and electric field (E). Further investigation of the ionospheric disturbances using GPS data was conducted to accompany ionosonde data observations. The derived $VTEC$ and its perturbation were used extensively in the search for mechanisms. The ionosonde and GPS data sets reveal TIDs and neutral wind composition changes as the driving mechanisms of the ionospheric disturbances over South Africa. Finally an anomalous amplitude scintillation observed with the Hermanus GISTM was analysed, but no conclusion was drawn.

Chapter 6

Discussion and conclusion

6.1 Introduction

This chapter discusses the observations and results of the research and submits a proposal for future work on SF and scintillation over South Africa. The aim of this study was to identify and characterise ionospheric irregularities causing SF and ionospheric scintillation at mid-latitude stations in South Africa, using data from instruments operating in the HF and L-band spectrum. The results presented in this thesis provide a suitable foundation and motivation for the development of a SF and scintillation prediction model for South Africa.

6.2 Discussion

The effects of ionospheric irregularities on the South African ionosphere was investigated by analysing SF and scintillation signatures, based on ionosonde and GPS data sets. A statistical SF database was derived by manually scanning ionograms covering an eight-year (2001-2008) period. The mechanisms causing ionospheric SF and scintillation were analysed, based on the variability of the ionospheric parameters (i.e. hmF2 and h'F) during the SF events. The SF events in this study were distinguished by high solar activity (11 April, 2001 and 15-16 November, 2001 SF events), moderate solar activity (18-20 February, 2005 SF event) and low solar activity (24-25 September, 2006 and 22-23 May, 2008 SF events). The L-band GPS observations were used to complement the ionosonde HF observations. Geomagnetically induced disturbances were investigated using the ACE satellite geomagnetic and solar wind data.

The ionosonde data from Madimbo (22.38°S, 30.88°E), Grahamstown (33.32°S, 26.50°E)

and Louisvale (28.51°S, 21.24°E) provided evidence that SF frequently occurs over South Africa. SF occurrence was characterised in terms of the monthly probability. Using the monthly SF probability, the dependence of SF occurrence on days, seasons and solar activity was characterised statistically for the period of this study. The diurnal SF probability was found to be highest between 23:00 and 00:00 UT for all seasons and types of SF during the two years chosen (2001 and 2005), except during autumn and spring (for RSF) in 2001 at Madimbo. The results reveal that MSF and FSF are the dominant seasonal irregularity structures observed from the Madimbo and Grahamstown ionosonde stations. The seasonal mid-latitude peak of MSF and FSF was in winter and this is consistent with the results obtained by Lambert (1988). RSF was observed mainly at Madimbo during a high solar activity period. However, higher MSF and FSF probability was more prevalent during low solar activity than high solar activity periods. The SF pattern correlated with solar activity for the two mid-latitude stations (Madimbo and Grahamstown) is consistent with that of Wang *et al.* (2010). This study revealed a weak negative correlation between solar activity and the probability of MSF at both stations, and a weak positive correlation between solar activity and RSF at the Madimbo station only. No correlation was found between SF and solar activity for both Madimbo and Grahamstown stations. Wang *et al.* (2010) also found that the occurrence of SF is independent of solar activity during each season. Therefore, ionosonde data showed that mixed SF (MSF) and frequency SF (FSF) are the dominant SF irregularities over South Africa.

Ionospheric measurements by the ionosondes (at Madimbo, Grahamstown and Louisvale) and selected dual frequency GPS receivers, revealed that the F-region ionosphere over South Africa was perturbed during SF events. The storm -induced perturbations had both positive (increased electron density) and negative (decreased electron density) effects on the ionosphere. These positive and negative storm effects were observed via the influence on the ionospheric plasma parameters, such as electron density and plasma turbulence. Yizengaw *et al.* (2005) showed that rapid heating and expansion of the atmosphere in the high latitude regions due to enhanced energy inputs by particle precipitation and enhanced electric fields could cause a reduction in F-region ionisation. Rapid heating and expansion of the atmosphere results in the depletion of the atomic to molecular ratio and changes the chemical composition. The current study demonstrates the occurrence of TEC depletion over South Africa during geomagnetic storms and sub-storms. The cause of the depletions are strongly linked with changes in the auroral latitudes as explained by Yizengaw *et al.* (2005). The intense electric fields and the enhanced equatorward neutral winds (i.e. TIDs) transport the composition changes that are generated in the high latitudes to mid- and low latitudes,

causing a reduction in the F-region ionisation.

The analysis of ionosonde data for the 11 April, 2001 SF event revealed an upliftment of the ionosphere during the peak of the storm (Figure 5.14). Similarly, the $VTEC$ perturbation for the same day shows both depletion and enhancement during the pre-midnight hours (Figure 5.16 (a)). During the 15-16 November 2001 SF event, although there was only minor storm activity, the SF intensity was very high, as shown on the ionograms in Figures 5.12 and 5.13. The difference between these two events could be attributed to the latitudinal difference. The 18-20 February, 2005 SF event which occurred during a moderate storm and moderate solar activity, seems to be linked to the increased energy input from the auroral latitudes. Therefore, the source of the irregularity that caused this extended SF event is probably the Joule heating transported by GWs or TIDs. On the other hand, the SF event of 24-25 September, 2006 exhibits both positive and negative storm effects. The changes in the composition of neutral winds and TIDs seem to be responsible for the generation of plasma irregularities during this event. The SF event of 22-23 May, 2008 occurred during multiple sub-storm activities. The $VTEC$ perturbations for this period reveal a turbulent ionosphere under the influence of wave-driven TID activity. This implies that waves or TIDs may be generated under geomagnetically quiet conditions.

The Rayleigh-Taylor (R-T) instability mechanism is widely believed to cause ionospheric SF irregularity. The linear growth rate of this instability (equation 2.5) suggests that many competing processes are responsible for the generation of SF. Abdu *et al.* (2000) however, states that the day-to-day variability of SF remains the least understood. In addition, Abdu *et al.* (2000) explains that the day-to-day variability is controlled by the SF seeding perturbation source which initiates the R-T instability. Several other factors, including GWs, have been cited as the main cause of the day-to-day variability. However, other key factors in understanding the origin of SF are the F layer height changes and the vertical plasma drift.

6.3 Conclusion

This study confirmed the occurrence of three types of SF (RSF, MSF and FSF) over the South African mid-latitude region. The three types of SF showed different responses for diurnal, seasonal and solar activity variation. The statistical database developed for this study can be used as a tool to develop a prediction model for the occurrence of SF. However, some of the data was incomplete due to gaps in GPS data from 2001 to 2005. Scintillation data was only available from July 2010, thus providing only a small period during which to

monitor the GPS scintillation phenomenon in the mid-latitude environment. Therefore, a substantial effort is required to improve the GISTM database in order to confirm occurrence of GPS ionospheric scintillation over South Africa. Some of the SF observations made at Madimbo and Grahamstown ionosonde stations were initiated by storm activity and others occurred during geomagnetically quiet periods. It was observed that MSF and FSF tend to appear frequently in the pre-midnight and post-midnight hours. Most of the observed RSF at Madimbo station occurred between 22:00 and 04:30 UT with a few cases between 18:00 and 21:30 UT, during high solar activity.

6.4 Future work

This study was limited to three ionosonde stations (Madimbo, Grahamstown and Louisvale) and selected dual frequency GPS receiver stations in South Africa. Future work should involve all four ionosonde stations (Table 5.1) and more GPS stations in South Africa and in other selected mid-latitude areas around the world. An extension of this study should consider analysis of the variation of SF over a whole solar cycle period. Other factors believed to cause daily variability, such as particle precipitation, vertical plasma drift, atmospheric GWs, thermospheric winds and F2 layer height changes, should be followed up using a global instrumentation network. Future work should also focus on developing an extensive scintillation database (at least four years) in order to monitor the GPS scintillation phenomenon over South Africa. Lastly, the nature and size of the irregularities responsible for the different types of SF should be examined and classified. The current research provides a background and motivation for developing a GISTM network for South Africa, and should form the basis upon which a scintillation and/or SF model for this region is developed.

References

Aarons J., "Global morphology of ionospheric scintillations", *Proceedings of the IEEE*, volume 70, pp. 360–378, 1982.

Abdu M.A., "Outstanding problems in the equatorial ionosphere-thermosphere electrodynamics relevant to spread F", *Journal of Atmospheric and Solar-Terrestrial Physics*, **63**, pp. 869–884, 2001.

Abdu M.A., Sobral J.H.A. and Batista I.S., "Equatorial spread F statistics in the American longitudes: some problems relevant to ESF description in the IRI scheme", *Advances in Space Research*, **25**, pp. 113–124, 2000.

Altadill D., Apostolov E.M., Boška J., Laštovička J. and Šauli P., "Planetary and gravity wave signatures in the F-region ionosphere with impact on radio propagation predictions and variability", *Annals of Physics*, **47**(2/3), pp. 1109–1119, 2004.

Basu S., Groves K.M., Quinn J.M. and Doherty P., "A comparison of TEC fluctuations and scintillations at Ascension Island", *Journal of Atmospheric and Solar-Terrestrial Physics*, **61**, pp. 1219–1226, 1999.

Beach T.L. and Kintner P.M., "Simultaneous Global Positioning System observations of equatorial scintillations and total electron content fluctuations", *Journal of Geophysical Research*, **104**(A10), pp. 22553–22565, 1999.

Belehaki A. and Tsagouri I., "Study of the thermospheric-ionospheric response to intense geomagnetic storms at middle latitudes", *Physics and Chemistry of the Earth*, **26**(5), pp. 353–357, 2001.

Belehaki A. and Tsagouri I., "On the occurrence of storm-induced nighttime ionization enhancements at ionospheric middle latitudes", *Journal of Geophysical Research*, **107**(A8), doi:10.1029/2001JA005029, 2002.

Bencze P., Burešová D., Laštovička J. and Märcz F., "Behaviour of the F1-region, and Es and spread-F phenomena at European middle latitudes, particularly under geomagnetic storm conditions", *Annals of Geophysics*, **47**(2/3), pp. 1131–1143, 2004.

Bhaneja P., Earle G.D., Bishop R.L., Bullett T.W., Mabie J. and Redmon R., "A statistical study of midlatitude spread F at Wallops Island, Virginia", *Journal of Geophysical Research*, **114**(A04301), doi:10.1029/2008JA013212, 2009.

Blanc M. and Richmond A., "The ionospheric disturbance dynamo", *Journal of Geophysical Research*, **85**(A4), pp. 1669–1686, 1980.

Buresova D., "Effects of geomagnetic storms on the bottomside ionospheric F region", *Advances in Space Research*, **35**, pp. 429–439, 2005.

Chiu M.C., Von-Mehlem U.I., Willey C.E., Betenbaugh T.M., J. J. Maynard J.A.K., Conde R.F., Gray W.T., Jr. J.W.H., Mosher L.E., McCullough M.G., Panneton P.E., Staiger J.P. and Rodberg E.H., "ACE Spacecraft", *Space Science Reviews*, **86**, pp. 257–284, 1998.

Conker R.S., El-Arini. M.B. and Hegarty C.J., "Modeling the effects of ionospheric scintillation on GPS/SBAS availability", , 2000.

Danilov A.D. and Lastovicka J., "Effects of geomagnetic storms on the ionosphere and atmosphere", *International Journal of Geomagnetism and Aeronomy*, **2**(3), pp. 5830–5838, 2001.

Datta-Barua S., Doherty P.H., Delay S.H., Dehel T. and Klobuchar J.A., "Ionospheric scintillation effects on single and dual frequency GPS positioning", *Proceedings of ION GPS/GNNS 2003, Portland, OR*, pp. 336–346, 2003.

Davies K., *Ionospheric radio*, Peter Peregrinus, London, 1990.

Dierendonck A.J.V., Klobuchar J. and Hua Q., "Ionospheric scintillation monitoring using commercial single frequency C/A code receivers", *Proceedings of ION GPS-93, Institute of Navigation, Salt Lake City, UT*, 1993.

Du J., Wilkinson P., Thomas R. and Cervera M., "Determination of equatorial ionospheric scintillation S4 dual frequency GPS", *URSI Commission G, Workshop, La Trobe University, Australia*, 2000.

Dubey S., Wahi R. and Gwal A.K., "Effects of ionospheric scintillation on GPS receiver at equatorial anomaly region Bhopal", *URSI XXVIIIth General Assembly, New Delhi, India*, 01238, 2005.

Dyson P.L., "Topside spread F at midlatitudes", *Journal of Geophysical Research*, **73**, pp. 2441–2446, 1968.

Earle G.D., Bhaneja P., Roddy P.A., Swenson C.M., Barjatya A., Bishop R.L., Bullett T.W., Crowley G., Redmon R., Groves K., Cosgrove R. and Vadas S.L., "A comprehensive rocket and radar study of midlatitude spread F", *Journal of Geophysical Research*, **115**(A12339), doi:10.1029/2010JA015503, 2010.

Fagundes P.R., Sahai Y., Batista I.S., Abdu M.A., Bittencourt J.A. and Takahashi H., "Observations of day-to-day variability in precursor signatures to equatorial F-region plasma depletions", *Annales Geophysicae*, **17**, pp. 1053–1063, 1999.

Fejer B.G., "Low-latitude ionospheric disturbance electric field effects during the recovery phase of the 19-21 October 1998 magnetic storm", *Journal of Geophysical Research*, **108**(A12), doi:10.1029/2003JA010190, 2003.

Fejer B.G. and Scherliess L., "Mid- and low-latitude prompt-penetration ionospheric zonal plasma drifts", *Geophysical Research Letters*, **25**(16), pp. 3071–3074, 1998.

Foppiano A.J. and Rodger A.S., "F-region ionospheric irregularities over King George Island and Argentine Islands - a comparative study", *Antarctic Science*, **3**, pp. 411–417, 1994.

Forte B. and Radicella S.M., "Comparison of ionospheric models with experimental data for satellite navigational systems", *Annales of Geophysics*, **48**(3), pp. 20–43, 2005.

Foster J.C. and Rich F.J., "Prompt mid-latitude electric field effects during severe geomagnetic storms", *Journal of Geophysical Research*, **102**, pp. 1–5, 1997.

Foster J.C. and Rideout W., "Storm enhanced density: magnetic conjugacy effects", *Annales Geophysicae*, **25**, pp. 1791–1799, 1997.

Fremouw E.J., "Early results from the DNA wideband satellite experiment - complex-signal scintillation", *Radio Science*, **13**(1), pp. 167–187, 1978.

Fremouw E.J. and Secan J.A., "Application of stochastic inverse theory to ionospheric tomography", *Radio Science*, **27**(5), pp. 721–732, 1992.

Fuller-Rowell T.J., Codrescu M.V., Moffett R.J. and Quegan S., "Response of the thermosphere and ionosphere to geomagnetic storms", *Journal of Geophysical Research*, **99**(A3), pp. 3893–3914, 1994.

Galushiko V.G., Paznukhov V.V., Yampolski Y. and Foster J., "Incoherent scatter radar observations of AGW/TID events generated by the solar terminator", *Annales Geophysicae*, **16**, pp. 821–827, 1998.

Garrard T., Davis A., Hammond J. and Sears S., "The ACE Science Center", *Space Science Reviews*, **86**, pp. 649–663, 1998.

Hajkowicz L.A., "Morphological and ionospheric aspects of quasiperiodic scintillations", *Journal of Atmospheric and Terrestrial physics*, **39**, pp. 833–841, 1977.

Hajkowicz L.A., "Simultaneous recordings of VHF scintillation occurrences over a wide range of southern latitudes", *Indian Journal of Radio and Space Physics*, **18**, pp. 2–9, 1989.

Hajkowicz L.A., "Types of ionospheric scintillations in southern mid-latitudes during the last sunspot maximum", *Journal of Atmospheric and Terrestrial Physics*, **56**(3), pp. 391–399, 1994.

Hajkowicz L.A., Bramley E.L. and Browing R., "Drift analysis of random and quasiperiodic scintillations in the ionosphere", *Journal of Atmospheric and Terrestrial physics*, **43**(7), pp. 723–733, 1981.

Hajkowicz L.A. and Dearden D.J., "Observations of random and quasi-periodic scintillations in southern mid-latitudes over a solar cycle", *Journal of Atmospheric and Terrestrial Physics*, **50**(6), pp. 511–517, 1988.

Hajkowicz L.A. and Minakoshi H., "Mid-latitude ionospheric scintillation anomaly in the Far East", *Annales of Geophysics*, **21**(2), pp. 577–581, 2003.

Hernández-Pajares M., Juan J.M. and Sanz J., "Medium-scale traveling ionospheric disturbances affecting GPS measurements: Spatial and temporal analysis", *Journal of Geophysical Research*, **111**, doi:10.1029/2005JA011474, 2006.

Ho C.M., Mannucci A.J., Sparks L., Pi X. and Lindqwister U.J., "Ionospheric total electron content perturbations monitored by the GPS global network during two northern hemisphere winter storms", *Journal of Geophysical Research*, **103**(A11), pp. 409–420, 1998.

Hoang T.L., Abdu M., MacDougall J. and Batista I.S., "Longitudinal differences in the equatorial spread F characteristics between Vietnam and Brazil", *Advances in Space Research*, **45**, pp. 351–360, 2010.

Hoffmann-Wellenhof B., Lichtenegger H. and Collins J., *Global Positioning System theory and practice*, Wien New York, Springer-Verlag, 1992.

Huang C.S., Kelley M.C., Machuzak J.S., Gentile L.C. and sultan P.J., "Nonlinear evolution of equatorial spread F, gravity waves, velocity shear, and day-to-day variability", *Journal of Geophysical Research*, **101**(A11), pp. 521–532, 1996.

Huang C.Y., Burke W.J., Machuzak J.S., Gentile L.C. and Sultan P.J., "Equatorial plasma bubbles observed by DMSP satellites during a full solar cycle: toward a global climatology", *Journal of Geophysical Research*, **107**(A12), doi:10.1029/2002JA009452, 2002.

Huang W.Q., Xiao Z., Xiao S.G., Zhang D.H., Hao Y.Q. and Suo Y.C., "Case study of apparent longitudinal differences of spread F occurrence for two midlatitude stations", *Radio Science*, **46**, doi:10.1029/2009RS004327, 2011.

Hunsucker R.D. and Hargreaves J.K., *The high-latitude ionosphere and its effects on radio propagation*, New York,Cambridge University Press, 2003.

Jakowski N., Schlüter S. and Sardón E., "Total electron content of the ionosphere during the geomagnetic storm on 10 January 1997", *Journal of Atmospheric and Solar-Terrestrial Physics*, **61**, pp. 299–307, 1999.

Kelley M., Fejer B. and Gonzales C., "An explanation of anomalous equatorial ionospheric electric fields associated with a northward turning of the interplanetary magnetic field", *Geophysical Research Letters*, **6**(4), pp. 301–304, 1979.

Kelley M.C., *The Earth's ionosphere: Plasma Physics and Electrodynamics*, Amsterdam, academic Press, second edition, 2009.

Kintner P., Ledvina B.M. and de Paula E.R., "GPS and ionospheric scintillation", *Space Weather*, **5**, p. S09003, doi:10:1029/2006SW000260, 2007.

Kumar S. and Singh A.K., "The effect of geomagnetic storm on GPS derived Total Electron Content (TEC) at Varanasi, India", *23rd National Symposium on Plasma Science and Technology (PLASMA-2008)*, 208, Journal of Physics: conference series, 1982.

Kumar V.V., Parkinson M.L., Dyson P.L. and Polglase R., "Solar and geomagnetic activity effects on mid-latitude F-region electric fields", *Annales of Geophysics*, **26**, pp. 2911–2921, 2008.

Lambert S., "Frequency and duration f disturbances in the mid-latitude F region of the ionosphere", *Radio Science*, **23**(4), pp. 693–707, 1988.

Liu H., Lühr H. and Watanabe S., "A solar terminator wave in thermospheric wind and density simultaneously observed by CHAMP", *Geophysical Research Letters*, **36**, doi: 110.1029/2009GL038165, 2009.

Mansilla G.A., "Mid-latitude ionospheric effects of a great geomagnetic storm", *Journal of Atmospheric and Terrestrial Physics*, **66**(12), pp. 1085–1091, 2004.

Martins C.R., Mendillo M.J. and Aarons J., "Toward a synthesis of equatorial spread F onset and suppression during geomagnetic storms", *Journal of Geophysical Research*, **110**, p. A07306, 2005.

McComas D.J., Blame S.J., Barker P., Feldman W.C., Phillips J.L., Riley P. and Griffee J.W., "Solar Wind Electron Proton Alpha Monitor (SWEPAM) for the Advanced Composition Explorer", *Space Science Reviews*, **86**, pp. 563–612, 1998.

McKinnell L., Paradza M., Cilliers P., Abdu M. and de Souza J., "Predicting the probability of occurrence of spread-F over Brazil using neural networks", *Advances in Space Research*, **39**, pp. 1047–1054, 2010.

McKinnell L.A., Opperman B. and Cilliers P.J., "GPS and Ionosonde TEC over Grahamstown, South Africa: first comparisons", *Advances in Space Research*, **39**, pp. 816–820, 2007.

McNamara L.F., *The ionosphere: communications, surveillance, and direction finding.*, Malabar, FL, Krieger, 1991.

Mendillo M., "Storms in the ionosphere: patterns and processes for total electron content", *Reviews of Geophysics*, **44**, 2006.

Michael C.K., Haldoupis C., Michael J.N., Jonathan J.M., Belehaki A., Shalimov S. and Victor K.W., "Case studies of coupling between the E and F regions during unstable sporadic-E conditions", *Journal of Geophysical Research* , **108**(A12), 2003.

Mikhailov A. and Schlegel K., "Physical mechanism of strong negative storm effects in the daytime ionospheric F region observed with EISCAT", *Annales Geophysicae*, **16**, pp. 602–608, 1998.

Mikhailov A., Skoblin M. and Föster M., "Daytime F2-layer positive storm effects at middle and lower latitudes", *Annales Geophysicae*, **13**, pp. 532–540, 1995.

Moldwin M., *An Introduction to Space Weather*, Cambridge, Cambridge University Press, 2008.

Pi X., Mannucci A.J., Lindqwister U.J. and Ho C.M., "Monitoring of global ionospheric irregularities using the worldwide GPS network", *Geophysical Research Letters*, **24**(18), pp. 2283–2286, 1997.

Pi X., Mendillo M. and Fox M.W., "Diurnal double maxima patterns in the F region ionosphere: substorm-related aspects", *Journal of Geophysical Research*, **98**(A8), pp. 677–691, 1993.

Prölss G.W., "Common origin of positive ionospheric storms at middle latitudes and the geomagnetic activity effect at low latitudes", *Journal of Geophysical Research*, **98**(A4), pp. 5981–5991, 1993.

Purohit P.K., Bhattacharya S., Tiwari R. and Gwal A.K., "Study of space weather on GPS performance at low latitude station Bhopal and high latitude station Maitri, Antarctica", *International Journal of Engineering Science and Technology*, **2**(12), pp. 7856–7865, 2010.

Radicella B.F.S.M. and Ezquer R.G., "A different approach to the analysis of GPS scintillation data", *Annals of Geophysics*, **45**(3/4), pp. 551–561, 2002.

Reinisch B., Galkin I.A., Khmyrov G., Kozlov A. and Kitrosser D.F., "Automated collection and dissemination of ionospheric data from the digisonde network", *Advances in Radio Science*, **2**, pp. 241–247, 2004.

Rezende L.F.C., de Paula E.R., Stephany S., Kantor I.J., Muella M.T.A.H., de Siqueira P.M. and Correa1 K.S., "Survey and prediction of the ionospheric scintillation using data mining techniques", *Space Weather*, **8**, 2010.

Rino C.L., "A power law phase screen model for ionospheric scintillation: 1. weak scatter", *Radio Science*, **14**(6), pp. 1135–1145, 1979.

Rufenach C.L., "A radio scintillation method of estimating the small-scale structure in the ionosphere", *Journal of Atmospheric and Terrestrial Physics*, **33**, pp. 1941–1951, 1971.

Sastri J.H., "Post-midnight onset of spread-F at Kodaikanal during the June solstice of solar minimum", *Annales Geophysicae*, **17**, pp. 1111–1115, 1999.

Secan J.A., Bussey R.M., Fremouw E.J. and Basu S., "High-latitude upgrade to the Wideband ionospheric scintillation model", *Radio Science*, **32**(4), pp. 1567–1574, 1997.

Sethi N.K., Dabas R.S. and Vohra V.K., "Diurnal and seasonal variations of hmF2 deduced from digital ionosonde over New Delhi and its comparison with IRI 2001", *Annales Geophysicae*, **22**, pp. 453–458, 2004.

Smith C.W., L'Heureux J., Ness N.F., M. H. Acuña L.F.B. and Scheifele J., "The ACE Magnetic Fields Experiment", *Space Science Reviews*, **86**, pp. 613–632, 1998.

Soicher H., Gorman F., Tsedilina E.E. and Weitsman O.V., "Spread-F during quiet and disturbed periods at midlatitudes", *Advances in Space Research*, **20**, pp. 2199–2202, 1997.

Somsikov V.M., "On mechanisms for the formation of atmospheric irregularities in the solar terminator region", *Journal of Atmospheric and Terrestrial Physics*, **57**, pp. 75–83, 1995.

Stone E.C., Frandsen A.M., Mewaldt R.A., Christian E.R., Margolies D., Ormes J.F. and Snow F., "The Advanced Composition Explorer", *Space Science Reviews*, **86**, pp. 4–22, 1998.

Subbarao K.S.V. and Murthy B.V.K., "Seasonal variation of equatorial spread F", *Annales Geophysicae*, **12**, pp. 33–39, 2006.

Tsurutani B.T., McPherron R.L., Gonzalez W.D., Lu G., Gopalswamy N. and Guarnieri F.L., *Recurrent magnetic storms: corotating solar wind streams*, Washington, D.C, American Geophysical Union, second edition, 2006.

Unnikrishnan K., Saito A., Otsuka Y., Yamamoto M., and Fukao S., "Transition region of TEC enhancement phenomena during geomagnetically disturbed periods at mid-latitudes", *Annales Geophysicae*, **23**, pp. 3439–3450, 2005.

Wang G.J., Shi J.K., Wang X. and Shang S.P., "Seasonal variation of spread-F observed in Hainan", *Advances in Space Research*, **41**, pp. 639–644, 2008.

Wang G.J., Shi J.K., Wang X., Shang S.P., Zherebtsov G. and Pirog O.M., "The statistical properties of spread F observed at Hainan station during the declining period of the 23rd solar cycle", *Annales of Geophysics*, **28**, pp. 1263–1271, 2010.

Wanninger L., "Ionospheric monitoring using IGS data", *Proceedings of the 1993 IGS Workshop, University of Berne, Berne*, pp. 351–360, 1993.

Wernik A.W., Lucilla A. and Materassi M., "Ionospheric irregularities, scintillation and its effects on systems", *Acta Geophysica Polonica*, **52**(2), pp. 237–249, 2004.

Yamamoto A., Ohta Y., Okuzawa T., Taguchi S., Tomizawa I. and Shibata T., "Characteristics of TEC variations observed at Chofu for geomagnetic storms", *Earth Planets Space*, **52**, pp. 1073–1076, 2000.

Yeh K.C. and Liu C.H., "Radio wave scintillation in the ionosphere", *Proceedings of the IEEE*, volume 70, pp. 324–360, 1982.

Yizengaw E., Dyson P., Essex E. and Moldwina M., "Ionosphere dynamics over the southern hemisphere during the 31 March, 2001 severe magnetic storm using multi-instrument measurement data", *Annales Geophysicae*, **23**, pp. 707–721, 2005.

Yizengaw E., Moldwina M., Dyson P. and Essex E., "Using tomography of GPS TEC to routinely determine ionospheric average electron density profiles", *Journal of Atmospheric and Solar-Terrestrial Physics*, **69**, pp. 314–321, 2007.